THE SOURCES, FORMATION AND PROPERTIES OF SOLUBLE ORGANIC AEROSOLS: RESULTS FROM AMBIENT MEASUREMENTS IN THE SOUTHEASTERN UNITED STATES AND THE LOS ANGELES BASIN

A Dissertation
Presented to
The Academic Faculty

by

Xiaolu Zhang

In Partial Fulfillment
of the Requirements for the Degree
Doctor of Philosophy in the
School of Earth and Atmospheric Sciences

Georgia Institute of Technology
August 2012

THE SOURCES, FORMATION AND PROPERTIES OF SOLUBLE ORGANIC AEROSOLS: RESULTS FROM AMBIENT MEASUREMENTS IN THE SOUTHEASTERN UNITED STATES AND THE LOS ANGELES BASIN

Approved by:

Dr. Rodney J. Weber, Advisor
School of Earth and Atmospheric Sciences
Georgia Institute of Technology

Dr. Armistead G. Russell
School of Civil and Environmental Engineering
Georgia Institute of Technology

Dr. Michael H. Bergin
School of Earth and Atmospheric Sciences
Georgia Institute of Technology

Dr. Jason D. Surratt
Department of Environmental Sciences and Engineering
University of North Carolina at Chapel Hill

Dr. Nga Lee (Sally) Ng
School of Earth and Atmospheric Sciences
Georgia Institute of Technology

Date Approved: May 9, 2012

To my parents

ACKNOWLEDGEMENTS

First and foremost, I sincerely thank my advisor, Dr. Rodney Weber, for his continuous and generous support throughout my Ph. D study. I am truly grateful to him for trusting me and admitting me to his group in the first place, when I was a new college graduate with only geochemistry background. During the past six years I worked with him, I have learned so much from his vision, knowledge and experience in atmospheric sciences, as well as from his hands-on guidance both in the lab and in the field. Words cannot fully express my heartfelt gratitude. Most of all, I thank him for his tolerance when I made mistakes, for his patience when my progress was not fast enough, and for his high expectation on me which is one important motivation that keeps me moving forward. I would like to acknowledge my Ph.D. thesis committee members, Drs. Michael Bergin, Sally Ng, Armistead Russell, and Jason Surratt, for taking time out of their busy schedules to read my thesis and providing constructive feedback on my research.

I was fortunate to have the opportunity to collaborate with a number of excellent scientists during the CalNex field campaign. I would like to thank Dr. Jason Surratt and Ying-Hsuan Lin from the University of North Carolina at Chapel Hill for their enormous help with data analyses and important contribution in paper writing, Dr. André Prévôt and Peter Zotter from Paul Scherrer Institut for providing the radiocarbon data and the insightful discussions at various conferences, Dr. Jose Jimenez and Patrick Hayes from the University of Colorado Boulder for providing the AMS data and invaluable manuscript comments, Dr. Paul Ziemann from the University of California Riverside for providing space and logistic help for Riverside measurements. I greatly appreciate Dr.

Joost de Gouw from NOAA Chemical Sciences Division for providing data and manuscript feedbacks, as well as for his support and career advice. I am also very grateful to my research collaborators on the EPA FRM project, Dr. Mei Zheng from Peking University and Dr. Neil Frank from USEPA Air Quality Assessment Division, for providing unique perspective and insight on the papers resulted from this study.

I acknowledge my fellow past and present Weber's group members, especially Dr. Chris Hennigan, Dr. Amy Sullivan, Dr. Neeraj Rastogi, Dr. Vishal Verma, Eric Parker, Jennifer Williams, Kayla Burns, and Thom Muccillo, for their assistance in my experimental work and helpful suggestions on general scientific questions. I appreciate Dr. Michelle Oakes, Jiumeng Liu and Laura King whom I shared most of my time with at Georgia Tech, for their long-term friendship and all the joyful moments we spent together. Special thanks to Dr. Arsineh Hecobian, a very close friend of mine, who is always there when I seek for help, who not only provides good advice on my research projects, but also shares with me the wisdom of life. I would like to thank my friends, especially Wenxian Zhang, Jin Liao, Lujia Feng, Kevin Chao, Zheng Lu, and Boris Galvis, as well as the fellow students in EAS and CEE departments. I enjoyed their company very much.

Finally, I thank my husband Zhen, the love of my life who stays with me through the ups and downs, and also a great friend and a wonderful colleague. I thank him and my parents back in China for their unconditional love and continuous support that made all these possible.

TABLE OF CONTENTS

LIST OF TABLES

LIST OF FIGURES

LIST OF SYMBOLS AND ABBREVIATIONS

SYMBOLS

$\mathring{A}_a$: Absorption Angström exponent

b_{ap}: Light absorption coefficient

b_{ap365}: Light absorption coefficient at 365 nm

Ca^{2+}: Calcium ion

CO: Carbon monoxide

F_p: WSOC partitioning coefficient; Fraction of total WSOC in the particle phase

κ: Hygroscopicity parameter

K^+: Potassium ion

K_p: Temperature-dependent partitioning coefficient

Mg^{2+}: Magnesium ion

Na^+: Sodium ion

NH_4^+: Ammonium ion

NO_3: Nitrate radical

NO_3^-: Nitrate ion

NO_x: Nitrogen Oxides ($NO + NO_2$)

NO_y: Total reactive nitrogen

O_3: Ozone

SO_2: Sulfur dioxide

SO_4^{2-}: Sulfate ion

λ: Wavelength

ABBREVIATIONS

ACSM: Aerosol Chemical Speciation Monitor

AMIGAS: 2008 August Mini-Intensive on Georgia Aerosol at SEARCH

AMS: Aerosol Mass Spectrometer

BB: Biomass Burning

BC: Black Carbon

BVOC: Biogenic Volatile Organic Compound

CALNEX: California Nexus; Research at the Nexus of Air Quality and Climate Change

CIMS: Chemical Ionization Mass Spectrometer

CMB: Chemical Mass Balance

CCN: Cloud Condensation Nuclei

CSN: Chemical Speciation Network

CTM: Chemical Transport Model

DAD: Diode Array Detection

EC: Elemental Carbon

ECMWF: European Centre for Medium-Range Weather Forecasts

EPA: Environmental Protection Agency

ESI-HR-Q-ToFMS: High Resolution Quadrupole Time-of-Flight Mass Spectrometry equipped with an Electrospray Ionization source

EST: Eastern Standard Time

FRM: Federal Reference Method

HOA: Hydrocarbon-like Organic Aerosol

HPAEC-PAD: High-Performance Anion-Exchange Chromatography with Pulsed Amperometric Detection

HULIS: HUmic-Like Substances

IC: Ion Chromatography

IEPOX: Isoprene-derived epoxydiols

IVOC: Intermediate Volatility Organic Compound

JST: Jefferson Street site

LA: Los Angeles

LOD: Limit Of Detection

LV-OOA: Low-Volatility Oxygenated Organic Aerosol

LWC: Liquid Water Content

LWCC: Liquid Waveguide Capillary Cell

MAE_{365}: Mass Absorption Efficiency at 365 nm

MC: Mist Chamber

MEGAN: Model of Emissions of Gases and Aerosols from Nature

MeOH: Methanol

MLH: Mixed Layer Height

MODIS: MODerate-resolution Imaging Spectroradiometer

NAAQS: National Ambient Air Quality Standards

NB: Non Biomass Burning

NR: Non-Refractory

OA: Organic Aerosol

OC: Organic Carbon

OOA: Oxygenated Organic Aerosol

OM: Organic Matter

PAH: Polycyclic Aromatic Hydrocarbon

PDT: Pacific Daylight Time

PILS: Particle-Into-Liquid Sampler

PM_1: Particulate Matter with aerodynamic diameter less than 1μm

$PM_{2.5}$: Particulate Matter with aerodynamic diameter less than 2.5 μm

POA: Primary Organic Aerosol

RH: Relative Humidity

RSD: Relative Standard Deviation

SEARCH: Southeastern Aerosol Research and Characterization

SOA: Secondary Organic Aerosol

SV-OOA: Semi-Volatile Oxygenated Organic Aerosol

SVOC: Semi-Volatile Organic Compound

TOC: Total Organic Carbon

TOR: Thermal/Optical Reflectance

TOT: Thermal/Optical Transmittance

UPLC: Ultra Performance Liquid Chromatography

UV: Ultraviolet

VIS: Visible

VOC: Volatile Organic Compound

WSOC: Water-Soluble Organic Carbon

$WSOC_g$: Gas-phase Water-Soluble Organic Carbon

$WSOC_p$: Particle-phase Water-Soluble Organic Carbon

YRK: Yorkville site

SUMMARY

Organic aerosol (OA) is an important component of tropospheric fine aerosol, and can have a large influence on climate, visibility and human health. Secondary organic aerosol (SOA) often comprises a large fraction of the total OA, and is a major contributor to poor air quality in urban environments. However, due to the complexity of SOA, its sources, formation mechanisms, and some chemical and physical properties remain poorly understood. This thesis presents results from online and offline observations of ambient soluble fine aerosol chemical composition and physical properties, with the goal of better understanding the sources and formation of SOA in regions dominated by biogenic emissions (e.g., the southeastern U.S.) and anthropogenic emissions (e.g., the Los Angeles Basin).

As part of the thesis work, 900 archived Federal Reference Method (FRM) filters from 15 sites over the southeast during the year of 2007 were analyzed for $PM_{2.5}$ chemical composition and physical properties. Secondary components (i.e. sulfate aerosol and SOA) were the major contributors to the $PM_{2.5}$ mass over the southeast, whereas the contribution from biomass burning varied with season and was negligible (2%) during summer based on fire count data and levoglucosan concentrations. Excluding biomass burning influence, FRM water-soluble organic carbon (WSOC) was spatially homogeneous throughout the region, similar to sulfate, yet WSOC was moderately enhanced (27%) in locations of greater predicted isoprene emissions in summer. A Positive Matrix Factorization (PMF) analysis identified two major source types for the summer WSOC; 22% of the WSOC were associated with ammonium sulfate, and 56% of

the WSOC was associated with brown carbon and oxalate. On smaller spatial scale, a substantial urban/rural gradient of WSOC (31%) was found through comparisons of online WSOC measurements at one urban/rural pair (Atlanta/Yorkville) in August 2008, indicating important contribution from anthropogenic emissions. The measured Atlanta urban excess, combined with the estimated boundary layer heights, gave an estimated Atlanta daily WSOC production rate in August of 0.55 mgC m^{-2} hr^{-1} between mid-morning and mid-afternoon.

A comparative study between Atlanta and LA reveals a number of contrasting features between the two cities, including gas-particle partitioning of WSOC and formic acid, as well as the light-absorbing properties of the soluble organic aerosols. WSOC gas-particle partitioning, investigated through the fraction of total WSOC in the particle phase, F_p, exhibited differing relationships with ambient RH and organic aerosols in the two urban environments. In Atlanta, evidence for WSOC partitioning to aerosol water is observed throughout the day, but is most prevalent in the morning. During drier periods (RH<70%), F_p was in proportion to the organic mass, suggesting that both particle water and OA can serve as an absorbing phase. In contrast, despite the higher average RH, in LA the aerosol water was not an important absorbing phase, instead, F_p was correlated with OA mass. Particle water concentrations from thermodynamic predictions based on measured inorganic aerosol components do not indicate significant differences in aerosol hygroscopicity. In terms of light absorption, fresh LA secondary organic carbon had a consistent brown color and a bulk absorption per soluble carbon mass at 365 nm that was 4 to 6 times higher than freshly-formed Atlanta soluble organic carbon. The chemical speciation analysis of aqueous filter extracts identified nitro-aromatics as one component

of LA brown SOA. Interpreting soluble brown carbon as a property of freshly-formed anthropogenic SOA, the difference in absorption per carbon mass between these two cities suggests most fresh secondary water-soluble organic carbon formed within Atlanta is not from an anthropogenic process similar to LA.

The observed differences in WSOC partitioning behaviors and SOA optical properties may be attributed to the contrasting volatile organic compounds (VOC) mixture between the two cities, i.e. the predominance of anthropogenic precursors in LA and the uniquely abundant biogenic emissions in Atlanta. In addition, different organic aerosol composition may also play a role, as Atlanta OA is expected to have a substantially more aged regional character. The findings of this work have significantly contributed to the current state of knowledge regarding SOA sources, formation pathways and properties, provide fundamental information for SOA modeling efforts, and have important implications for control strategies and regulations of ambient aerosols in urban regions.

CHAPTER 1

INTRODUCTION

1.1 Organic aerosols in the atmosphere

Atmospheric aerosols can absorb and scatter solar radiation and consequently have a significant direct impact on global climate and regional radiative forcing. Additionally, aerosols have a substantial but highly uncertain indirect effect as they can serve as cloud condensation nuclei (CCN), modify cloud albedo and lifetime, and thereby affect the Earth's radiation budget [*IPCC*, 2007]. Particulate matters with an aerodynamic diameter less than 2.5 μm ($PM_{2.5}$) have an adverse effect upon human health [*Seagrave et al*., 2006]. These particles are small enough to penetrate deep into the lungs of people and often contain toxic compounds such as heavy metals and polycyclic aromatic hydrocarbons (PAHs) [*Lighty et al*., 2000]. Epidemiology studies have shown that fine particles result in more respiratory diseases and premature death than do larger particles [*Dockery et al*., 1993; *Schwartz et al*., 1993].

Organic aerosols (OA) are major components of tropospheric fine aerosols, contributing ~20-50% to the total $PM_{2.5}$ mass at continental mid-latitudes [*Saxena and Hildmann*, 1996] and as high as 90% in tropical forested areas [*Roberts et al*., 2001]. Organic compounds that are directly emitted into the atmosphere in the particle phase are referred to as primary organic aerosols (POA). The sources of POA include biomass burning, fossil fuel combustion, cigarette smoking, food cooking and primary biogenic aerosols [*Kanakidou et al*., 2005 and references therein]. Organic aerosols that are formed in the atmosphere from gas-phase precursors through multistep oxidation

processes and subsequent condensation onto existing particles are referred to as secondary organic aerosols (SOA). SOA often comprise a large fraction of the total OA [*Zhang et al.,* 2007], and are major contributors to poor air quality in urban environments [*Docherty et al*., 2008; *de Gouw and Jimenez*, 2009], especially during summer when more intensive photochemical processes lead to highly oxidizing conditions. The precursor volatile organic compounds (VOCs) of SOA are derived from a variety of natural and anthropogenic sources, including biogenic hydrocarbons, such as isoprene [*Kroll et al*., 2006], monoterpenes [*Hoffmann et al*., 1997; *Ng et al*., 2007] and sesquiterpenes [*Cahill et al*., 2006], as well as aromatic compounds [*Odum et al*., 1997] and possibly a host of other unidentified semi-volatile organic species from anthropogenic emissions [*Robinson et al*., 2007; *de Gouw et al*., 2011].

On a global scale, bottom-up models estimate total biogenic SOA fluxes of 12-70 Tg yr^{-1}, approximately 5-6 times large than the estimated anthropogenic SOA fluxes (2-12 Tg yr^{-1}) [*Kanakidou et al*., 2005; *Henze et al*., 2008; *Hallquist et al*., 2009], indicating the important contribution from biogenic emissions globally. Anthropogenic SOA contributes up to 65% of the total SOA mass in the north hemisphere in winter and contributes less than 15% during summer when biogenic VOC emissions were large [*Tsigaridis and Kanakidou*, 2003]. However, recent field observations show that the anthropogenic SOA has been underestimated by the model estimates over a factor of 10 [*de Gouw et al*., 2005; *Volkamer et al*., 2006], likely due to the missing anthropogenic SOA precursors as well as the highly uncertain SOA yields reported by chamber studies. In addition, a number of ambient studies have reported enhancement of biogenic SOA formation in urban areas with substantial anthropogenic emissions [*Weber et al*., 2007;

Spracklen et al., 2011; *Worton et al*., 2011; *Setyan et al*., 2012], which adds one more degree of uncertainty to the complex SOA chemistry.

1.2 Formation of secondary organic aerosols

The global SOA budget is highly uncertain due to current understanding of emission inventories and chemistry. Recent field observations reported unexpected high SOA loadings in the ambient air that cannot be explained by current models [*de Gouw et al.,* 2005*; Volkamer et al.,* 2006]. Top-down estimates based on mass balance of VOCs suggest a global SOA source ranging from 120-1820 Tg yr^{-1}, roughly an order of magnitude larger than bottom-up estimates using VOC emission inventory and their particulate mass yields determined in the laboratory [*Spracklen et al*., 2011]. Some of the uncertainty in the SOA budget and the discrepancy between model simulation and field observations are due largely to the incomplete understanding of the SOA formation mechanisms.

SOA formation is generally thought to occur through gas-particle partitioning of semi-volatile organic compounds (SVOCs) formed by the gas-phase oxidation of VOCs [*Seinfeld and Pankow*, 2003]. Results from chamber experiments suggest that the partitioning of SVOCs is highly dependent on the quantity of pre-existing OA mass [e.g., *Odum et al*., 1996]. The observed SOA mass in chambers has been well described by an equilibrium absorptive partitioning model [*Pankow*, 1994], although the system may not be in equilibrium and thus may be kinetically-controlled under certain conditions [*Perraud et al*., 2012]. However, it has been challenging to extend this model to the complex ambient atmosphere given the wide spectrum of SVOCs of unclear identity and

physiochemical properties [*Hallquist et al*., 2009]. Model simulations that incorporate SOA formation from traditional VOC precursors represented by absorptive partitioning to OA tend to significantly underestimate ambient SOA mass by up to an order of magnitude in polluted regions [*de Gouw et al*., 2005; *Heald et al*., 2005; *Volkamer et al*., 2006]. Newer models including primary SVOC and intermediate volatility species (IVOC) result in much improved predictions, but it is unclear whether this is for the right reasons [*Hodzic et al*., 2010; *Dzepina et al*., 2011].

A growing body of evidence indicates that reactions in the atmospheric aqueous phase are important contributors to aerosol formation and can help explain observations that cannot be accounted for using traditional gas-phase chemistry. For example, the presence of the high-molecular-weight compounds (i.e. oligomers, humic-like substances) in ambient particles [*Surratt et al*., 2007; *Stone et al*., 2009] and the higher oxygen-to-carbon (O:C) ratio observed in the ambient air relative to chamber experiments [*Aiken et al*., 2008; *Ng et al*., 2010] may be explained by an aqueous phase oxidation process [*Ervens et al*., 2011]. Furthermore, there is evidence that absorptive partitioning to particle water can lead to SOA formation [*Blando and Turpin*, 2000; *Volkamer et al*., 2009]. Gas-phase water-soluble organic species (e.g., glyoxal and methylglyoxal) have been shown to undergo heterogeneous oxidation in the aqueous phase leading to reduced vapor pressures and SOA [*Volkamer et al*., 2007; *Ervens and Volkamer*, 2010; *Lim et al*., 2010]. Recent studies suggest that the mass of SOA formed through this mechanism may be substantial [*Hennigan et al*., 2008a; *Chang et al*., 2009; *Parikh et al*., 2011].

Another potential reason for the large discrepancy between model results and in-

situ observations is the formation of SOA from precursors that are not traditionally considered. For example, recent laboratory work have demonstrated that isoprene-derived epoxydiols (IEPOX) formed from the photooxidation of isoprene under low-NO_x conditions are likely the key intermediates in the formation of isoprene SOA, and these IEPOX and IEPOX-derived SOA constituents have been identified in the ambient aerosol samples collected in the southeastern U.S. [*Chan et al*., 2010b; *Lin et al*., 2012]. Besides, *Robinson et al*. [2007] propose that some fraction of POA evaporates upon dilution with ambient air and these organic vapors subsequently undergo oxidation and re-partition to the aerosol phase and form SOA. In environmental chamber experiments, *Robinson et al*. [2007] found that taking into account the SOA mass formed from SVOCs and IVOCs could bring the model predictions to much better agreement with observations. Likewise, results from regional [*Hodzic et al*., 2010] and global [*Pye and Seinfeld*, 2010] modeling studies have also shown the important potential role of S/IVOC chemistry in the SOA budget. Most recently, evidence of significant contribution of IVOCs to SOA formation was observed in the atmosphere. *de Gouw et al*. [2011] found that C_{14} to C_{16} hydrocarbons were the major precursors of the SOA observed downwind from the Deepwater Horizon oil spill. However, the molecular structure of these hydrocarbon compounds remains unclear and in-situ measurement data of S/IVOCs under ambient condition are still quite sparse due to measurement limitation. Laboratory chamber studies on S/IVOCs have been limited to single surrogate compounds whereas most of the IVOC species remain in the "unresolved complex mixture" [*Robinson et al*., 2007]. The contribution from evaporation of POA followed by re-condensation of these S/IVOCs may be important on regional scales, especially in urban regions where POA

emissions from diesel exhaust and wood smoke are abundant.

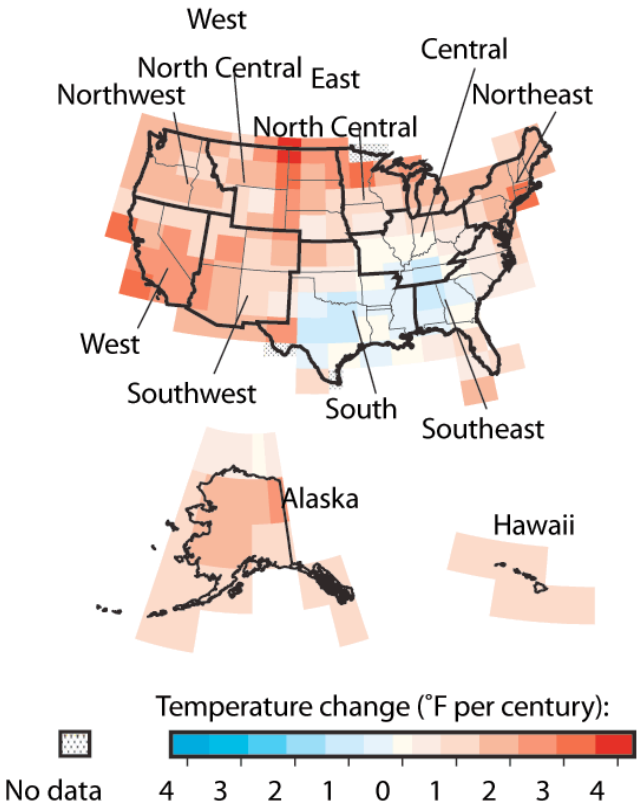

Figure 1.1 Annual mean temperature anomalies over 1901-2005. Figure courtesy: U. S. EPA and data courtesy: NOAA's National Climatic Data Center. Figure is downloaded from: (http://www.epa.gov/climatechange/science/recenttc.html).

1.3 Regions of interest

SOA formation in urban atmospheres has received extensive attention in the past years and has been investigated through multiple field studies conducted in major urban areas around the world [e.g., *de Gouw et al.*, 2008; *Aiken et al.*, 2009; *Williams et al.*, 2010; *Stone et al.*, 2010; *Hersey et al.*, 2011]. In this work, online and offline measurements of gas and aerosol phase components were carried out and contrasted in

two regions in the United States, the southeast and the Los Angeles Basin along the west coast, to understand the sources and formation processes of ambient secondary organic aerosols. These two regions were chosen due largely to their distinctly different meteorology, topography, and population density, as well as the emissions of SOA precursors.

Much of the thesis work is focused on characterizing the sources and formation of fine aerosols in the southeastern United States. The southeast has a generally rural environment interspersed with a number of urban areas, where, including the Atlanta metropolitan area, the fine particle ($PM_{2.5}$) National Ambient Air Quality Standards (NAAQS) are often exceeded [*Cohan et al*., 2007]. On the other hand, the U.S. EPA reported that the annual mean temperature anomalies over the southern and southeastern U.S. in the past century (1901 to 2005) were significantly lower than other parts of the country (Figure 1.1). Meanwhile, *Portmann et al*. [2009] showed that changes in regional climate over the 20^{th} century were most pronounced over the southern U.S.. Previous studies based on in-situ and satellite observations of aerosol optical depth suggest that aerosols over these regions may be the cause. The direct effects of aerosols on radiative forcing are estimated to produce a summertime cooling of -11 ± 6 W m^{-2} [*Carrico et al*., 2003] in urban Atlanta, and a greater radiative cooling of -3.9 W m^{-2} in summer than in winter over the entire southeastern U.S. [*Goldstein et al*., 2009]. These estimates are significant compared to the global mean CO_2 radiative forcing of 1.66 W m^{-2} and the global mean aerosol direct radiative forcing of -0.5 ± 0.4 W m^{-2} [*IPCC*, 2007]. This substantial cooling haze over the southeast is thought to be largely from secondary organic aerosols (SOA) of biogenic origin [*Goldstein et al*., 2009]. The southeastern

U.S. has the highest predicted biogenic emission (e.g., isoprene and monoterpenes) of northern mid-latitudes, with significant amount of anthropogenic emissions from mobile sources in large urban areas like Atlanta. In addition, emissions from frequent wildfires and prescribed burnings in spring and residential wood burning in winter are also important contributors to ambient fine aerosols in this region. For these reasons, the southeastern U.S. is ideal to study biogenic-anthropogenic interactions, given the proximity of natural emissions with a variety of anthropogenic pollution sources, and has been a focus area in many ambient studies in the past.

The Los Angeles area has long suffered from heavy air pollution and is considered a laboratory for air quality studies. Despite decades of aggressive emission controls, the LA area is still among the most polluted regions in the U.S., with the annual $PM_{2.5}$ averages regularly exceeding the national standard during the past decade [*CARB*, 2010]. Multiple ground-based [*Croes and Fujita*, 2003; *Docherty et al*., 2011; *Hersey et al*., 2011] and airborne [*Jacob et al*., 2010] field campaigns have been carried out in the LA Basin, aiming to characterize aerosols in this area. The CalNex 2010 (California Research at the Nexus of Air Quality and Climate Change) field study was undertaken in the LA Basin and the central valley during May to July 2010, with one goal being to better understand the sources and formation processes contributing to regional SOA loading. The metropolitan Los Angeles (LA) is one of the largest urban centers in the United States, spanning a land area of approximately 12,600 km^2 that includes a population of over 17 million people (2010 United States Census). SOA is a major source of LA fine particle mass and is formed mainly from anthropogenic emissions in this area [*Docherty et al*., 2008; *Hersey et al*., 2011; *Zhang et al*., 2011; *Bahreini et al*., 2012;

Hayes et al., 2012]. Compared to LA, the Atlanta metropolitan region has a significantly lower population density, with 5.3 million people (2010 United States Census) spread across an area of 21,700 km^2. Urban Atlanta also has substantial summertime SOA production [*Lim and Turpin*, 2002], but with important contributions from both biogenic and anthropogenic emissions [*Weber et al*., 2007; *Goldstein et al*., 2009].

Due to the significant differences in the emissions of SOA precursors as well as the general meteorology and geography between these two environments, a comparative study utilizing novel measurements of SOA and its components will provide valuable insight and facilitate the understanding of SOA sources and formation processes, which will also have important implications on the control strategies and regulation of fine aerosols in areas under similar conditions.

1.4 Motivation and scope of this work

This dissertation investigates several important aspects of aerosols in the ambient environment, with a particular focus on the sources, formation and properties of SOA in the southeastern United States. Specific questions that will be addressed in this work include:

- **Can levoglucosan and water-soluble potassium be used as robust biomass burning tracers? How much does biomass burning emission contribute to ambient $PM_{2.5}$ in different seasons over the southeastern U.S.?**
- **What are the major sources of SOA in the southeast? To what extent does anthropogenic pollution impact biogenic SOA formation?**
- **Can SOA light-absorbing properties provide insights on the sources and**

formation of SOA?

- **Is aqueous chemistry an important SOA formation route in the southeast and LA?**

Through conducting online and offline ambient measurements of gas-phase species and soluble $PM_{2.5}$ components, this study addresses the essential scientific questions listed above by providing detailed analyses and thorough discussions on the observational results. Specifically, this thesis evaluates and validates the use of levoglucosan as a biomass-burning tracer, and based on this finding, estimates the contribution of biomass burning to ambient $PM_{2.5}$ level over the southeast through covariance analysis (Chapter 2). Using WSOC as a quantitative measure of SOA, this work characterizes the regional nature of SOA through analysis of spatial and temporal distributions of WSOC, and highlights the important roles of both biogenic and anthropogenic emissions in SOA formation over the southeast region and estimates an urban Atlanta WSOC production rate based on simultaneous online measurements at an urban/rural paired sites (Chapter 3). Through a comparative study of WSOC light-absorbing properties (Chapter 4) and gas-particle partitioning behaviors (Chapter 5) in Atlanta and LA, the latter being a typical urban environment predominately influenced by anthropogenic emissions, it is concluded that much of the observations in the southeastern U.S., including the weakly-absorbing fresh SOA components and the clear dependence of WSOC partitioning on aerosol liquid water, can be attributed to unique VOC emissions (i.e. dominated by biogenic emission with considerable amount of anthropogenic impact) in the southeast compared to other parts of the country.

CHAPTER 2

BIOMASS BURNING IMPACT ON AMBIENT $PM_{2.5}$ OVER THE SOUTHEASTERN UNITED STATES

2.1 Background

Biomass burning is a major source of ambient $PM_{2.5}$ (particulate matter with aerodynamic diameter less than 2.5μm) and has significant impacts on human health [*Lighty et al*., 2000], regional to global air quality [*Lelieveld et al*., 2001] and climate [*Penner et al*., 1992; *Hobbs et al*., 1997]. Numerous studies have attempted to assess the impact of biomass burning on local and regional $PM_{2.5}$ concentrations. Typically, either source-oriented or receptor-oriented methods are used to quantify biomass burning contributions. Source-oriented approaches use chemical transport models (CTMs) to simulate the emissions from biomass burning sources, but are limited by large uncertainties in fire emission inputs [*Zeng et al*., 2008; *Tian et al*., 2009]. Receptor-oriented approaches quantify source contribution through measurements of specific marker species for biomass burning [e.g., *Schauer et al*., 1996; *Rogge et al*., 1998; *Schauer and Cass*, 2000; *Zheng et al*., 2002] and have been used more widely.

A number of chemical species have been used as particle-phase biomass burning emission tracers. Water-soluble potassium (K^+) has been used extensively as an inorganic tracer to apportion biomass burning contributions to ambient aerosol [*Ramadan et al*., 2000; *Kim et al*., 2003a, b; *Ma et al*., 2003; *Liu et al*., 2005; *Lee et al*., 2008]. K^+ is not an ideal tracer as it has other sources, such as sea salt and soil dust [*Wang et al*., 2005; *Duvall et al*., 2008]. Attempts have been made to eliminate these sources by calculating

non-sea-salt non-dust K^+ [*Cachier et al*., 1991; *Puxbaum et al*., 2007; *Pio et al*., 2008], but this requires knowledge of the source characteristics and an assumption that they are invariant among different locations and seasons. Organic compounds are the largest component produced from fires and there are specific compounds found to be exclusively emitted from biomass burning. The most commonly used organic tracer is levoglucosan, a sugar anhydride produced during the combustion of cellulose [*Simoneit et al*., 1999; *Puxbaum et al*., 2007; *Zheng et al*., 2007; *Sullivan et al*., 2008].

$PM_{2.5}$ concentrations are high in the southeastern U.S. [*Goldstein et al*., 2009] and the impact of biomass burning emissions in this region has been extensively studied [*Tanner et al*., 2004; *Liu et al*., 2005; *Zheng et al*., 2006, 2007; *Lee et al*., 2008; *Zeng et al*., 2008; *Tian et al*., 2009; *Yan et al*., 2009]. *Zeng et al*. [2008] suggested that prescribed fire emissions can result in a daily increase of $PM_{2.5}$ mass up to 25 μg m^{-3}, leading to $PM_{2.5}$ nonattainment in regions affected by the fires. *Tian et al*. [2009] attributed 55% and 80% of $PM_{2.5}$ to prescribed burning in January and March of 2002, respectively. Receptor model studies using levoglucosan as a biomass-burning tracer suggested that wood burning is the dominant contributor (9-51%) to OC and one of the major sources of $PM_{2.5}$ at several urban and rural sites in the southeast during September 2003 and January 2004 [*Zheng et al*., 2006, 2007]. Using both PMF and CMB receptor models and K^+ as a tracer, *Lee et al*. [2008] attributed 5-20% of the $PM_{2.5}$ mass to biomass burning emissions at four sites in Georgia and Alabama from January 2000 to December 2002.

These previous studies indicated that biomass burning is a major $PM_{2.5}$ source with contributions that vary with seasons; however, they are based on data for only a few months at a limited number of sites and are further restricted by uncertainties in biomass

burning emissions and tracer concentrations. In this study, an extensive data set of $PM_{2.5}$ mass concentrations and chemical speciation was generated from archived FRM filters acquired from state regulatory agencies for the year of 2007. This study compares K^+ and levoglucosan as biomass-burning tracers and employs a PMF analysis to quantify average mass contributions from biomass burning and other sources over the southeastern U.S. throughout 2007.

2.2 Experimental methods

2.2.1 FRM filter sampling

State agencies use an EPA Federal Reference Method (FRM) to determine ambient $PM_{2.5}$ mass at sites throughout the country to assess compliance with National Ambient Air Quality Standards (NAAQS). Once mass has been determined gravimetrically, the filters are stored and are eventually discarded. For this study, archived FRM filters that had been in storage (in the dark at a $T < -20°C$) for roughly a year were acquired from state regulatory agencies in Georgia (GA Department of Natural Resources), South Carolina (SC Department of Health and Environmental Control) and Alabama (AL Department of Environmental Management and the Jefferson Co. Department of Health). The FRM method for collecting ambient fine particles onto Whatman 47 mm Teflon filter substrates involved 24-hour integrated sampling at a nominal flow rate of 16.7 L/min with $PM_{2.5}$ sharp cut cyclone size selector or $PM_{2.5}$ WINS impactor and with no gas-denuders [*Patashnick et al*., 2001]. Fifteen sampling sites throughout the southeastern U.S. were chosen within the EPA FRM monitoring network, on the basis of geographic location, site type (i.e. urban and rural) and source influences. Among these fifteen sites, eight were urban and seven were rural. Table 2.1

lists the sites, and their locations are shown in Figure 2.1. A subset of all field samples corresponding to a one-in-six-day sampling schedule produced 60 filters for analysis per site and a total of 900 filters. In addition to these filters, a series of field blanks (36 filters) and replicated filters (43 filters) were included for quality control.

Table 2.1 Locations and types of the FRM sampling sites in this study.

No.	State	City	Site name	Latitude	Longitude	Type
1	GA	Decatur	South Dekalb*	33.6881	-84.2902	Urban
2	GA	Rome	Rome*	34.2611	-85.3230	Urban
3	GA	Augusta	AUG-BRS*	33.4339	-82.0224	Urban
4	GA	Macon	Macon*	32.7773	-83.6412	Urban
5	GA	Yorkville	Yorkville	33.9285	-85.0453	Rural
6	GA	Sandersville	Sandersville	32.9747	-82.8089	Rural
7	GA	Columbus	COL-CRS*	32.4309	-84.9318	Urban
8	GA	Athens	ATNS-UGA*	33.9179	-83.3446	Urban
9	AL	Birmingham	N'BHM*	33.5530	-86.8149	Urban
10	AL	Wylam	Wylam	33.4997	-86.9241	Urban
11	AL	Providence	Providence	33.4596	-87.3055	Rural
12	AL	Ashland	Ashland	33.2849	-85.8036	Rural
13	AL	Crossville	Crossville	34.2886	-85.9699	Rural
14	SC	Long Creek	Long Creek	34.8053	-83.2377	Rural
15	SC	Trenton	Trenton	33.7400	-81.8536	Rural

* Sampling stations with co-located EPA Speciation sites.

2.2.2 Chemical analyses

This suite of filters was extracted in water and a number of chemical components and physical properties were quantified. Each archived FRM Teflon filter was placed in a pre-cleaned 30 mL Nalgene amber HDPE bottle and extracted with 30 mL of 18-MΩ Milli-Q water via 30-minute sonication. The liquid extract was then filtered using a 0.45 μm PTFE syringe filter and transferred to a separate pre-cleaned 30 mL Nalgene amber bottle. Various chemical analyses were performed on aliquots from these bottles, which were stored in the refrigerator (~4°C) for at most one week until all analyses were

completed.

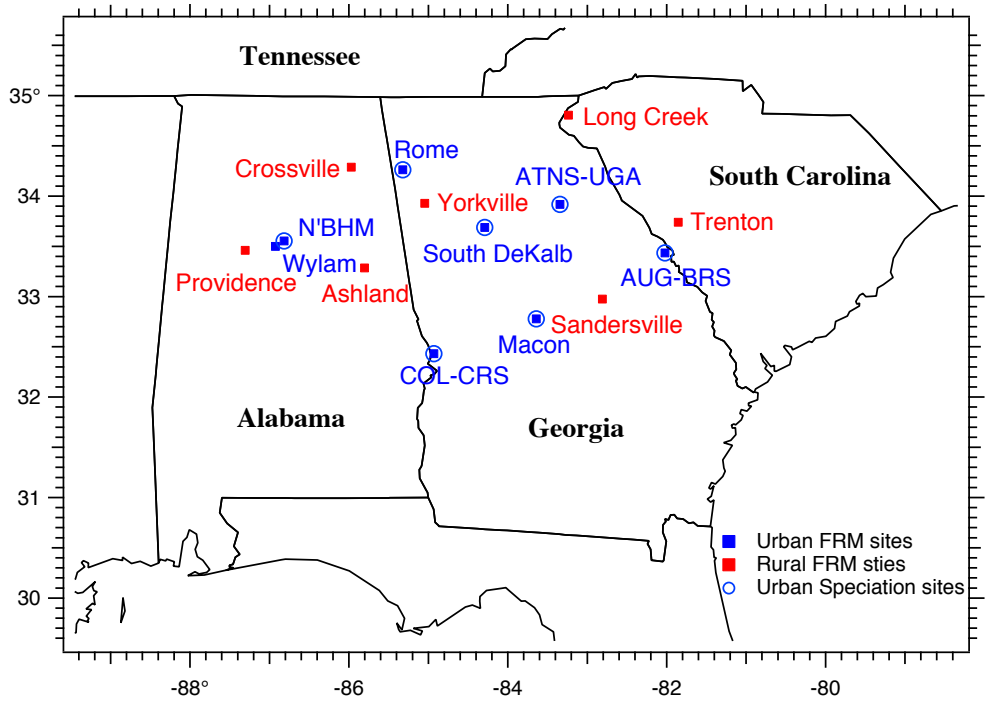

Figure 2.1 Map of the EPA FRM and co-located Speciation sampling sites used in this study. Site names and locations are given in Table 2.1.

For each species quantified, overall uncertainty was determined based on a sum of squares that included measurement uncertainties (e.g., liquid extraction volumes, etc.), variability in calibrations performed throughout the analyses of all 900 filters, variability in field blanks and water blanks, and precision based on variability of a standard placed at intervals of every tenth sample throughout the sample queues.

Water-soluble organic carbon (WSOC) in the extract was quantified using a Sievers Model 800 Turbo Total Organic Carbon analyzer (GE Water Systems, Boulder, CO; for more details see *Sullivan et al*. [2004]). The instrument was calibrated using a

series of sucrose standards (N=5, linear regression r^2=0.9998; variability in slope based on three separate calibrations throughout the analysis period was ~3%). The method limit of detection (LOD) of 0.33 μg Carbon m^{-3} (μg C m^{-3}) for WSOC was estimated by three times the standard deviation of field blanks, translated to ambient air concentration assuming, in all cases, a flow rate of 16.7 L/min and 24 hour sampling period. Overall measurement uncertainty was 9%.

High-performance anion-exchange chromatography with pulsed amperometric detection (HPAEC-PAD) was utilized to quantify various carbohydrate compounds, including levoglucosan. This technique involved a Dionex DX-500 series ion chromatograph coupled with Dionex ED 50 electrochemical detector with a gold working electrode operating in integrating amperometric mode, and a Dionex CarboPac PA-1 anion-exchange column with gradient elution of 200 mM NaOH at a flow rate of 0.5 mL min^{-1}. The elution profile was as follows: 0-8 min, isocratic elution with 10 mM NaOH; 8-25 min, linear gradient elution from 10 mM to 60 mM NaOH; 25-38 min, column cleaning step with 180 mM NaOH; and 38-56 min, column re-equilibration step with 10 mM NaOH. Detailed descriptions of eluent preparation, peak detection and calibrations of HPAEC-PAD have been presented elsewhere (Engling et al., 2006; Sullivan et al., 2008). Calibrations were based on serial dilutions from a stock solution made by dissolving individual compounds in solid form (purchased from Sigma-Aldrich) with Milli-Q water. The LOD for the various carbohydrates was estimated at 6 ng m^{-3} and the overall measurement uncertainty for levoglucosan was 21%. Previous studies have found that the peaks of levoglucosan and arabitol, a sugar alcohol from fungal spores, cannot be fully separated by a CarboPac PA-1 column [*Caseiro et al*., 2007; *Sullivan et al*., 2008],

as a result the integrated peak area of levoglucosan was corrected for this interference by arabitol. Ambient mannitol and arabitol concentrations correlate well and a ratio of 1.5 between the two has been obtained in PM_{10} samples (Bauer et al., 2008). Since mannitol can be quantitatively measured with the CarboPac PA-1 column, the arabitol concentration was determined by dividing mannitol by 1.5. The peak area of arabitol was then calculated and subtracted from the levoglucosan peak area. This correction adds uncertainty to the measured levoglucosan concentration, as using a uniform conversion factor from mannitol to arabitol assumes a same mannitol/arabotol ratio for $PM_{2.5}$ samples and does not necessarily reflect the varied ratio as a function of physical environments (i.e. temperature), aerosol sources, etc. This uncertainty is larger in summer (can be on order of 25%) when levoglucosan concentrations are typically low than in winter when levoglucosan is most abundant (on order of 3%) (Figure 2.2).

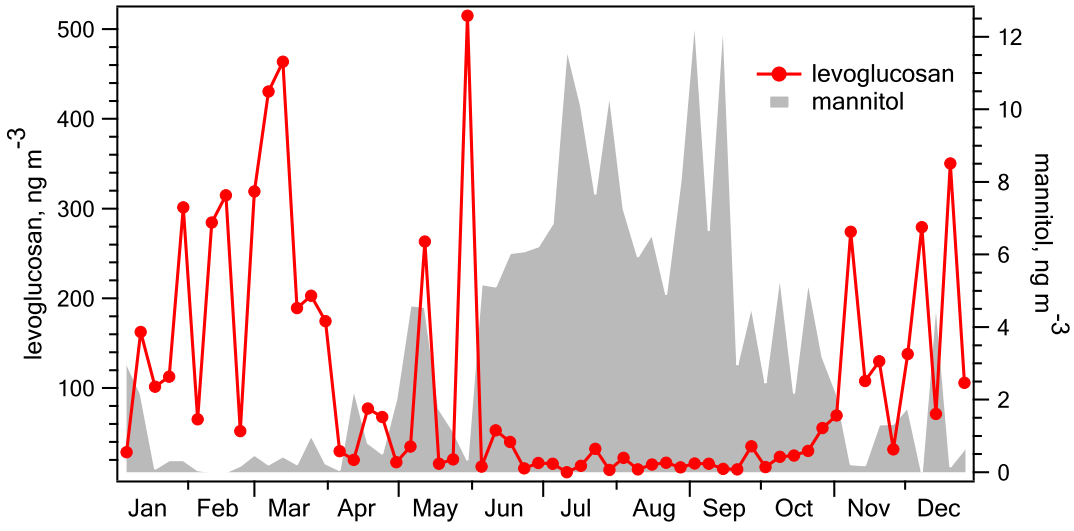

Figure 2.2 Mean concentrations of levoglucosan and mannitol for all the sites in 2007.

To validate the HPAEC-PAD method, levoglucosan concentrations were determined via independent GC-MS measurements [*Zheng et al*., 2006] from a series of quartz fiber filters (N=33) collected from May. 2004 to Apr. 2005. A portion of the same filters was extracted in water and levoglucosan was measured by HPAEC-PAD following the method described above. The two datasets showed good agreement, with a linear regression r^2 of 0.92, and a zero intercept regression slope of 1.09±0.04 (± one STD). No significant underestimation by the HPAEC-PAD method due to arabitol correction was found. On average levoglucosan concentrations determined by HPAEC-PAD for the summertime filters were 14% lower than those determined by GC-MS.

Water-soluble anions (chloride, nitrate, sulfate and oxalate) and cations (sodium, ammonium, potassium, magnesium and calcium) were quantified on a dual channel Dionex DX-500 Ion Chromatograph with suppression and conductivity detection, employing a Dionex AS11-HC anion column and Dionex CS12A cation column. Calibrations were based on NIST traceable liquid standards. Measurement uncertainties were 40% for Na^+, 28% for NH_4^+, 63% for Mg^{2+}, 17% for K^+, 7% for SO_4^{2-} and 36% for oxalate. Ca^{2+} uncertainty was 755%, which was subsequently found to be due to a contaminated DI water supply. Thus, Ca^{2+} results are not reported. Instead, Mg^{2+} is used as a mineral dust indicator in the following analysis. LODs for the ions were in the range of 0.01 (K^+) to 0.1 (SO_4^{2-}) μg m^{-3}.

The UV-Vis light absorption spectra for the liquid extracts were determined with a 1-m path-length Liquid Waveguide Capillary Cell (LWCC-2100, World Precision Instrument, Sarasota, FL) to investigate the link between brown carbon and biomass burning. *Hecobian et al*. [2010] provides a detailed description of the method and results

investigating brown carbon sources, based in part on the FRM filters used in this work. Briefly, the method involved injecting 1 mL of FRM-filter extract through the LWCC via a syringe pump (Klohn, LTD; Las Vegas, NV). The absorption spectra between wavelengths of nominally 200 and 800 nm was saved 30 seconds after the sample entered the LWCC. After each measurement, the LWCC was flushed thoroughly with 1 mL of 0.6 N HCl and 3 mL of Milli-Q DI water, and the baseline was re-zeroed with reference to 18-MΩ Milli-Q water. The absorption was determined using the ratio of transmitted to incident light intensity following Beer's Law, such that the absorption is linear with the absorbers concentration and mass absorptivity, and LWCC path length (~1 m). We used the product of all three since in our samples the mass absorptivities were unknown. In this study, the average absorption between wavelengths 360 and 370 nm (b_{ap365}, in units of m^{-1}, see Equation 1 and 2 in *Hecobian et al*. [2010]) was used as a measure of brown carbon.

$PM_{2.5}$ mass concentrations were determined gravimetrically by each of the three state regulatory agencies following their protocols. It is important to note that FRM Teflon filters are not designed for $PM_{2.5}$ composition measurements. Although Teflon filters are known to be relatively inert to gas absorption, the un-denuded sampling method may contribute to positive artifacts. Furthermore, this sampling method and the yearlong storage of the Teflon filters may also lead to loss of semi-volatile components [*Watson et al*., 2009]. Effort has been made to estimate these semi-volatile components retained on FRM Teflon filters [*Frank*, 2006]. In this paper, known semi-volatile species such as nitrate are not discussed, and the reported WSOC and other components (including FRM $PM_{2.5}$ mass) should be viewed as a measure of the more non-volatile

species associated with ambient $PM_{2.5}$.

To assess the quality of the FRM filter data, the results were compared to a number of components, i.e. $PM_{2.5}$ mass, NH_4^+, K^+, and SO_4^{2-}, from seven co-located EPA Speciation sites (South Dekalb, Rome, Macon, AUG-BRS, COL-CRS, ATNS-UGA and N'BHM; see Table 2.1), where the chemical analyses were done through Research Triangle Institute on nylon filters and were completely independent of the FRM data. The results are shown in Figure 2.3. All components show good agreement between the two types of filters, with linear regression slopes from 0.88 to 1.15. It is noteworthy that the Speciation NH_4^+ concentrations were on average 15% higher than the FRM NH_4^+ concentrations (a slope of 1.15), reflecting possible loss of semi-volatile NH_4^+ associated with NO_3^- from the FRM filters.

2.2.3 MODIS fire counts

Fire counts detected by remote sensing have been used to examine seasonal biomass burning emissions [*Eva and Lambin*, 1998; *Duncan et al*., 2003; *Zeng et al*., 2008]. In this work, MODIS fire count data from the NASA Aqua satellite [*Giglio et al*., 2003] were used as a measure of outdoor biomass burning over the southeast in 2007. The data set had a horizontal resolution of 1 km × 1 km, and a time resolution of 1 day. The sum of fire counts in each month was used to investigate monthly and seasonal variations. Fire counts for seven states were used, including the three states in which our sampling sites were located and four other surrounding states to ensure that all possible biomass burning source regions were considered. An analysis of fires over continental United States indicated no evidence for long-range transport of smoke to the sites during

2007; however, episodic influence from longer-range transport of smoke cannot be ruled out.

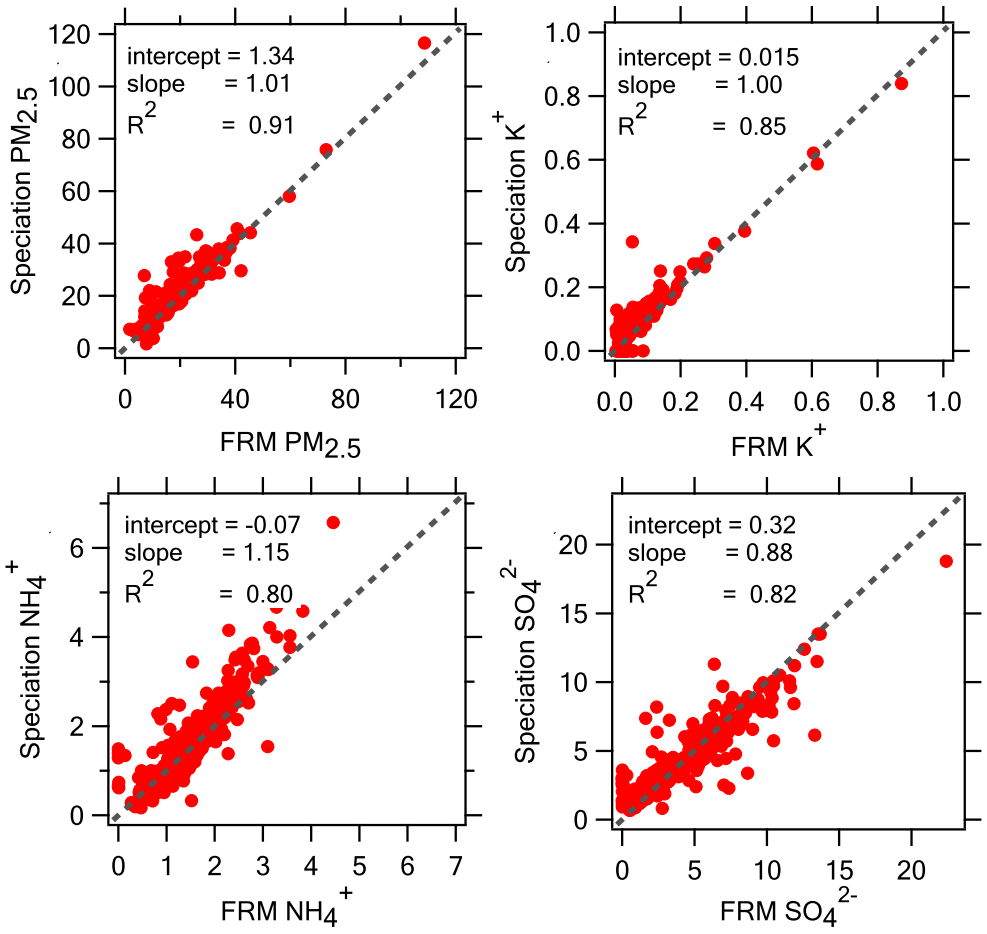

Figure 2.3 Intercomparison of $PM_{2.5}$ mass, K^+, NH_4^+, SO_4^{2-} concentrations (in µg m^{-3}) between seven co-located EPA FRM and Speciation sites. FRM K^+, NH_4^+ and SO_4^{2-} are from the methods used in the analysis of all sites presented in this study. In all cases N=420.

2.2.4 Positive Matrix Factorization (PMF) source apportionment

A PMF analysis on the chemical and physical data was used to quantify contributions from biomass burning and other sources to the FRM $PM_{2.5}$ mass

concentrations. Detailed information on EPA-PMF (v3.0) can be found on U.S. EPA website (http://www.epa.gov/heasd/products/pmf/pmf.html). Two datasets, (i.e. a concentration/physical property dataset and an uncertainty dataset) are required for PMF input. PMF is able to identify underlying covariance among chemical or physical parameters. While most previous PMF source apportionment studies use concentrations of chemical species as objects for analysis, in this work, along with chemical species (WSOC, Na^+, NH_4^+, K^+, Mg^{2+}, SO_4^{2-}, oxalate, xylose, and levoglucosan), the UV-Vis light absorption data at 365nm (b_{ap365}) from the FRM filter water-extract were also incorporated, as light absorption is an important aerosol property dependent on source and composition of the aerosols [*Andreae and Gelencser*, 2006]. Data from the 15 sampling sites on each sampling date were merged to form the concentration dataset. Considering potentially different source types for urban and rural sites, PMF analysis was also performed separately using two datasets from urban and rural sites, and the results, i.e. source composition profiles and contributions, showed little difference from those discussed in Sect. 2.3.3. Missing values for each component were replaced with the mean concentration of this component, and values below the LOD were replaced with half of the detection limit of the corresponding component [*Polissar et al*., 1998], ensuring that all values were positive. The uncertainty for each component was determined based on the methods discussed in Sect. 2.2.2. For missing data points and values below the LOD, the uncertainties were assigned as 4 and 5/6 times the concentration values, respectively [*Polissar et al*., 1998]. Numerous PMF runs were performed with 3-7 factors and various combinations of the concentration and absorption data set. Based on Q values (the objective function to be minimized) and physical interpretation of the solution, four

factors appeared to be the optimal solution. The model output files include factor profiles, relative factor contributions and residuals (unexplained fractions).

In order to quantify the contribution to $PM_{2.5}$ mass from each factor-related source, multivariate linear regression (MLR) analysis was performed to scale relative factor contributions to the measured total $PM_{2.5}$ mass. Light absorption data were not included in the regression analysis since it is not a mass concentration measurement.

2.3 Results and discussion

2.3.1 Spatiotemporal variations of levoglucosan and water-soluble potassium (K^+)

The 12 months of 2007 were separated into four seasons as: January, February and December (winter); March, April and May (spring); June, July and August (summer); September, October and November (fall). Table 2.2 presents the annual and seasonal mean concentrations of levoglucosan and K^+, together with those of $PM_{2.5}$ mass, water-soluble organic carbon (WSOC), ammonium (NH_4^+), sulfate (SO_4^{2-}), oxalate and xylose. Figure 2.4 shows the seasonal mean concentrations of levoglucosan and K^+ at each site.

Table 2.2 Annual and seasonal mean concentrations (± STD) of measured $PM_{2.5}$ components from FRM filters.

Component	Unit	Annual	Winter	Spring	Summer	Fall
$PM_{2.5}$	$\mu g\ m^{-3}$	15.56 ± 8.67	11.68 ± 6.25	17.33 ± 11.19	19.17 ± 7.87	13.61± 5.74
WSOC	$\mu gC\ m^{-3}$	2.07 ± 1.53	1.45 ± 1.01	2.47 ± 2.22	2.58 ± 1.21	1.70 ± 0.83
NH_4^+	$\mu g\ m^{-3}$	1.40 ± 0.71	1.06 ± 0.61	1.39 ± 0.63	1.78 ± 0.79	1.36 ± 0.63
K^+	$ng\ m^{-3}$	53.7 ± 104.1	45.0 ± 32.1	55.6 ± 51.8	70.8 ± 194.8	42.9 ± 46.2
SO_4^{2-}	$\mu g\ m^{-3}$	4.43 ± 2.99	2.60 ± 1.90	4.24 ± 2.40	6.41 ± 3.68	4.38 ± 2.46
Oxalate	$ng\ m^{-3}$	136.0 ± 91.3	82.6 ± 57.2	172.4 ± 110.5	173.2 ± 85.6	108.3 ± 59.5
Levoglucosan	$ng\ m^{-3}$	107.5 ± 221.9	169.9 ± 180.3	180.3 ± 339.2	18.7 ± 44.7	55.7 ± 134.7
Xylose	$ng\ m^{-3}$	1.23 ± 2.44	1.71 ± 2.12	1.99 ± 3.84	0.52 ± 0.78	0.68 ± 1.31

2.3.1.1 Levoglucosan

In general, levoglucosan concentrations obtained in this study were comparable with those in previous studies in the same region [*Zheng et al*., 2007; *Ding et al*., 2008], but were considerably higher than those at other locations in the U.S., such as Pittsburgh, PA (annual mean at ~21 ng m^{-3}) [*Robinson et al*., 2006], suggesting much larger impact from biomass burning in the southeast. The annual mean concentration of levoglucosan for all sampling sites was 107.5 ng m^{-3} (Table 2.2). Clear seasonal variations of levoglucosan concentrations were observed, with significantly higher concentrations in spring and winter and minimum levels in summer. Mean concentrations for spring and winter were 180 ng m^{-3} and 170 ng m^{-3}, respectively; whereas the mean summer concentration was only 19 ng m^{-3}, which is within the range of levels (5 to 52 ng m^{-3}) reported by *Puxbaum et al*. [2007] at six background stations in Europe. Significantly enhanced levoglucan concentrations at several sites were detected for several days in spring. For instance, 2,950 ng m^{-3} of levoglcusoan was recorded at the Macon site on May 12, almost 2 orders of magnitude higher than the level observed six days before (31 ng m^{-3}). Similarly, on May 30, levoglucosan concentrations at COL-CRS, N'BHM, Wylam, Ashland and Providence all exceeded 1,000 ng m^{-3}, much higher than those at other sites on the same day (3.93-346 ng m^{-3}). Such unusual levoglucosan concentrations at these sites were due to significant but sporadic impacts from unique wildfire events in spring of 2007. Extensive wildfires started in the Okefenokee Swamp in southern Georgia/northern Florida in April and spread across Georgia and adjacent states during the following two months [*Yan et al*., 2010].

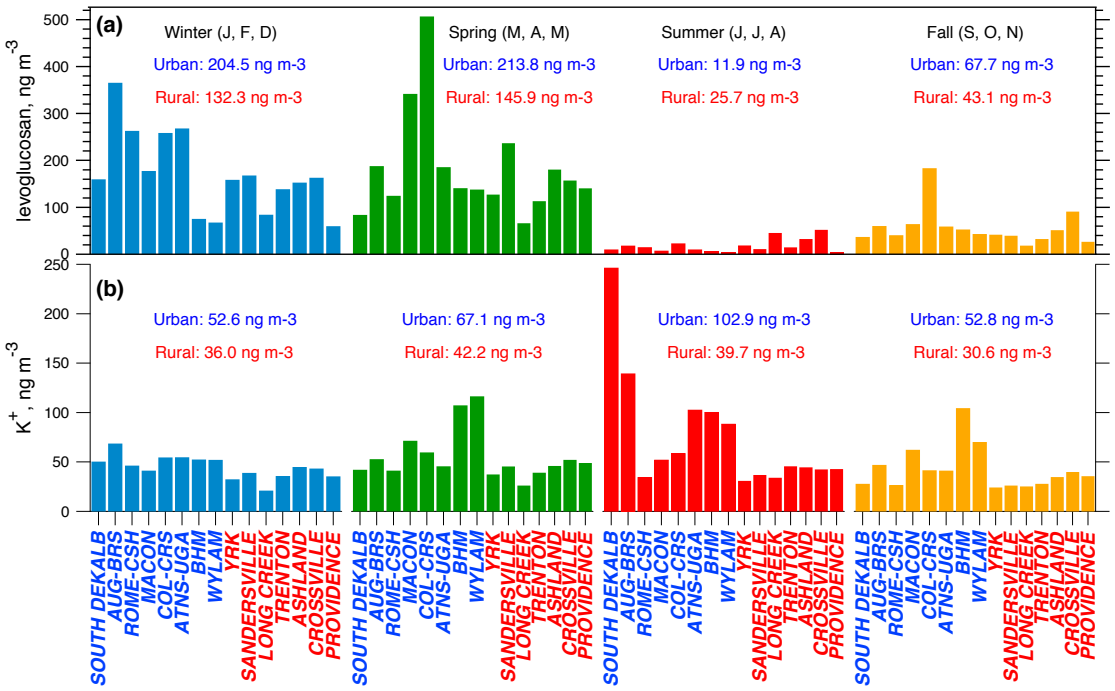

Figure 2.4 Seasonal (Winter, Spring, Summer, Fall) variations of levoglucosan (a) and K^+ (b) concentrations at each site during 2007. Site names in blue and red are urban and rural sites, respectively. The mean concentrations of levoglucosan and K^+ by urban/rural segregation for each season are given in the plots.

Figure 2.4a also shows the spatial distributions of levoglucosan for different seasons. In general, there were significant site-to-site variations, suggesting varied impacts from biomass burning emissions among the sampling sites. Winter and spring showed the largest variations in terms of absolute concentrations. In spring, variability was largely due to the sporadic impacts from wildfire events at different sites. In winter, biomass burning was likely mainly in the form of residential wood burning (discussed in more detail below), thus spatial variability at these time periods likely reflect population densities and frequency of burning in different regions. Levoglucosan concentrations in urban sites were generally higher than those in rural sites, except during summer when

rural sites tended to have slightly higher levoglucosan concentrations, implying that residential wood burning in urban areas is an important source of levoglucosan when other forms of biomass burning, such as wildfires, are absent. High spatial variability was observed for levoglucosan during all seasons, as indicated by the large relative standard deviations (RSD, standard deviations of concentrations in each season divided by the corresponding seasonal mean concentration) (51-79%).

2.3.1.2 Water-soluble Potassium (K^+)

Compared to levoglucosan, K^+ concentrations exhibited different spatiotemporal variability. First, K^+ had an opposite seasonal pattern to levoglucosan with much less seasonal variability (from 45 ng m^{-3} in winter to 71 ng m^{-3} in summer, Table 2.2). Smaller site-to-site concentration differences suggested by the lower RSD values (25-75%) for all four seasons indicate more uniform K^+ concentrations compared to levoglucosan. The significantly higher levels of K^+ at South Dekalb and AUG-BRS sites during summer (Figure 2.4b) were due to K^+ spikes detected at these two sites on July 5, likely reflecting pyrotechnique (fireworks) emissions. Excluding these data, RSD value in summer (75%) would be much smaller, and K^+ concentrations would be even more uniform (The July 5 sampling day was excluded from all further analysis). Similar to levoglucosan, K^+ tended to have slightly higher concentrations at urban sites (Figure 2.4b).

A comparison of 24-hr averaged levoglucosan and K^+ shows different degrees of correlation in winter and summer (Figure 2.5). In winter, when biomass burning was expected to be more prevalent, levoglucosan and K^+ were reasonably correlated (r^2=0.59), suggesting their common emission sources. In summer, however, there was

almost no correlation between levoglucosan and K^+ (r^2=0.02), reflecting distinctly different behaviours of these two tracers when biomass-burning emissions are expected to be significantly lower. Higher relative uncertainty in summertime levoglucosan concentrations due to the scaling of arabitol to mannitol (Sect. 2.2.2) may have also contributed to the poor correlation.

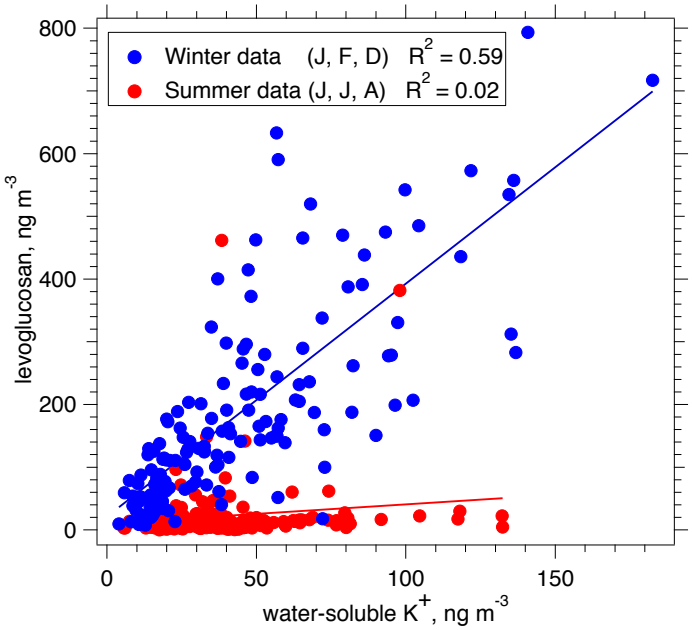

Figure 2.5 Relationship between levoglucosan and water-soluble K^+ concentrations in winter (January, February and December) and summer (June, July and August). Data on July 5 2007 were not plotted and excluded from the regression calculation due to abnormally elevated levels of K^+ associated with 4th of July fireworks.

2.3.2 Relationships between K^+, levoglucosan and MODIS fire counts

MODIS fire count data can be used as a measure of wildfire and prescribed burning events, two of the major forms of biomass burning over the southeast [*Zeng et al.*, 2008]. Other forms of biomass burning such as residential wood burning cannot be detected by remote sensing and thus are not reflected in the fire counts. Since our

sampling dates are evenly distributed in each month, the monthly fire counts over the region encompassing our sampling sites should reflect the outdoor biomass burning impacts on the measured $PM_{2.5}$ mass and composition.

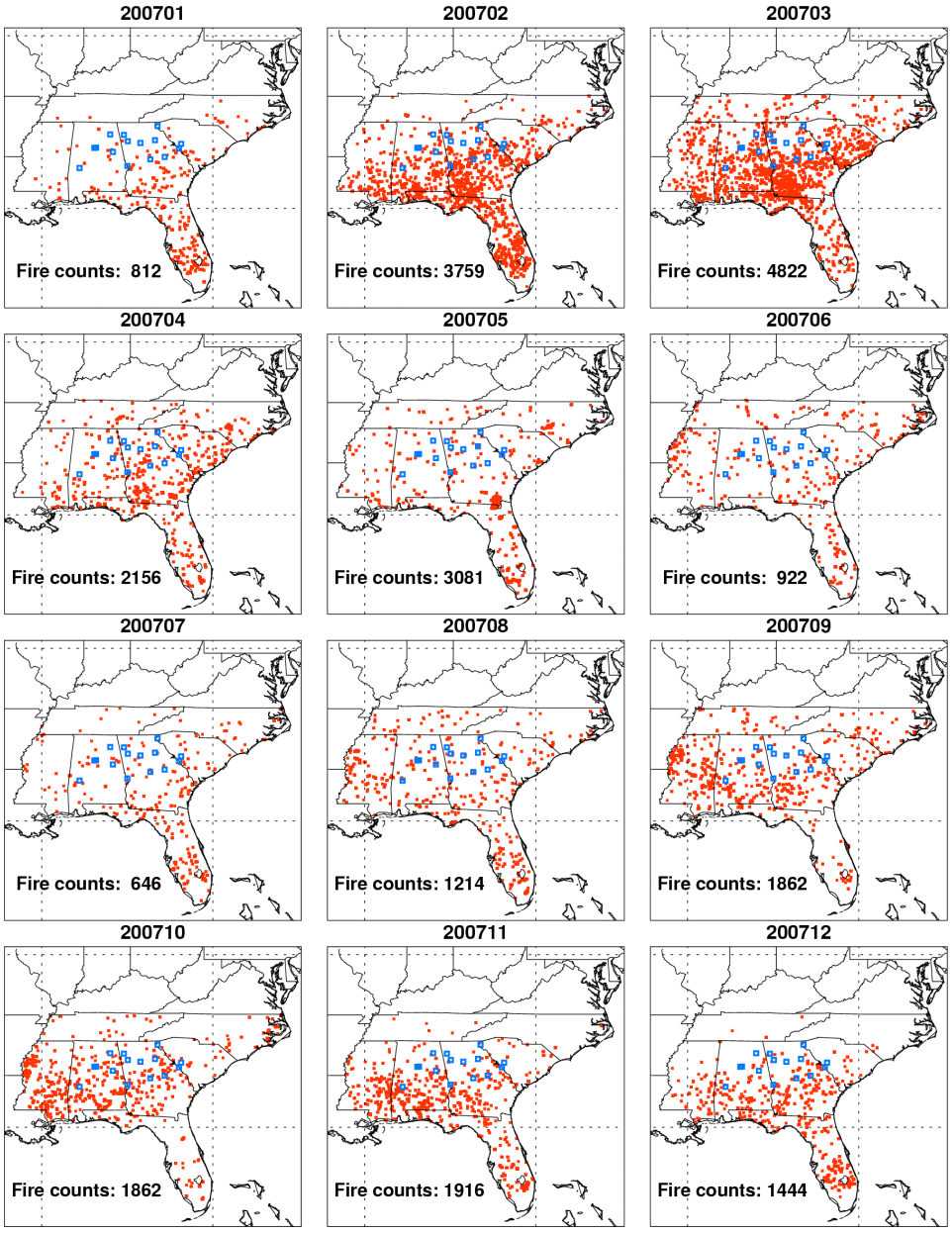

Figure 2.6 Monthly MODIS Aqua fire counts (red points) in 2007 over seven states in the southeastern U.S.. FRM sampling sites are shown as blue square symbols.

In 2007 there was a distinct seasonal variation of fire counts, with maximum in spring (counts ranging from 2156 to 4822) and minimum in summer (646-1214) (Figure 2.6), indicating extensive outdoor biomass burning events in spring, and fewer such events in summer. The highly concentrated fire points in May along Georgia-Florida boarder (Figure 2.6) were identified as the Okefenokee Swamp fires discussed above.

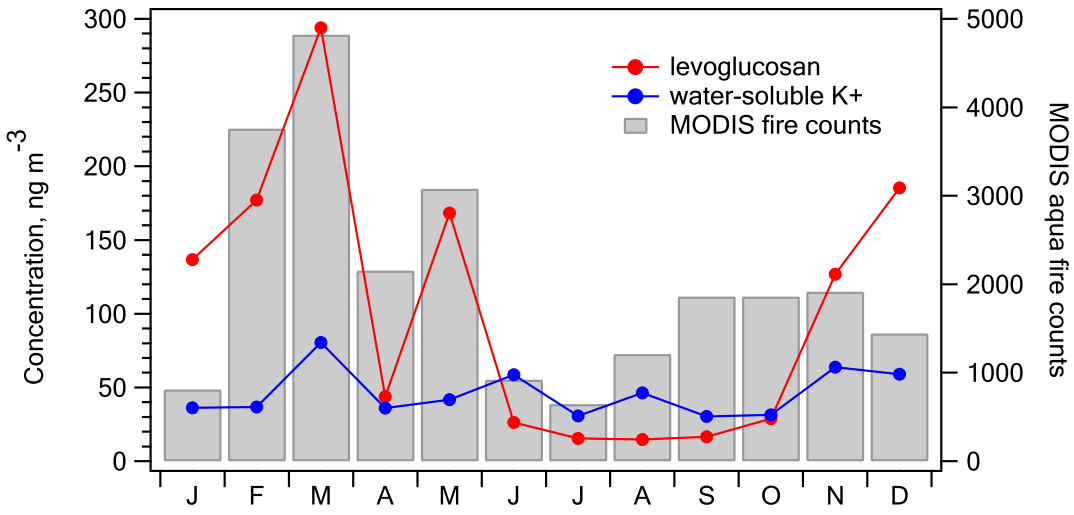

Figure 2.7 Monthly mean levoglucosan and water-soluble potassium concentrations from all sites compared with monthly mean MODIS Aqua fire counts from seven states in the southeastern US.

The relationships between monthly fire counts and monthly mean concentrations of levoglucosan and K^+ are shown in Figures 2.7 and 2.8. Monthly fire counts tracked levoglucosan concentrations well. For example, fire counts dropped from a March peak of 4822 by a factor of 8 to 646 in July, corresponding to levoglucosan concentrations changing from 294 ng m^{-3} to 15 ng m^{-3}, a factor of 9 decrease. The exceptions in January and December (Figure 2.7) when levoglucosan appeared to deviate from fire counts were

likely due to residential wood burning as a source of levoglucosan being prevalent in these two months, yet could not be detected as fire counts by satellite [*Tian et al*., 2009]. Levoglucosan and K^+ concentrations are also shown as a function of fire counts in Figure 2.8. For the levoglucosan and fire counts correlation, r^2 was 0.54; excluding January and December, r^2 was 0.86. K^+ concentrations showed poor correlation with fire counts throughout the year (r^2=0.16, and 0 excluding January and December in Figure 2.8). Since residential burning is minimal in summer, while fire count data also showed a large decrease in outdoor burning during summer, biomass burning emissions in summer was expected to be significantly lower than the cooler seasons. Levoglucosan had a similar trend as fire counts, whereas K^+ did not. The scatters at the lower concentrations in summer months may be due to some fraction of levoglucosan being lost through oxidation [*Hennigan et al*., 2010], as well as the larger measurement uncertainty of levoglucosan in summer (Sect. 2.2.2). The difference in levoglucosan concentrations in January and December when fire counts were low (Figure 2.8) suggests residential wood burning throughout the southeastern U.S., on average, contributed roughly 135 ng m^{-3} to 145 ng m^{-3} of levoglucosan during these two months. This corresponds to approximately 2.6 μg m^{-3} of $PM_{2.5}$ mass (based on an average emission factor determined in Sect. 2.3.3.3).

The distinct seasonal trends of levoglucosan and K^+, with only the former tracking fire counts well, appear to be evidence that levoglucosan is a better tracer of biomass burning (including wildfire and prescribed burning) than K^+. Although poor correlation between levoglucosan and K^+ may also be due to highly variable emissions, which as shown in laboratory studies depend on burning conditions and types of material

burned [*Sullivan et al*., 2008], this alone cannot explain the distinct temporal trends of K^+ and levoglucosan. The lack of correlation between fire counts and K^+ clearly points to additional significant sources of K^+ other than biomass burning, such as soil dust, sea salt, vegetation and meat cooking [*Lawson and Winchester*, 1979; *Morales et al*., 1996; *Schauer et al*., 1999], which at time can limit its use as a unique indicator of biomass burning emissions.

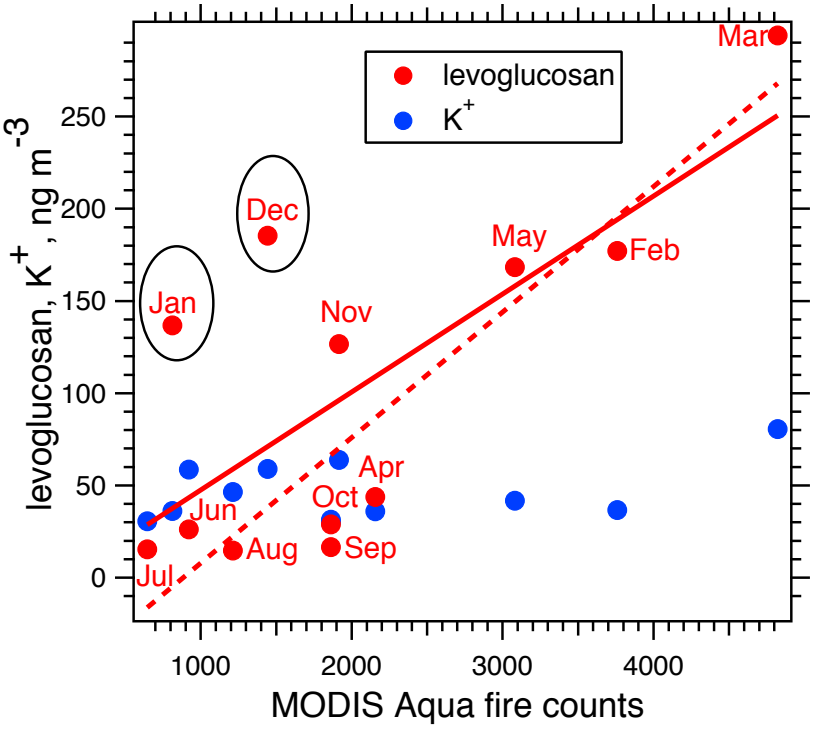

Figure 2.8 Correlations of monthly mean concentrations of levoglucosan and K^+ versus fire counts. The red solid line is the fit of levoglucosan-fire counts correlation (r^2=0.54). The red dashed line is the fit without January and December (r^2=0.86).

A receptor modelling study was conducted to comprehensively understand the sources of $PM_{2.5}$ in the southeast and was also used to further assess the performances of these two biomass burning tracers.

2.3.3 Source apportionment of $PM_{2.5}$ using PMF

2.3.3.1 Source profiles and relative contributions

Composition profiles for the 4 factors resolved by PMF are shown in Figure 2.9 (left panel). Values in the composition profiles represent average fractions (in percent) of those species distributed amongst the four factors. Relative contributions of the four factors obtained from the PMF output were averaged among all sampling sites for each sampling date, shown on the right panel, to illustrate their temporal variation throughout the year.

Factor 1 is characterized by high levels of levoglucosan (i.e. 77% of levoglucosan is in factor 1), xylose (50%), and UV-Vis light absorption (b_{ap365}) (55%). Also associated with this factor are K^+ (16%), WSOC (14%), oxalate (11%), and NH_4^+ (7%). Factor 1 composition profile is consistent with biomass burning emissions. Levoglucosan is the dominant component and almost exclusively associated with this factor, consistent with it being a unique biomass burning tracer [*Simoneit et al*., 1999; *Schkolnik and Rudich*, 2006]. Xylose is also a carbohydrate emitted in biomass burning [*Simoneit*, 2002]. Consistent with the discussions in Sect. 2.3.1–2.3.2, PMF analysis indicates that K^+ is not a unique biomass-burning tracer, while it is more associated with other factors, mostly factor 2 (43%), as shown below. Biomass burning emissions also produce significant levels of brown carbon [*Andreae and Gelencser*, 2006; *Hecobian et al*., 2010], which explains the presence of light absorption (b_{ap365}) in this factor. Oxalate has also been found in biomass burning smoke [*Kundu et al*., 2009]. The appreciable amount of WSOC associated with this factor is consistent with previous studies suggesting biomass burning and secondary organic aerosol (SOA) formation are the two major sources of WSOC

[*Fuzzi et al*., 2006; *Sullivan et al*., 2006; *Weber et al*., 2007; *Saarikoski et al*., 2008]. The seasonal pattern of factor 1 shows that averaged over the southeast, biomass burning is most prevalent in the cold months compared to its little impact in summer, with wildfire events in the springtime in South Georgia.

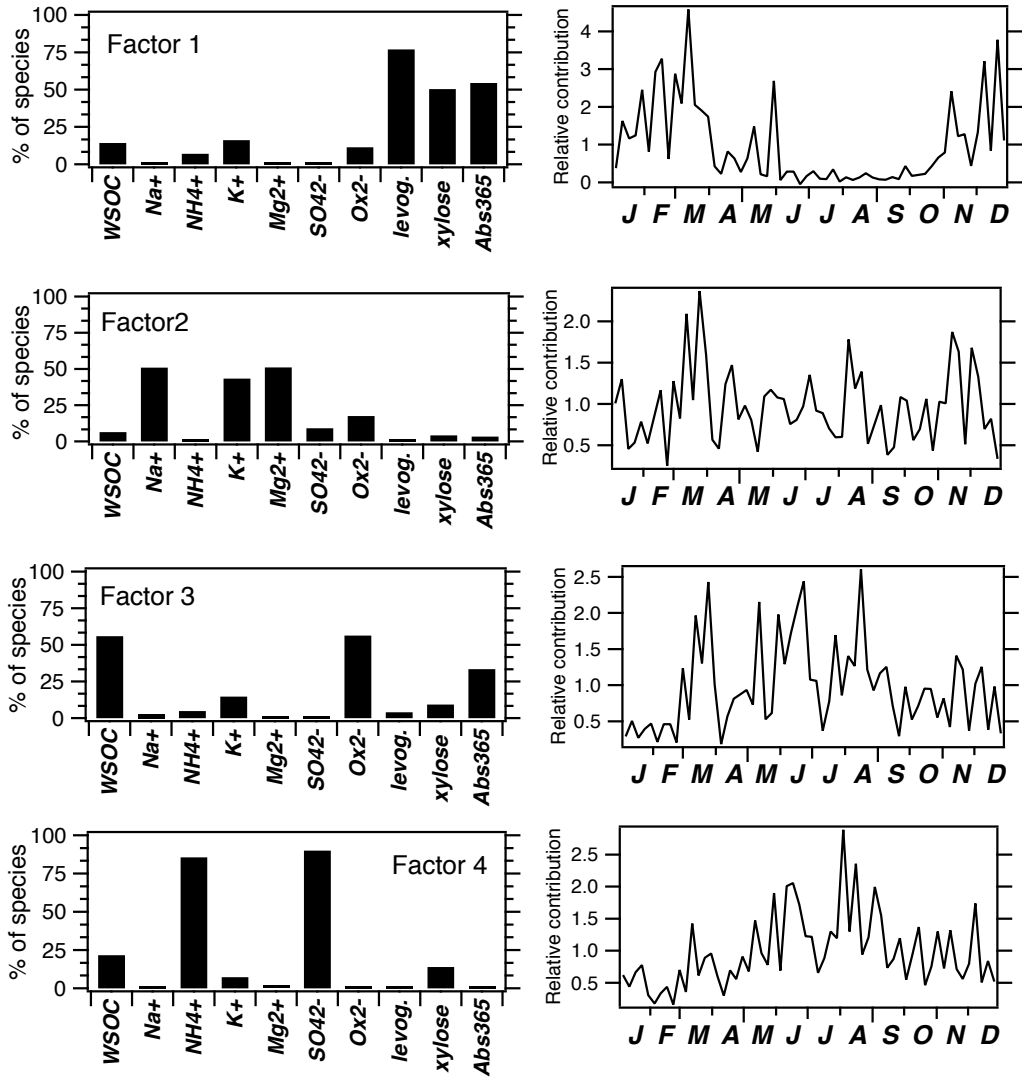

Figure 2.9 Composition profiles (% of total of each species) for the four factors resolved by PMF based on data from the whole year (2007) at all sites (left panel), and the time series of relative contribution of each factor (right panel).

Factor 2 is characterized by refractory material: Na^+ (51%), K^+ (43%), and Mg^{2+} (51%), indicating $PM_{2.5}$ from mineral dust [e.g., *Lee et al*., 1999]. These refractory materials are likely related to coarse-mode particles, windy conditions and possibly long-range transport. The factor 2 time series has no clear seasonal pattern.

Factors 3 and 4 are thought to be linked to secondary aerosol formation. Factor 3 has the highest percentages of WSOC (56%) and oxalate (56%), along with light-absorbing species (i.e. brown carbon) (34%), and K^+ (15%). Factor 4 is distinguished by NH_4^+ (86%) and SO_4^{2-} (90%), as well as a considerable amount of WSOC (22%), but little oxalate and little light-absorbing species. In this factor, the molar ratio of NH_4^+ to SO_4^{2-} is 1.6, indicating that for much of the southeast sulfate is not fully neutralized, as noted in other studies [*Lee et al*., 2008] (Note, any NH_4^+ associated with nitrate is not considered). Both factors are correlated with temperature (r^2=0.62 for F3 and r^2=0.81 for F4), and the high levels of WSOC in both factors and the abundant sulfate in factor 4 are attributed to secondary aerosol formation processes that are known to be prevalent during summer [*Lim and Turpin*, 2002; *Kondo et al*., 2007; *Weber et al*., 2007; *Miyazaki et al*., 2009]. The differences between factors 3 and 4 and the linking of WSOC, oxalate and light absorbing organics (brown carbon) suggest insights into secondary organic aerosol formation, which is investigated further in Chapter 3.

2.3.3.2 Contributions of factors to yearly $PM_{2.5}$ mass, levoglucosan, K^+ and WSOC

Using multivariate linear regression (MLR), the four factors isolated by PMF, along with the residual, can be used to estimate source contributions (percent of total mass and concentrations in μg m^{-3}) to overall $PM_{2.5}$ mass and various $PM_{2.5}$ components.

Results are summarized in Table 2.3 and Figures 2.10 and 2.11.

Table 2.3 Seasonal and annual source contributions of each PMF factor to $PM_{2.5}$ mass (% of $PM_{2.5}$ mass).

	Winter	Spring	Summer	Fall	Annual
Biomass Burning (F1)	27	15	2	7	13
Refractory (F2)	7	6	6	6	6
Secondary Light Abs WSOC (F3)	16	27	31	26	25
Secondary Sulfate/WSOC (F4)	30	32	46	44	38
Residual	20	20	16	16	18

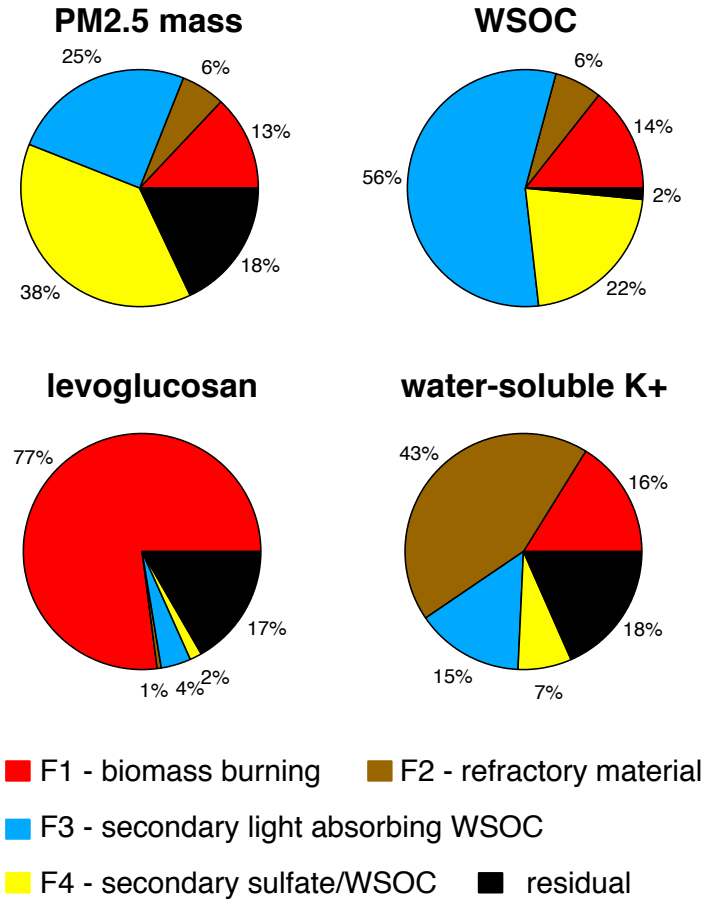

Figure 2.10 PMF results showing annually averaged source contributions to $PM_{2.5}$ mass, WSOC, levoglucosan, and water-soluble K^+.

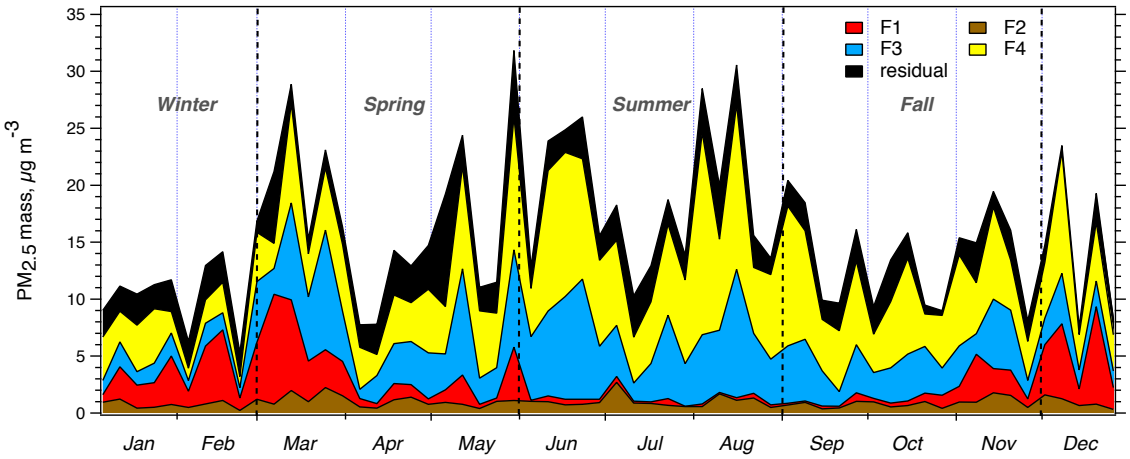

Figure 2.11 Time series of $PM_{2.5}$ composition by four factors resolved by PMF and masses predicted by multivariant linear regression (MLR).

Annually, the four factors resolved by PMF explained 82% of the total $PM_{2.5}$ mass (Figure 2.10). The largest contribution (38%) was from factor 4 (secondary sulfate/WSOC), followed by 25% from factor 3 (secondary light absorbing WSOC), and 13% from factor 1 (biomass burning). The 18% of the total $PM_{2.5}$ mass from residual likely reflects contributions from sources related to unmeasured species contributing to $PM_{2.5}$ mass, such as elemental carbon (EC) and water-insoluble organic species, which can be associated with primary emissions from both biomass burning and fossil fuel combustion. At the seven co-located EPA Speciation sites (see Sect. 2.2.2, all located at urban areas), measurements were made of organic and elemental carbon by Thermal Optical Reflectance (TOR) and Transmittance (TOT) and several elements by Energy Dispersive X-Ray Fluorescence (EDXRF). Incorporating OC, EC, Ca, Cu and Fe data along with the FRM chemical species/light absorption data that were measured at these seven sites, a PMF analysis on this dataset resolved 5 factors (Figure 2.12). A mobile source emission factor characterized by abundant EC (70%) and Cu (57%) was

identified, contributing 8% of the $PM_{2.5}$ mass on an annual basis. Meanwhile, the residual fraction dropped from 18% to 7%. The other 4 factors were very similar to the PMF analysis based on just the FRM data shown in Figures 2.9, 2.10 and 2.11.

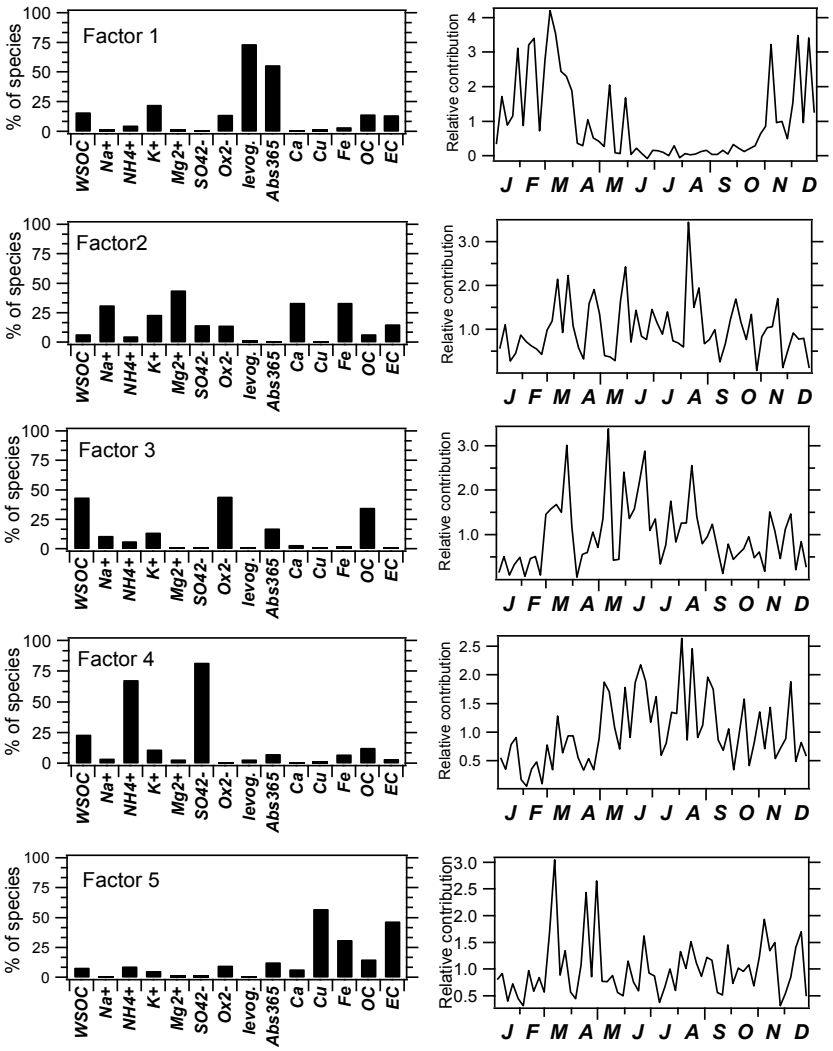

Figure 2.12 Composition profiles (% of total of each species) for the five factors resolved by PMF based on FRM and Speciation datasets for the whole year (2007) at 7 EPA (urban) FRM/Speciation sites (left panel), and the time series of relative contribution of each factor (right panel). Factors 1 through 4 are similar to those in Figure 2.9. Factor 5 has characteristics of a mobile source emission profile.

Relative contributions of various sources (factors) to WSOC, levoglucosan, and K^+ are also shown in Figure 2.10. On an annual basis, most of the WSOC is associated with secondary light absorbing WSOC source (56%), followed by secondary sulfate/WSOC (22%) and biomass burning (14%). For levoglucosan, the dominant source is the biomass-burning factor (77%). In contrast, K^+ has several sources, with refractory material (43%) being the largest, and each of the other three sources contributing from 7 to 16%.

Table 2.3 shows the separated fractional contributions of the factors to $PM_{2.5}$ mass by season. Although biomass burning only contributed 13% on an annual basis, it accounted for 27% of the $PM_{2.5}$ during winter and only 2% in summer, consistent with the PMF results that included Speciation data, in which case biomass burning contributed 29% and 1% in winter and summer, respectively (Table 2.4). Factors involving secondary aerosol formation processes (F3 and F4) show the opposite trend, contributing 46% in winter and 77% in summer. This rather large relative increase in summertime secondary sources corresponds to an average WSOC increase of roughly 1 $\mu gC\ m^{-3}$ from winter to summer (Table 2.2).

Table 2.4 Seasonal and annual source contributions of each PMF factor to $PM_{2.5}$ mass (% of $PM_{2.5}$ mass) based on FRM and Speciation datasets.

	Winter	Spring	Summer	Fall	Annual
Biomass Burning (F1)	29	15	1	8	13
Refractory (F2)	11	15	14	14	13
Secondary Light Abs WSOC (F3)	10	22	24	17	20
Secondary Sulfate/WSOC (F4)	29	34	47	45	39
Mobile source emission (F5)	9	9	7	9	8
Residual	12	5	7	7	7

Figure 2.11 is similar to the time series plot for each factor (Figure 2.9, right panel), but in this case the contributions in terms of estimated mass of each factor (source) throughout the year are given. While refractory material (F2) contributions remained consistently low (<7%), secondary sulfate/WSOC was the largest $PM_{2.5}$ contributor throughout the year (30-46%), partially due to the relatively large and uniform distribution of sulfate in this region [*Kim et al*., 2003a, b; *Liu et al*., 2005]. Biomass-burning sources (F1) dominated in winter and on average made little contribution to $PM_{2.5}$ mass in summer. The secondary light absorbing WSOC factor (F3) also shows enhancement in summer, but was higher relative to the other secondary factor (F4) in March during a period of unusually warm weather. The source of this factor is investigated further in Chapter 3.

2.3.3.3 Comparisons to other studies

Studies using a variety of techniques have investigated contributions of biomass burning to air quality in the southeast. These results are compared to the PMF analysis using the FRM filter data presented here. First, $PM_{2.5}$ mass to levoglucosan ratios from emission studies have been found to vary from 9.7±2.4 g/g for hardwoods to 24.4±4.3 g/g for softwoods [*Fine et al*., 2002], and 11.5 g/g for a prescribed burning episode in Georgia during April 2004 [*Lee et al*., 2005]. From PMF factor 1, the biomass burning factor, the annual $PM_{2.5}$ mass to levoglucosan ratio was 18.3±5.4 (± STD) g/g, roughly midway between hard and softwood emissions, but higher than emissions from prescribed burning. Emission studies have also characterized ratios of K^+ to levoglucosan, with median ratios in the range of (0.03-0.16) [*Fine et al*., 2001; 2002; 2004a; b; *Lee et*

al., 2005], depending on the type of material burnt. For factor 1 the K^+/levoglucosan ratio was 0.10, similar to the emission profiles. In contrast, for the FRM dataset the ratio is 0.50 in terms of annual mean and 0.26 for winter. These values are not in the range found in the studies mentioned above, likely due to other sources for K^+.

Our PMF-predicted annual mean contribution of 13% from biomass burning is comparable with previous PMF results using K^+ alone as the tracer. For example, *Kim et al*. [2003a, 2003b] estimated 14% in Atlanta, and *Liu et al*. [2005] estimated 13% for the southeastern U.S. However, different seasonal patterns were found in our study and those PMF studies using K^+. Our PMF results suggest significant biomass burning contribution in winter (27%), and a small impact (2%) in summer, consistent with a Chemical Mass Balance analysis based on Molecular Markers (CMB-MM) using levoglucosan as the biomass-burning tracer (0.4% in summer) [*Zheng et al*., 2007]. In contrast, previous PMF studies using K^+ predicted similar biomass-burning contributions for all the seasons [e.g., *Kim et al*., 2003a; *Liu et al*., 2005]. The discrepancy depends on the choice of biomass burning tracer used. During periods of significant biomass burning emissions, typically the colder months, levoglucosan and K^+ tend to be correlated (Figure 2.5) and the predicted biomass burning impacts are similar, using either levoglucosan or K^+ as the tracer. During these periods the biomass-burning source for K^+ appears to dominate over other sources. However, due to the relatively higher contributions of non-biomass burning K^+ sources observed in summer, it is expected that a source apportionment analysis using K^+ alone as a tracer would overestimate biomass burning emission during those periods.

Alternatively, levoglucosan may be substantially depleted in the summer due to

photochemical oxidation reactions, leading to a large underestimation of summertime biomass-burning contribution [*Hennigan et al*., 2010; *Hoffmann et al*., 2010]. This, however, is not consistent with the low fire counts in summer. Considering such uncertainties and that the results from previous studies might overestimate biomass burning contribution in summer (>10%) due to non-biomass burning K^+ sources [e.g., *Kim et al*., 2003a; *Liu et al*., 2005], we conclude that biomass burning contribution in summer is likely in the range of 2-10%. In winter, levoglucosan is relatively stable and likely provides a reasonable estimate of biomass burning contributions to $PM_{2.5}$ levels. Based on a number of studies, including this work, typical winter contribution of biomass burning to $PM_{2.5}$ in the southeast (on a mass basis) is estimated to be near 25%, which in December and January appears to be mostly from residential wood-burning.

2.4 Conclusions

We investigate the biomass burning impact on $PM_{2.5}$ in the southeastern U.S. in 2007 through analysis of chemical and physical properties of over 900 24-h integrated FRM Teflon filters collected by state regulatory agencies.

Two commonly used biomass burning tracers, i.e. levoglucosan and K^+, were compared in conjunction with MODIS Aqua fire counts. Levoglucosan concentrations showed large seasonal variations and correlated well with fire counts, except in winter (January and December) when residential wood burning not detected by satellites led to increased levoglucosan. During these months, residential burning was estimated to contribute 2.6 μg m^{-3}, on average, to the ambient $PM_{2.5}$ mass throughout the region. K^+ concentrations exhibited no apparent seasonal trends and poor correlation with fire

counts. Levoglucosan and K^+ correlated well (r^2=0.59) in winter, suggesting their common origin from biomass burning when its emissions were relatively high. In other seasons, K^+ poorly correlated with levoglucosan apparently due to additional K^+ sources other than biomass burning. Both levoglucosan and K^+ concentrations were higher at urban sites than at rural sites, with levoglucosan showing larger spatial variations than K^+. Comparison of K^+ and levoglucosan measurements in conjunction with fire count data suggests that K^+ was not a good tracer for biomass burning emissions due to multiple sources in addition to biomass burning, whereas levoglucosan was a reasonable indicator of biomass burning emissions, including emissions from wildfires and prescribed burnings, as well as emissions from wood combustion for residential heating. Although chamber study results show that levoglucosan reacts with the hydroxyl radical at atmospherically relevant concentrations [*Hennigan et al*., 2010], the good correlation between fire counts and levoglucosan concentrations suggest that this was not a large effect. This may be due to little biomass burning occurring in summer when this effect would be most important due to enhanced photochemistry, whereas in winter and spring when biomass burning emissions were higher and from local sources (e.g., residential or prescribed burning along with the occasional wildfire), relatively fresh emissions and slow photochemistry minimize this effect.

Positive Matrix Factorization (PMF) was applied to analyze $PM_{2.5}$ sources from the FRM data. Four factors were resolved, including a biomass burning factor characterized by high levels of levoglucosan and light absorbing compounds (brown carbon), a refractory component characterized by K^+, Na^+ and Mg^{2+}, and two secondary aerosol components, one characterized by high WSOC, organic acids (oxalate) and light

absorbing compounds, and the other by high SO_4^{2-}, NH_4^+, and WSOC. Secondary sulfate/WSOC component was the largest source of $PM_{2.5}$ in all seasons and combined, the two secondary sources dominated in all seasons. The biomass burning source contributed 13% to the $PM_{2.5}$ mass annually, 27% in winter, and only approximately 2% in summer. The refractory component contributed the least and was consistent throughout the year. Overall, the results show that K^+ is a poor biomass burning tracer especially in summer and can lead to large over-prediction of biomass burning contributions by source apportionment analyses. Extensive photochemical degradation of levoglucosan may lead to under-prediction of biomass buring in summer; however, in this study there was reasonable consistency between levoglucosan concentrations and summertime outdoor burning quantified by remotely sensed fire count data.

CHAPTER 3

SPATIAL AND SEASONAL VARIATIONS OF WSOC OVER THE SOUTHEASTERN UNITED STATES

3.1 Background

A number of ambient studies have been carried out to understand secondary organic aerosol (SOA) formation over the Southeastern United States [*Lee et al*., 2010 and references therein]. Based on ratios of organic carbon to elemental carbon (OC/EC), *Lim and Turpin* [2002] found that secondary OC contributed approximately half of the measured OC in urban Atlanta, and the hourly contribution could occasionally range up to 88%. Using water-soluble organic carbon (WSOC) as a measure of SOA carbon during summer, *Weber et al*. [2007] and *Hennigan et al*. [2009] reported similar secondary OC fractions, and those fractions were consistently higher (~75%) in rural areas due to reduced contributions of primary OC [*Weber et al*., 2007]. *Zheng et al*. [2006] investigated the spatial distribution of carbonaceous aerosols in the southeast using molecular marker-based chemical mass balance (CMB-MM) modeling and found that the urban excess of OC was mainly from vehicle emissions and meat cooking based on results of the urban-rural pair in Alabama. *Blanchard et al*. [2011] also reported that most of the Atlanta urban excess OC was from motor vehicle emissions with a fossil carbon source based on analysis of SEARCH (Southeastern Aerosol Research and Characterization) filter data. *Gao et al*. [2006] analyzed polar organic components from 24-hour filter samples collected at four SEARCH sites in the summer of 2004 and found direct evidence for atmospheric processing of biogenic emissions (i.e. terpene oxidation)

as a source of HUmic-LIke Substances (HULIS). Also based on filter samples collected at these four sites in 2004-2005, *Ding et al*. [2008] examined the spatial and seasonal trends of biogenic SOA tracers and found significant correlations between 2-methyltetrols, an isoprene oxidation product, and WSOC. Radiocarbon (^{14}C) analysis on $PM_{2.5}$ WSOC collected in urban Atlanta in summer during periods of minimal biomass burning emissions showed that roughly 70 to 80 % of the carbon in WSOC was modern rather than fossil. This suggested that most WSOC mass was linked to biogenic VOCs, assuming the main source of WSOC was SOA formation [*Weber et al*., 2007]. *Schichtel et al*. [2007] estimated the average fraction of contemporary carbon was 92% in the summer and 81% in the winter of 2004 based on radiocarbon data from $PM_{2.5}$ total carbon (OC and EC) collected at the Great Smoky Mountains National Park in Tennessee. However, most of these studies were based on filter samples with low time resolution collected from a limited number of sites over relatively short time periods and all are susceptible to filter sampling artifacts.

The findings in this study add to these ambient results by investigating the spatial and seasonal variability of secondary aerosols over the southeastern U.S. based on measurements of WSOC, sulfate and other $PM_{2.5}$ chemical components extracted from 900 Federal Reference Method (FRM) filters collected at 15 sites throughout the year of 2007. These results demonstrate the potential of the large array of FRM filters collected by various regulatory agencies for investigating fine aerosol sources and properties of the non-volatile components. This chapter focuses on non-biomass burning contributions to $PM_{2.5}$; biomass-burning contributions based on this data set are discussed in Chapter 2. Additionally, one summer month of online WSOC and other gas and aerosol data with

high time resolution sampled at an urban/rural paired site in Georgia in 2008 provide a complement to the 24-hour integrated filter data and allow examination of SOA sources and formation on a much shorter time scale (diurnal) and with less susceptibility to sampling artifacts. The comparison of WSOC diurnal trends between urban and rural areas provides important insights on the roles of biogenic and anthropogenic emissions in SOA formation in the southeast.

3.2 Experimental methods

3.2.1 Filter sampling and measurements

The collection and chemical analyses of the filter samples from the fifteen EPA FRM and seven co-located EPA CSN sites (Figure 3.1c) were described in detail in Chapter 2 Sect 2.2, and thus are not repeated here.

3.2.2 Online WSOC measurements

From August 2 to September 15 2008, as part of the 2008 August Mini-Intensive on Georgia Aerosol at SEARCH (AMIGAS) field study, online $PM_{2.5}$ WSOC measurements were conducted using a Particle-Into-Liquid Sampler (PILS) coupled with a TOC analyzer [*Sullivan et al*., 2004] simultaneously at two SEARCH sites in Georgia, i.e. Jefferson Street (JST) and Yorkville (YRK). JST (33.777 N, 84.416 W) is an urban site approximately 4 km northwest of central Atlanta and is located in a mixed commercial/residential area. YRK (33.929 N, 85.045 W) is a rural site approximately 55km northwest of metro Atlanta. Detailed descriptions of the sampling sites were given by *Hansen et al*. [2003]. The ambient fine particles were concentrated into a continuous liquid flow via a PILS with an upstream URG $PM_{2.5}$ cyclone and a parallel plate carbon

denuder [*Eatough et al*., 1993]. Three background WSOC measurements were performed daily (at 3:00, 10:00 and 19:00 EST) throughout the study period by diverting the sampling flow through a Teflon filter (47 mm dia., 2.0 μm pore size, Pall Life Sciences). Ambient WSOC data were blank-corrected and reported at 10-min resolution. During the AMIGAS campaign, WSOC data at both sites were available for 25 days from August 12 to September 6 2008, along with a suite of gas and meteorological data that were routinely measured at these SEARCH sites.

The two PILS-TOC systems deployed at the two SEARCH sites were compared side-by-side prior to and after the field campaign on the roof of the Environmental Science and Technology building on the Georgia Institute of Technology campus for a period of 4 days. The data collected by the two instruments were highly correlated (r^2 = 0.96) and showed good agreement with a linear regression slope of 0.88 and an intercept of 0.13 μgC m^{-3}. The YRK WSOC data were modified to account for this small systematic difference.

3.2.3 Gridded monthly isoprene emission fluxes from MEGAN-ECWMF global inventory

Monthly averaged isoprene emission data over the southeast (30-36°N, 80-89°W) were obtained from the website: http://tropo.aeronomie.be/models/isoprene.htm. The global emissions of isoprene were calculated at 0.5° resolution, based on the MEGAN (Model of Emissions of Gases and Aerosols from Nature) version 2 [*Guenther et al*., 2006] and a detailed multi-layer canopy environment model for the calculation of leaf temperature and visible radiation fluxes. The calculation was driven by meteorological fields provided by analyses of the European Centre for Medium-Range Weather

Forecasts (ECMWF) [*Müller et al.*, 2008] and included air temperature, cloud cover, downward solar irradiance, wind speed, and volumetric soil moisture in four soil layers.

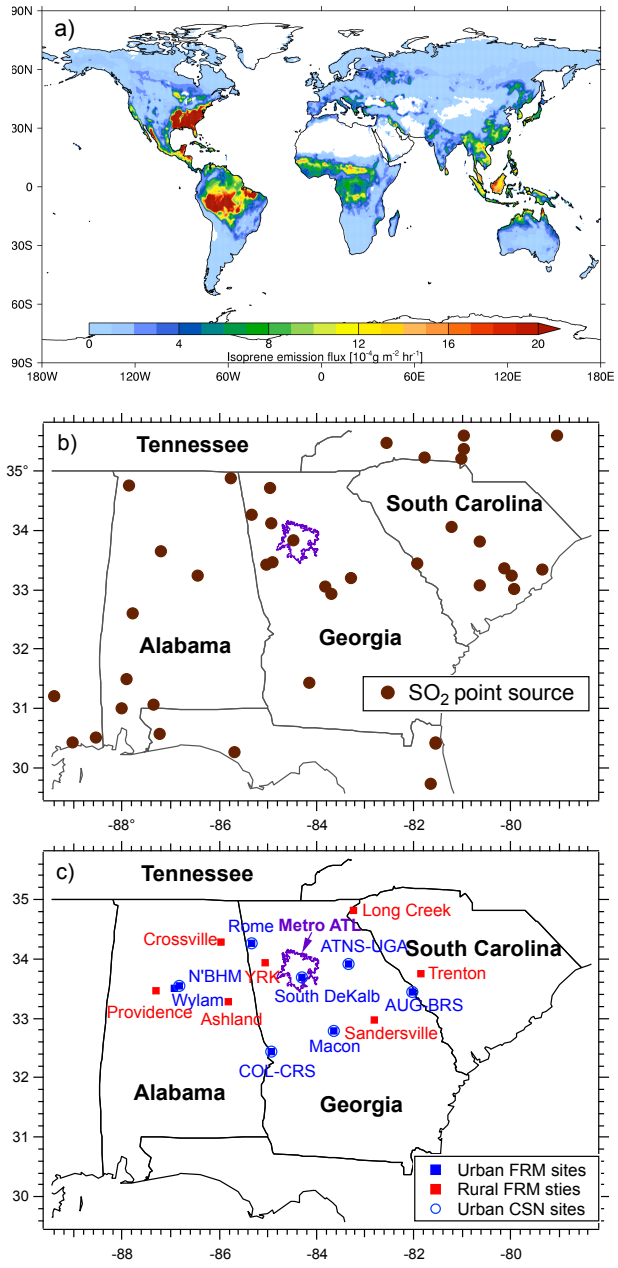

Figure 3.1 Maps of a) MEGAN-ECMWF global isoprene emissions in August of 2007, b) SO_2 point sources based on EPA National Emission Inventory (NEI) 1999, and c) geographic locations of EPA FRM and co-located CSN sampling sites.

3.3 Results and discussion

3.3.1 Characteristics of fine aerosol composition over the southeast – a "sulfate-organic-rich" fine aerosol with widely uniform concentrations

Seasonal average mass concentrations of $PM_{2.5}$ and a number of its key chemical components at each of the 15 sampling sites are presented in Figure 3.2. Levoglucosan, an exclusive and relatively stable biomass burning emission tracer, had a large cold-warm season contrast due to enhanced domestic biomass burning emissions in the winter, as can be seen from the generally higher levoglucosan concentrations at urban sites, as well as more frequent wildfires and prescribed burnings in the spring; the large inter-site variability was due to random plume impacts (see *Zhang et al*. [2010] for a detailed discussion of biomass burning emissions from this data set). A possible secondary effect of accelerated loss of levoglucosan via photo-oxidation in the summer [*Hennigan et al*., 2010] may also account for some of the seasonal difference. To minimize the contribution of biomass burning to primary WSOC ($WSOC_{BB}$) and focus on secondary WSOC, a surrogate of SOA carbon [*Sullivan et al*., 2004, 2006; *Hennigan et al*., 2009; *Miyazaki et al*., 2009], filter samples with levoglucosan concentration greater than 50 ng m^{-3} were not included in the following analysis and discussion. The remaining data were assumed to be largely non-biomass-burning WSOC ($WSOC_{NB}$), which in warmer seasons was mainly comprised of secondary WSOC (as will be shown below), with minor contributions of primary WSOC from mobile source emissions at urban sites [*Hecobian et al*., 2010]. In colder seasons (e.g., winter), the fraction of primary $WSOC_{NB}$ could be higher due to reduced secondary formation from photochemistry.

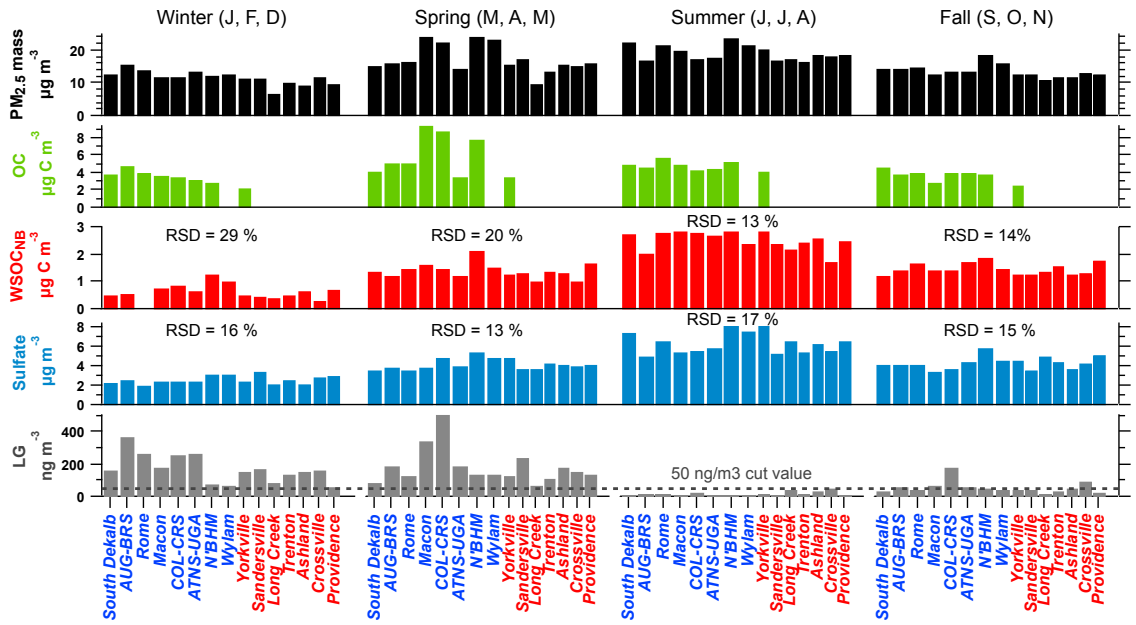

Figure 3.2 Seasonal mean concentrations of a) $PM_{2.5}$ mass, b) OC, c) $WSOC_{NB}$ (non-biomass burning), d) sulfate and e) levoglocosan (LG) at each of the 15 FRM sampling sites. OC data are only available at 7 of the 8 urban sites and 1 rural site. RSD stands for seasonal average relative standard deviations of $WSOC_{NB}$ and sulfate data. The initials after each season indicate the months included. Urban sites are labeled in blue and rural sites are labeled in red.

Organic aerosol (OA) mass (calculated by assuming an OM/OC ratio of 1.6) and ammonium sulfate were the two largest components of $PM_{2.5}$ mass throughout the year at all sites (Table 3.1), consistent with previous studies [*Tanner et al.*, 2004; *Weber et al.*, 2007; *Hand et al.*, 2012]. On average, OM and ammonium sulfate accounted for 39 ± 6% and 50 ± 5% of the total $PM_{2.5}$ mass, respectively. The minor contributors to $PM_{2.5}$ mass included EC (~7% in urban areas) and other refractory materials such as mineral dust and sea salt that were enriched in K^+ and Mg^{2+} (6 % from a PMF analysis detailed by *Zhang et al.* [2010]).

Table 3.1 Annual and seasonal averaged fractions (%) of organic aerosol mass (OM), water-soluble organic aerosol mass (WSOM), and ammonium sulfate in $PM_{2.5}$ and $WSOC_{NB}/OC_{NB}$ mass ratios, where OM is 1.6×OC, WSOM is 2.0×WSOC, and the subscript NB represents non-biomass-burning, using levoglucosan concentration (less than 50 ng m^{-3}) as a criteria.

	$OM/PM_{2.5}$ mass		$(NH_4)_2SO_4/PM_{2.5}$ mass		$WSOM_{NB}/PM_{2.5}$ mass		$WSOC_{NB}/OC_{NB}$ (levog.< 50 ng m^{-3})	
	Urban	Rural*	Urban	Rural	Urban	Rural	Urban	Rural*
Annual	43.7	34.7	40.7	50.4	23.5	26.3	51.9	55.8
Winter	44.0	34.3	32.8	41.4	20.2	25.5	45.2	59.6
Spring	49.1	33.2	39.7	47.0	24.8	26.7	46.8	41.2
Summer	40.9	36.1	49.1	53.6	26.4	28.9	56.3	52.6
Fall	40.5	33.1	46.2	56.7	22.9	24.3	51.2	69.7

* OM(OC) data are only available at one rural site: Yorkville (YRK).

Scatter plots in Figure 3.3 show the tight correlations of $WSOC_{NB}$ and sulfate with $PM_{2.5}$ mass in urban and rural sites. The high R^2 values for both $WSOC_{NB}$ (0.70 at urban to 0.75 at rural sites) and sulfate (0.60 at urban to 0.66 at rural sites) with $PM_{2.5}$ mass indicate the widespread presence of these two $PM_{2.5}$ components throughout the southeast. Contributions from primary species to the total fine aerosol mass likely account for the slightly lower regression slopes and R^2 values for both components at urban sites (Figure 3.3). Assuming a WSOM/WSOC ratio of 2.0 [*Turpin and Lim*, 2001], $WSOM_{NB}$ (a proxy of SOA mass) and ammonium sulfate together contributed up to 76% at urban and 82% at rural sites of the total $PM_{2.5}$ mass in the summer (Table 3.1). The large mass fractions of $WSOM_{NB}$ and sulfate and their strong correlations with $PM_{2.5}$ mass implies that the secondary processes leading to the formation of both components largely influence and contribute substantially to the fine particle loadings over the

southeast throughout the year, which has significant implications on $PM_{2.5}$ control strategies and possible $PM_{2.5}$ responses to a changing climate [*Goldstein et al.*, 2009].

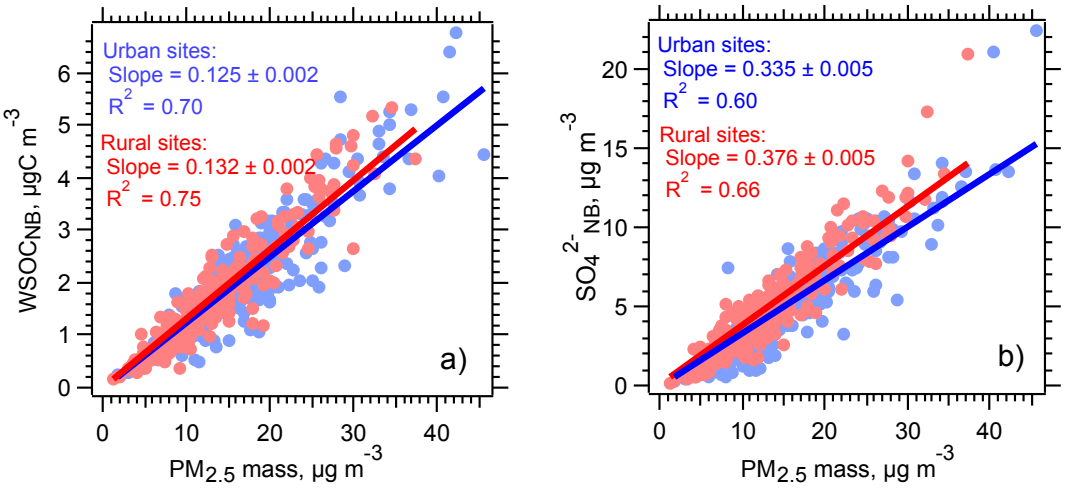

Figure 3.3 Scatter plots of a) $WSOC_{NB}$ (non-biomss burning) and b) $Sulfate_{NB}$ versus $PM_{2.5}$ mass concentrations. Slope and R^2 of the linear fit are shown separately for urban and rural sites.

3.3.2 Seasonal and spatial variability of WSOC based on FRM filter data

3.3.2.1 Seasonality of WSOC and other $PM_{2.5}$ components

The monthly mean concentrations of $WSOC_{BB}$ and $WSOC_{NB}$ shown in Figure 3.4 indicated that the biomass burning influences on WSOC were mostly in winter and spring, whereas during summer and early fall (September and October), $WSOC_{BB}$ was nearly negligible. Figure 3.4 also shows the monthly mean sulfate concentrations and temperature averaged over all 15 sites as well as the predicted isoprene emission flux over the sampling domain (30-36°N, 80-89°W). Pronounced seasonality for concentrations of $PM_{2.5}$ mass (Figure 3.2), $WSOC_{NB}$ and sulfate were found, with maximum in summer and minimum in winter. The mean summer (JJA)-to-winter (JFD)

ratio (± one standard deviation) averaged across all the sites for sulfate, WSOC and OC concentrations was 2.5 ± 0.6, 1.9 ± 0.8, and 1.6 ± 1.1, respectively. When filtering out samples with significant levoglucosan concentrations (> 50 ng m^{-3}) to remove biomass-burning influence, these ratios were nearly doubled, i.e. 4.5 ± 0.4 for sulfate, 3.9 ± 0.5 for WSOC, and 2.2 ± 0.9 for OC. A lower summer/winter ratio for OC may reflect that roughly half OC was primary at urban sites (although less at rural sites), which was not expected to vary significantly with season [*Lim and Turpin*, 2002; *Weber et al*., 2007]. In contrast, the large summer-winter difference for $WSOC_{NB}$ and $sulfate_{NB}$ concentrations was most likely due to the summertime enhancement of secondary chemical processes (e.g., enhanced photochemistry due to higher oxidant levels and stronger solar radiation). As shown in Figure 3.4, $WSOC_{NB}$ and temperature (and to a lesser extent, $sulfate_{NB}$ and temperature) had a common seasonal pattern (for $WSOC_{NB}$ vs. T: $r^2 = 0.57$; sulfate vs. T: $r^2 = 0.38$), and there was a clear co-variability among these three from March to August; an unusually warm March had elevated $WSOC_{NB}$ and $sulfate_{NB}$, whereas a cooler July corresponded to lower concentrations. Much of this co-variability may be due to temperature effects on photochemistry and synoptic meteorology.

The enhanced emissions of precursor compounds (e.g., isoprene as a SOA precursor) during warmer months may also explain some of the seasonality observed for WSOC. Studies have found evidence for biogenic hydrocarbons as a major contributor of SOA mass over the southeast [*Gao et al*., 2006; *Weber et al*., 2007; *Ding et al*., 2008; *Goldstein et al*., 2009; *Chan et al*., 2010b; *Lin et al*., 2012]. Monthly mean predicted isoprene emission shown in Figure 3.4 had a large seasonal variability and roughly increased 4 fold from winter to summer. However, since sulfate also exhibited an evident

seasonality, yet SO_2 emissions did not have a strong seasonal dependence (U.S. EPA National Emissions Inventory, http://www.epa.gov/ttnchie1/trends/), the seasonal variability of $WSOC_{NB}$ based on 24-h filter data cannot be related specifically to temperature-induced biogenic emissions and resulting SOA formation. The observed seasonality for $WSOC_{NB}$ and sulfate may be due to a combination of various controlling factors, including synoptic meteorological events (e.g., stagnation and precipitation), transport and photochemistry. Emissions of precursor compounds may also play a role, but is probably minor from the analysis of this data set.

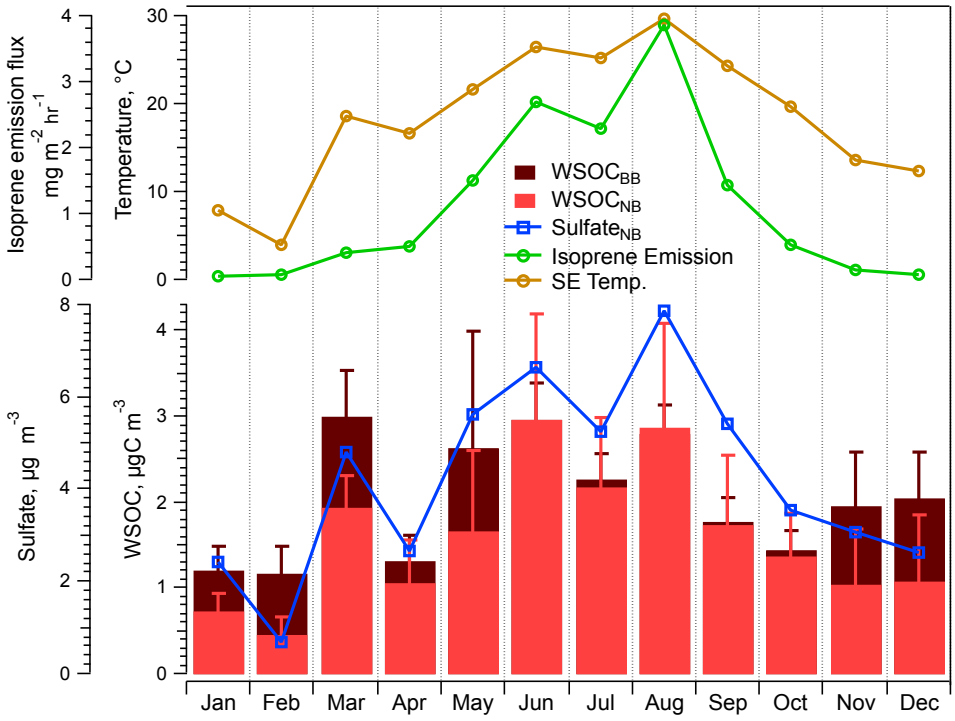

Figure 3.4 Monthly mean concentrations of $WSOC_{BB}$ (biomass burning) and $WSOC_{NB}$ (non-biomass burning), $sulfate_{NB}$ and temperature averaged over all sampling sites; regional average isoprene emission flux over the sampling domain (30-36°N, 80-89°W).

3.3.2.2 Spatial homogeneity of WSOC and sulfate

One of the notable features of Figure 3.2 is the insignificant site-to-site variation of $WSOC_{NB}$ and sulfate concentrations throughout all seasons, especially during warmer months. This is indicative of widely uniform concentrations of both secondary components throughout the region. Seasonally averaged relative standard deviations (RSD; standard deviation divided by mean for the season of interest) for $WSOC_{NB}$ and sulfate, as labeled in Figure 3.2 above each group, were mostly below 20% except for $WSOC_{NB}$ in the winter. A detailed site-to-site correlation analysis suggests that the concentrations of $WSOC_{NB}$ and sulfate were not only similar but also well correlated to those at other sites. Taking the South Dekalb (urban Atlanta) site as an example since it is located in the center of the sampling region, Figure 3.5 shows the correlation coefficients (r^2) of $WSOC_{NB}$ and sulfate concentration between South Dekalb and each of the other 14 sites as a function of estimated distance between sites. $WSOC_{NB}$ at South Dekalb was strongly correlated with that at all other sites as indicated by the high r^2 values (> 0.65). For example, for the Providence site, a rural site ~280 km away from South Dekalb, the r^2 of $WSOC_{NB}$ was as high as 0.93, suggesting the highly spatial homogeneity of $WSOC_{NB}$ (SOA), similar to previous finding by *Ding et al*. [2008]. The site-to-site correlation for sulfate was weaker than $WSOC_{NB}$, possibly owing to the spatial distribution of the SO_2 point source (Figure 3.1b). For example, the very low r^2 of sulfate between South Dekalb and Macon may be partially due to the large coal-fired power plant near the Macon site. For all the combination of 15 sites (N = 105), the mean (median) ± standard deviation of r^2 value was 0.64 (0.69) ± 0.25 for $WSOC_{NB}$ and 0.46 (0.48) ± 0.28 for sulfate.

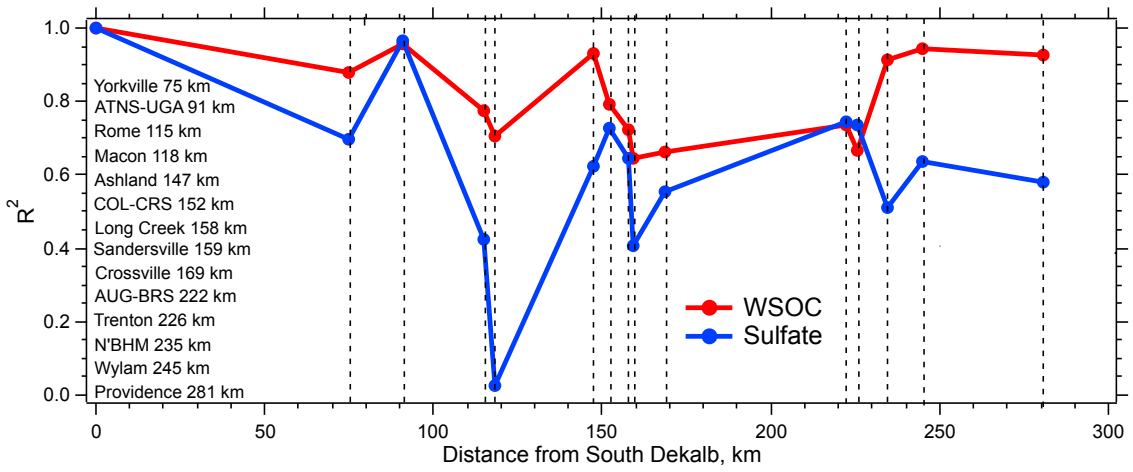

Figure 3.5 Site-to-site correlations of WSOC and sulfate between South Dekalb (a site within urban Atlanta) and other 14 sites in the southeast. Distance between South Dekalb and the other site is given in ascending order.

The observed large seasonal variation and spatial homogeneity of FRM filter-based WSOC (i.e. non-volatile WSOC) is consistent with biogenic VOC emissions that are both highly temperature dependent and widely distributed over the southeast. These patterns, together with observations of organic carbon in this region having a large modern (i.e. biogenic) carbon component [*Tanner et al*., 2004; *Weber et al*., 2007; *Bench et al*., 2007; *Schichtel et al*., 2007], support the hypothesis that biogenic VOC oxidation is the major SOA source in the southeast. However, similar (although to a lesser degree) seasonality and spatial uniformity have been observed for sulfate. Sulfate is formed from oxidation of SO_2 and the largest source of national SO_2 emission is coal-fired electric power plants, accounting for 73% of the total SO_2 emission in 2007 (U.S. EPA National Emissions Inventory). As shown in Figure 3.1b, the SO_2 point sources in the southeast are not uniformly distributed, unlike the VOC-emitting vegetation. Thus, as discussed in Sect. 3.3.2.1, it is more likely the observed spatial homogeneity for these secondary

compounds is largely due to meteorology, resulting in the well-mixed regional aerosol characteristic of the southeast. Both WSOC (SOA) and sulfate are long-lived secondary products with lifespan of days to a week. The southeast region is generally not well ventilated (unlike the coastal areas where the sea/land breeze circulation disperses the pollution daily [*Zhang et al*., 2012b]), especially during summer when high-pressure systems lead to frequent stagnation events. Therefore, the pollutants with long lifetime, such as SOA and sulfate, can build up and eventually spread across the whole southeast region. Thus, the regional $WSOC_{NB}$ per se does not exclusively indicate a widely distributed source of SOA (i.e. biogenic VOC oxidation). An alternative explanation is that the formation of $WSOC_{NB}$ is not independent of sulfate (e.g., WSOC formed through acid-catalyzed reaction) so the uniform distribution of sulfate has some impact on SOA formation and thus the distribution of $WSOC_{NB}$. Recent work by *Lin et al*. [2012] found that reactive uptake of gaseous IEPOX onto acidic seed aerosols yielded the same aerosol constituents that have been observed in the ambient aerosols in rural southeast. A study contrasting regional distributions of $WSOC_{NB}$ and a primary species such as EC would provide additional insight.

3.3.2.3 Spatial correlations of WSOC concentrations with isoprene emissions

Although $WSOC_{NB}$ was highly correlated and relatively uniformly distributed throughout the whole region, some of the spatial pattern may be linked to the spatial distribution of isoprene emissions. Figure 3.6a shows the color-coded mean predicted isoprene emission flux with $WSOC_{NB}$ concentrations at each sampling site for August 2007. In August, biogenic emissions and SOA formation are significant due to the large

vegetation mass, high temperature and intense solar radiation. Quantitative interpretations from Figure 3.6a are limited by the coarse grids (0.5°×0.5°) and known large uncertainties for isoprene emission estimates [*Guenther et al*., 2006]. However, some qualitative trends can be seen in Figure 3.6a. First, there was a rough west-to-east gradient in isoprene emissions and a corresponding $WSOC_{NB}$ zonal trend. $WSOC_{NB}$ concentrations were lower by roughly 27% at the five sites on the east end of the sampling region, which were also located in areas with less isoprene emissions. On smaller spatial scales, isoprene enhanced areas often corresponded to high $WSOC_{NB}$ (e.g., COL-CRS, Ashland and the three most western sites in AL). Interestingly, there were several sites in the vicinity of urban Atlanta that exhibited high $WSOC_{NB}$ concentrations yet were not in isoprene-enriched areas. It is possible that these sites were under stronger influence of anthropogenic emissions as seen from the satellite observed NO_2 column density in Figure 3.6b. Previous ambient studies have shown evidence for enhanced SOA formation from interactions between naturally emitted precursors with anthropogenic pollutants such as NO_x [*Weber et al*., 2007; *de Gouw et al*., 2008; *Worton et al*., 2011]. Environmental chamber studies also reported higher SOA yields for biogenic hydrocarbons in the presence of high NO_x levels [*Dommen et al*., 2006; *Chan et al*., 2010a]. Contributions from anthropogenic SOA formation in urban regions would also account for higher urban WSOC. The extent of the contribution from pure anthropogenic or anthropogenic-enhanced biogenic SOA to urban WSOC in the southeast is discussed in Chapter 4 and 5 as well as in the following section.

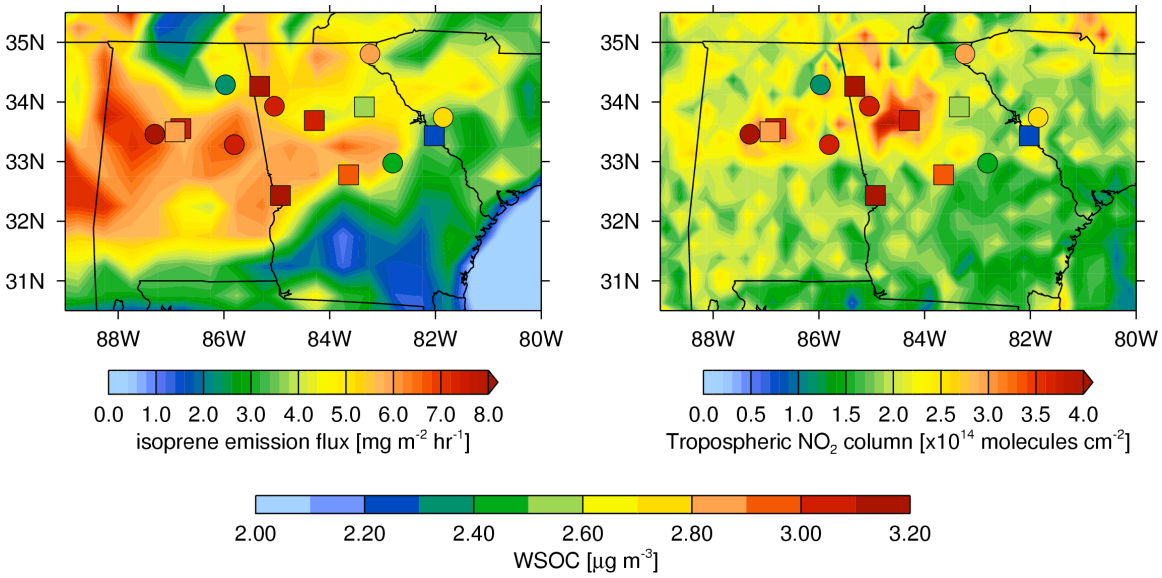

Figure 3.6 Spatial distributions of a) isoprene emission fluxes (0.5°×0.5°) predicted from MEGAN-ECWMF global inventory and b) tropospheric NO_2 column density from OMI on board NASA AURA satellite in August of 2007. Overlaid on the emission maps are the color-coded $WSOC_{NB}$ (non-biomass burning) concentrations at the 15 FRM sampling sites (urban: squares; rural: circles) in August of 2007 (Note that the $WSOC_{NB}$ color scale is set to investigate relatively small changes in absolute $WSOC_{NB}$ concentrations).

3.3.3 WSOC concentration gradient between urban and rural sites based on FRM filter data and online WSOC measurements

3.3.3.1 Urban/rural FRM filter

A small urban/rural gradient of FRM $WSOC_{NB}$ was evident for all four seasons (Figure 3.7), indicating an anthropogenic component for primary $WSOC_{NB}$ and/or SOA production in urban environments, consistent with the reported urban excess OC in the southeast [*Zheng et al.*, 2006; *Blanchard et al.*, 2011; *Hand et al.*, 2012]. The largest urban/rural difference was seen in winter (on average urban $WSOC_{NB}$ is 63% higher than rural $WSOC_{NB}$), whereas in other seasons the difference was within 20%. The much

higher urban $WSOC_{NB}$ in the winter was likely due to primary WSOC emitted from fossil fuel combustion and possibly residential wood burning (although data with leveoglucosan > 50 ng m^{-3} were filtered out) in urban areas. Based on the FRM filter data, the widespread SOA was only moderately enhanced by urban emissions, resulting in a small urban/rural gradient (10%) in the summer.

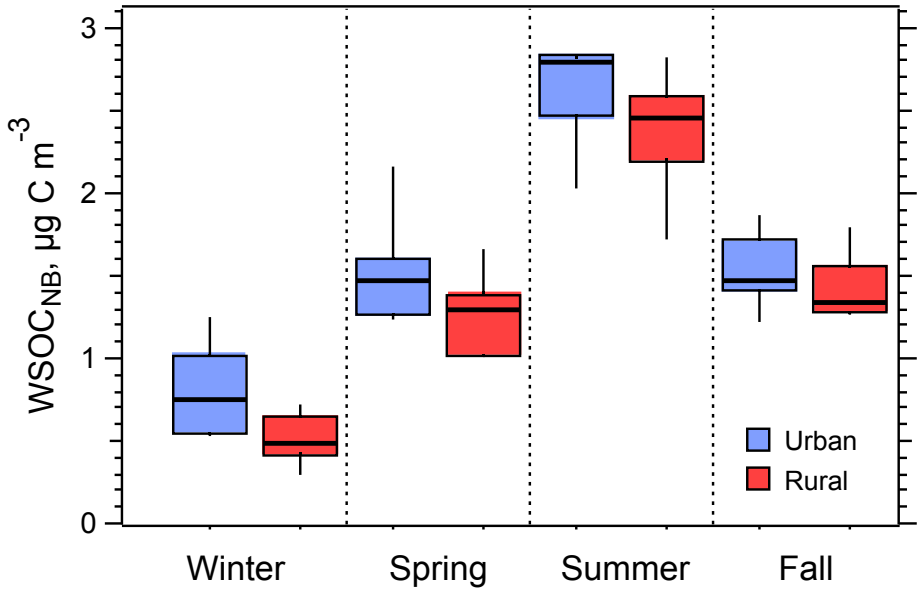

Figure 3.7 Box plots of the seasonal mean concentrations of $WSOC_{NB}$ (non-biomass burning) segregated for urban and rural sites. The plot shows median values (thick horizontal bar), 25th and 75th percentiles (lower and upper box bounds, respectively), and 10th and 90th percentiles (lower and upper whiskers, respectively) for each bin.

However, as noted earlier, filter sampling is subject to considerable negative artifact so that the semi-volatile SOA components may not be included. An online measurement is expected to have fewer sampling artifacts [*Weber et al*., 2003]. Factors associated with the summer urban/rural difference were explored by conducting real-time

in situ measurements at an urban/rural pair in Georgia: an Atlanta metropolitan site at Jefferson Street (JST) and a rural site at Yorkville (YRK, also a FRM site) in August of 2008. In the following analysis, WSOC was expected to be $WSOC_{NB}$ since little biomass burning contributions were observed in the southeast during summer [*Zhang et al*., 2010], although no companion measurements of biomass burning tracers were available.

3.3.3.2 Online measurements at JST and YRK

For the entire 1-month study, WSOC concentrations (10-minute averages) at JST and YRK were moderately correlated with an r^2 of 0.37. The time series of WSOC and other associated parameters at JST and YRK are shown in Figure 3.8. Between the two sites, WSOC exhibited both common and distinct temporal patterns. On a lower frequency scale (~daily), urban and rural WSOC generally tracked each other well, whereas on a higher frequency scale (~hourly), urban WSOC showed larger and more frequent fluctuations superimposed on the generally less variable lower frequency varying rural WSOC. Since YRK is often located upwind of JST and so is not subject to significant urban impact, as indicated by the consistently lower CO and NO_x concentrations (Figure 3.8), the more constant YRK WSOC likely represents the typical regional (i.e. rural) background levels, and the smooth variation is due to synoptic meteorological processes. For example, the consistently lower concentrations of a variety of species at both sites during August 21 – 26 were mainly due to higher wind speeds and frequent rain events. The air masses impacting both sites during this period originated either from the Gulf of Mexico or the Atlantic Ocean [*Padró et al*., 2011].

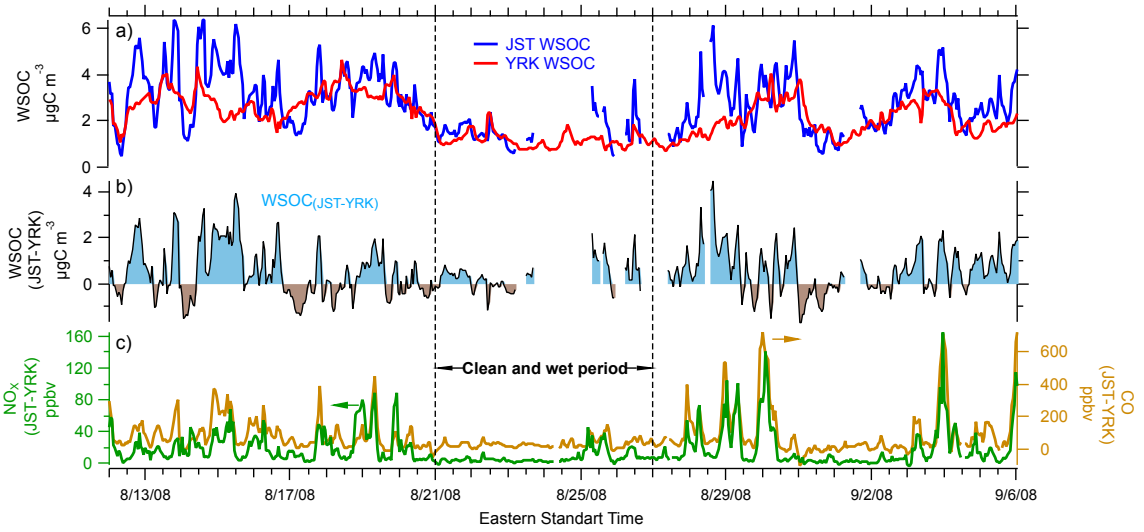

Figure 3.8 Time series of WSOC and other parameters measured at Jefferson St. (JST) and Yorkville (YRK) from Aug 12, 2008 to Sep 6, 2008 during the AMIGAS field campaign: a) absolute WSOC concentrations at two sites; b) WSOC difference (ΔWSOC) between the two sites (i.e. $WSOC_{JST}$ minus $WSOC_{YRK}$); c) CO and NO_X difference between the two sites (i.e. CO_{JST} minus CO_{YRK}, NO_{X_JST} minus NO_{X_YRK}).

The distinct WSOC pattern at the urban relative to the rural site is likely due to a combination of SOA precursor emissions and chemical formation processes. Based on data from emission inventories, isoprene emissions at these two sites are practically identical (Figure 3.6a), indicating that biogenic SOA precursors were not the main reason for the difference. Higher WSOC is generally associated with much higher CO and NO_x levels, which frequently occurs at the urban site. Occasionally, YRK WSOC was higher (e.g., on August 14, 17, 31) due to stagnation events. The scatter plot in Figure 3.9 clearly shows that the largest differences of WSOC between the two sites were observed at low wind speeds at JST and were often associated with higher CO concentrations at urban site, indicating local production of WSOC under anthropogenic influence.

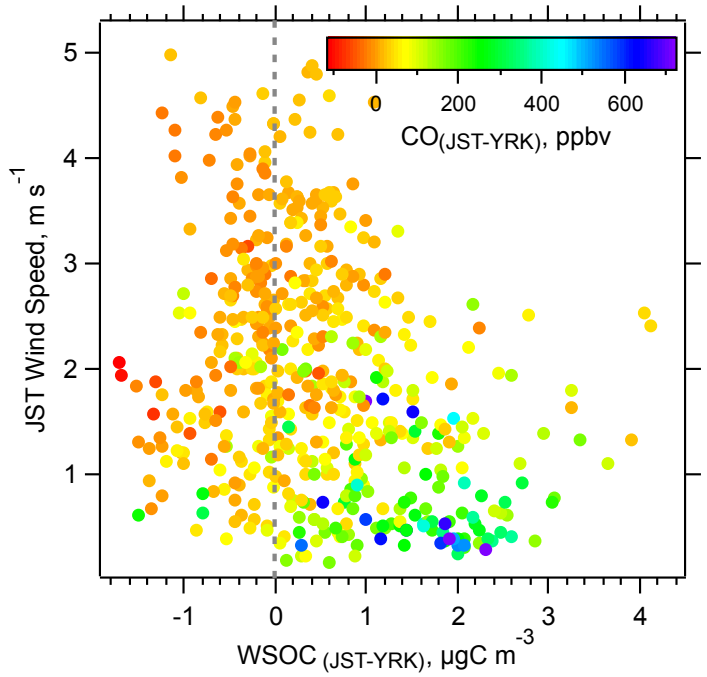

Figure 3.9 Differences between WSOC measured between the two sites ($WSOC_{(JST-YRK)}$) as a function of wind speed at JST, color coded by CO difference between the two sites ($CO_{(JST-YRK)}$).

Average diurnal trends for CO, O_3 and WSOC at JST and YRK also showed distinctly different patterns at these two sites (Figure 3.10a, b). WSOC and CO at YRK were nearly constant throughout the day. In contrast, JST CO clearly showed a characteristic morning rush hour peak at ~7 am and roughly a factor of 2 night-to-day enhancement, which was attributed to lower nighttime mixed layer height leading to higher CO concentrations from nighttime mobile source emissions. JST WSOC was constantly higher than YRK, again indicating the urban enhancement of SOA formation. Primary WSOC emissions can also make some contribution, as seen by the morning WSOC peak during rush hour, but this was clearly minor compared to secondary photochemical production when considering the effect of mixed layer expansion.

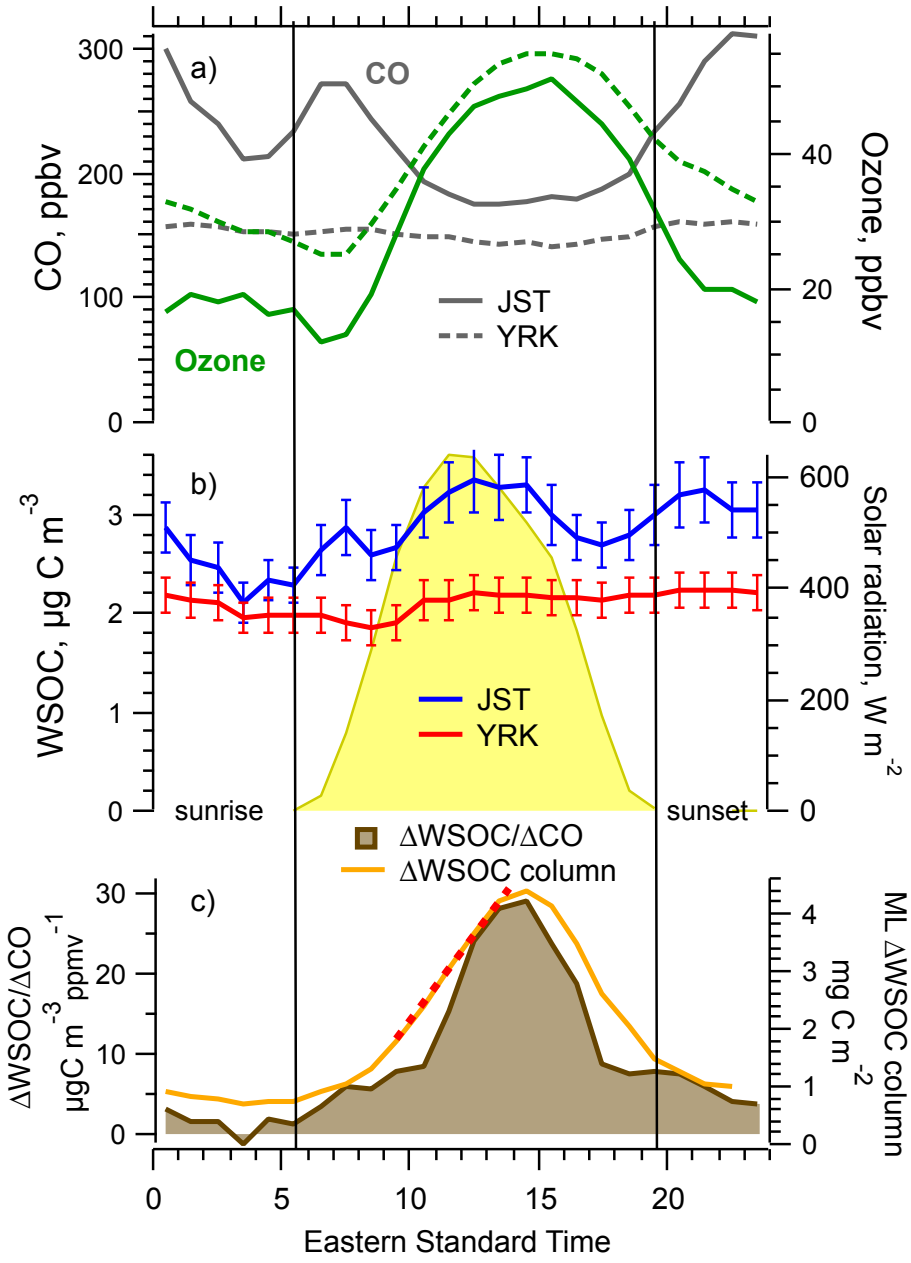

Figure 3.10 Composite diurnal profiles of a) CO, O_3 at JST and YRK, b) WSOC concentrations at JST and YRK, solar intensity at JST, and c) ΔWSOC/ ΔCO and mixed layer ΔWSOC column, where ΔWSOC/ΔCO = $WSOC_{(JST-YRK)}$/(CO–0.15ppmv), and mixed layer ΔWSOC column = $WSOC_{(JST-YRK)}$ × MLH (mixed layer height), during the AMIGAS sampling period. The red dotted line in panel (c) represents an estimate of urban WSOC production rate in unit of mgC m^{-2} hr^{-1}.

As a rough approximation, the effect of expanding mixed layer on WSOC variation can be determined by normalizing WSOC concentration to a conservative species (e.g., CO). Figure 3.10c shows the diurnal profile of ΔWSOC/ΔCO (= $WSOC_{(JST-YRK)}$/(CO_{JST} - 0.15 ppmv), where it assumes the CO emissions at JST are constant throughout the day (a significant over-simplification) and a CO background level of 0.15 ppmv (based on CO_{YRK}). The result shows that the major source of urban excess WSOC is photochemical production (e.g., ΔWSOC/ΔCO tracks solar radiation and O_3 concentrations), which is much more significant than the mobile emissions leading to primary WSOC during morning rush hour. An alternate approach to estimate the urban ΔWSOC production is to use the actual mixed layer height, in which case the column integrated WSOC concentration can be calculated by multiplying ΔWSOC concentrations by the mixed layer height. This product is directly related to the urban WSOC source per unit surface area, assuming WSOC concentrations above the mixed layer are negligible, no net advection of WSOC into the region or loss of WSOC by deposition to the surface, and WSOC within the mixed layer is uniformly distributed. Mixed layer heights were not measured during the AMIGAS study, so literature values reported by *Marsik et al*. [1995] were used instead. Figure 3.10c shows that the two approaches give similar diurnal profiles, both characterizing the photochemical production with normalized WSOC concentrations peaking at approximately 15:00 local time, roughly 1-2 hours later than when solar intensity reached its maximum value. The rate of increase in WSOC per unit surface area from morning to early afternoon (i.e. increasing slope of WSOC column) gave an average urban WSOC production rate during this time period of approximately 0.55 mgC m^{-2} hr^{-1}, or 1.1 mg m^{-2} hr^{-1} for WSOM mass (shown as the red dotted line in

Figure 3.10c). After the peak near 15:00, both ΔWSOC/ΔCO and mixed layer ΔWSOC column decreased to background levels, possibly owing to SOA production weakening and/or downward mixing of cleaner air mass from aloft [*Blanchard et al*., 2011]. At night there was low production of WSOC, indicated by the flat slopes, similar to findings from previous studies on Atlanta WSOC [*Hennigan et al*., 2009]. More extensive urban/rural paired online studies would be valuable since the estimates of urban production rates could be contrasted throughout the year.

The urban/rural comparison suggests that the anthropogenic emissions play an important role in the enhancement of WSOC (SOA) in urban areas. Anthropogenic emissions could be involved in SOA formation in several ways, such as direct contributions from anthropogenic SOA precursors, e.g., aromatics [*Henze et al*., 2008] and acetylene [*Volkamer et al*., 2009], evaporation and re-condensation of semi-volatile organic vapors [*Robinson et al*., 2007; *de Gouw et al*., 2011], NO_x effect on both biogenic and anthropogenic SOA yields [*Presto et al*., 2005; *Song et al*., 2005; *Ng et al*., 2007] as well as SOA formed through reaction of NO_3 radical with biogenic VOCs [*Surratt et al*., 2008; *Brown et al*., 2009]. Based on the real-time data, the urban excess WSOC was on average 31% of the rural (regional) WSOC. However, as shown in Figure 3.7, for FRM filter WSOC the urban/rural difference during summer was only ~10%. The inconsistency between filter and online data may be due to the loss of semi-volatile components of the urban excess WSOC from the FRM filters during sampling and storage. Consequently, the FRM WSOC data in both urban and rural areas showed little variation and tend to be highly correlated as discussed in Sect. 3.3.2.

Considering the urban/rural difference obtained from the online data, it is of

interest how anthropogenic emissions were involved in the formation of urban WSOC in Atlanta. *Zhang et al*. [2011] observed a similar average WSOC diurnal profile as shown in Figure 3.10 in Atlanta in the summer of 2010. Meanwhile, they made measurements of WSOC light absorption in Atlanta and Los Angeles and found that the freshly-formed urban WSOC (i.e. ΔWSOC) in Atlanta was much less light-absorbing (~4-6 times less) than those freshly formed in LA. The LA ΔWSOC is proved to be mainly from anthropogenic sources [*Zhang et al*., 2011; *Bahreini et al*., 2012]. As an approximation, taking light-absorbing WSOC as a measure of anthropogenic SOA suggests that in Atlanta up to 25% of the urban ΔWSOC was from direct contributions of anthropogenic VOCs, and the rest (75%) was related to formation of biogenic SOA, possibly enhanced under anthropogenic influence.

3.3.4 Sources of summertime regional FRM WSOC

A Positive Matrix Factorization (PMF) analysis using the FRM $PM_{2.5}$ chemical composition (WSOC, Na^+, NH_4^+, K^+, Mg^{2+}, SO_4^{2-}, oxalate, xylose, and levoglucosan) and light absorption data set from all 15 sites was performed to investigate the sources of $PM_{2.5}$ throughout the southeast region over the year of 2007. A detailed description and procedures for the PMF analysis were presented in Chapter 2. PMF results focusing on summertime FRM WSOC formation processes are discussed here.

The very different composition profiles of F3 and F4 (Figure 2.9) suggest different physical and/or chemical processes involved in the regional WSOC (SOA) formation. The limited number of species available for this factor analysis limits the identification of multiple sources and prohibits definitive identification of the sources or

processes leading to these two factors, but the differences between F3 and F4 are intriguing. In the following we speculate on possible sources of the regional WSOC in the southeast.

Factor 3: The association among oxalate, b_{ap365} and WSOC of F3 is notable for a number of reasons. First, these are all characteristics of biomass burning emissions (Factor 1 detailed in Chapter 2). Although biomass burning cannot be completely ruled out, it is unlikely to cause such a large fraction of the summertime FRM WSOC variability. Instead, numerous laboratory studies have shown that chemical processes in aqueous solutions produce both oxalate [*Sorooshian et al*., 2006; *Lim et al*., 2010] and light-absorbing organic compounds [*Bones et al*., 2010; *Sareen et al*., 2010], along with other aqueous SOA products including oligomers and high molecular weight multi-functional compounds that could be included in the overall WSOC in F3 [*Surratt et al*., 2007; *Nguyen et al*., 2012]. Collectively, these components have been grouped as HULIS [*de Haan et al*., 2009; *Shapiro et al*., 2009] and are linked to aqueous chemical aging of the aerosol, which uniquely explains the presence of high MW compounds [*Ervens et al*., 2011]. *Gao et al*. [2006] have detected polar organics that are similar to HULIS on filters collected in rural areas in the southeast and have shown evidence of atmospheric processing of biogenic emissions leading to HULIS as a typical pathway in the background (regional) atmosphere. *Hennigan et al*. [2009] and *Zhang et al*. [2012b] studied WSOC gas/particle partitioning in urban Atlanta and found evidence for WSOC partitioning to particle liquid water indicating that an aqueous chemical route is feasible. The fact that the PMF factor 3 explains much of the variability of WSOC mass concentrations suggests the importance of a potential summertime aqueous WSOC

formation route.

Factor 4: Previous aerosol source apportionment studies in the southeast and other locations have attributed factors with high organic carbon and ammonium sulfate loadings to be associated with secondary aerosol formation through a variety of pathways. Correlations between WSOC and sulfate in some locations show clear evidence for a cloud formation process [*Huang et al*., 2006]; however, the lack of oxalate associated with F4 seems to suggest this may not be the case in the southeast. WSOC-sulfate correlations may result from possible acid-catalyzed effects on SOA formation [*Liu et al*., 2005; *Kim and Hopke*, 2006], or simply could be related to long-range transport [*Saarikoski et al*., 2008]. We have noted the spatial and seasonal correlations of WSOC and sulfate and attributed some of this co-variability to both being secondary components with similar atmospheric lifetimes/loss processes. This would be consistent with F4 representing the regional/more aged aerosols mainly composed of sulfate and WSOC. A more comprehensive data set that includes speciated SOA tracer compounds (e.g., IEPOX and other known monoterpene, sesquiterpene, and aromatic tracers) as well as AMS and VOC/SVOC data is needed to better resolve the causes for differences between F3 and F4.

3.4 Summary

The spatial and seasonal variations of WSOC from the FRM filter samples (referred to as FRM WSOC) associated with fine aerosols in the southeastern U.S. were investigated through measurements of over 900 24-hour integrated FRM Teflon filters collected from 15 urban and rural sites in 3 states in the year of 2007. FRM WSOC was

contrasted with sulfate to examine possible causes of the spatial and seasonal variability. Online measurements of WSOC in August of 2008 at an urban/rural pair were compared to the FRM filter urban/rural differences and used for a more detailed analysis of the observed urban excess WSOC. The major findings of this study are:

1. In the southeast, FRM $PM_{2.5}$ was mainly composed of organic aerosol and ammonium sulfate. On average, OM (1.6 times OC) and sulfate accounted for 39% and 35% of the total $PM_{2.5}$ mass, respectively. Excluding biomass burning contributions (levoglucosan < 50 ng m^{-3}), FRM $PM_{2.5}$ mass was tightly correlated with both WSOC (r^2 of 0.70 urban, 0.75 rural) and sulfate (r^2 of 0.60 urban, 0.66 rural). WSOM (2.0 times WSOC) and ammonium sulfate together contributed up to 71% at urban and 78% at rural sites of the total $PM_{2.5}$ mass, indicating secondary processes largely influenced and substantially contributed to the fine particle loadings over the region throughout the year of 2007.

2. Pronounced seasonality was observed for FRM WSOC and sulfate. Both components showed maximum concentrations in the summer, apparently due to enhanced photochemistry and meteorology associated with elevated temperatures. Enhanced emissions of precursor compounds, such as biogenic hydrocarbons, may also have contributed to the seasonality of WSOC, but links to biogenic emissions and temperature were not as clear since both sulfate and WSOC responded in a similar way.

3. FRM WSOC and sulfate were widely distributed and fairly spatially uniform throughout the southeast, indicated by the significant site-to-site co-variability. Given the point source nature of sulfate precursor (SO_2), the large scale spatial homogeneity suggested that the dominant role played by secondary components in $PM_{2.5}$ mass

(ignoring biomass burning contributions present mainly in winter) combined with meteorology (a well-mixed region with limited ventilation) was the major cause for the large regional aerosol loading. Spatial uniformity cannot be mainly attributed to a widely distributed source of biogenic precursor VOCs. However, on smaller scales, spatial distributions of estimated isoprene emissions were consistent with relatively small differences in FRM WSOC, providing evidence of biogenic hydrocarbons as important SOA precursors.

4. Online measurements of WSOC between an urban/rural pair (Atlanta/Yorkville) indicated that on average urban WSOC was 31% higher than rural levels during the sampling period. The urban excess WSOC was clearly associated with local anthropogenic emissions since the WSOC enhancement was linked to CO and NO_x. In contrast, FRM WSOC urban/rural difference in summer was only ~10%, indicating that filters tend to produce a more uniform distribution, possibly due to poor temporal resolution and loss of semi-volatile organic species that were more likely associated with urban environments. Using the difference between the urban-rural WSOC and estimated boundary layer height, an urban Atlanta production rate of WSOC in August was calculated to be roughly 0.55 mgC m^{-2} hr^{-1} from morning to mid-afternoon.

5. A PMF analysis resolved two factors that explained 78% of the FRM WSOC variability. One factor that explained over half of the 2007 FRM WSOC variability was loaded with oxalate and brown carbon, consistent with a condensed phase SOA formation route. The other factor that accounted for roughly 1/4 of the FRM WSOC variability was associated with ammonium sulfate and may represent a regional aged SOA, or a possible acid catalyzed route. Further work is needed to investigate these hypotheses.

CHAPTER 4

LIGHT-ABSORBING ORGANIC AEROSOL IN ATLANTA AND LOS ANGELES BASIN

4.1 Background

Organic compounds that preferentially absorb light in the UV to lower visible wavelength range appear brown and are one light-absorbing component of atmospheric aerosols [*Andreae and Gelencser*, 2006]. Differing from black carbon (BC) or soot, brown carbon has a strong absorption-wavelength dependence and therefore has absorption Angström exponent (AAE, or $\mathring{A}_a$) larger than one. Brown carbon may influence photochemical processes [*Jacobson,* 1999] as well as regional radiative forcing [*Park et al.*, 2010] and modify light-absorbing and chemical properties of the clouds [*Jacobson*, 2012]. Some components of brown carbon have also been linked to adverse effects on human health (e.g., soluble nitro-aromatic compounds formed from oxidation of PAHs [*Gupta et al.*, 1996]).

Ambient observations and laboratory studies have shown that brown carbon has multiple sources. Brown carbon can be directly emitted from primary sources such as incomplete and smoldering combustion of both fossil and biomass fuels [*Duarte et al*., 2005; *Hoffer et al*., *2006*; *Lukacs et al*., 2007; *Hecobian et al*., 2010]. There is also evidence for brown carbon as a secondary organic aerosol (SOA) component produced from a variety of chemical ageing processes that often involve nitrogen, such as ageing of limonene ozonolysis products in solution with ammonium and amino acids [*Bones et al*., 2010], as well as aqueous phase reactions of carbonyls (e.g., glyoxal and methyglyoxal)

in acidic solutions [*Noziere et al*., 2005; *Sareen et al*., 2010], with amino acids [*Noziere et al*., 2007; *de Haan et al*., 2009a], methylamine [*de Haan et al*., 2009b] , or ammonium salts [*Shapiro et al*., 2009]. Along with these heterogeneous reaction routes, brown carbon can also be formed in the gas phase and partition to aerosols under dry conditions. Chamber studies show that brown SOA is formed directly from photooxidation of aromatics (i.e. toluene) under high-NO_x conditions [*Jaoui et al*., 2008; *Nakayama et al*., 2010; *Zhong and Jang*, 2011].

The prevalence and optical role of brown carbon are not well characterized. Particle light absorption coefficients (b_{ap}) are typically measured using optical instruments, such as the aethalometer, photo acoustic soot spectrometer (PASS), or particle soot absorption photometer (PSAP) at a fixed number of wavelengths, making quantifying brown carbon difficult and uncertain given that brown carbon is measured together with BC, the dominant aerosol absorber, and the contribution of brown carbon is often inferred by the difference between BC and total absorption [*Sandradewi et al*., 2008]. Further uncertainty arises due to other possible confounding factors such as absorption enhancement by the clear coatings formed over the BC cores [*Lack and Cappa*, 2010]. In addition, these optical measurements provide limited information on the complete absorption spectra over a wide wavelength range. In contrast, measurement of soluble brown carbon using various solvents provides detailed spectral information and does not suffer from the interference from BC or mineral dust absorption since undissolved particles can be removed from the solution; however, particle size-resolved information is lost [*Hecobian et al*., 2010].

Of particular interest is the water-soluble component of brown carbon associated

with secondary organic aerosols (SOA) in the absence of biomass burning. SOA formation leads to water-soluble organics and is a complex poorly understood process that contributes a substantial fraction to the fine particle mass and affects aerosol scattering, cloud activation and the toxicity properties of fine particles [*Hallquist et al*., 2009]. In this work, we report both online and offline measurements of soluble brown carbon at two urban environments, Pasadena/Riverside, California and Atlanta, Georgia, to examine the light-absorbing properties and formation processes of SOA in cites with contrasting emissions of volatile organic compounds (VOCs).

4.2 Experimental methods

4.2.1 Field sites

From mid-May to mid-June 2010, as part of the CalNex field campaign, online WSOC and light absorption measurements were carried out simultaneously at two ground sites, i.e. Pasadena and Riverside, California. Pasadena sampling was conducted on the California Institute of Technology campus (34.140582N, 118.122455W), ~16 km NE of downtown Los Angeles [*Hersey et al.*, 2011] (hereinafter referred to as the LA site). The Riverside site was located on the University of California-Riverside campus (33.97185N, 117.32266W), which is approximately 80km to the east-southeast of downtown Los Angeles. The sample inlet was situated 7 meters above ground level at the Pasadena ground site, and approximately 4.5 meters above ground at Riverside. Due to instrumentation issues, light absorption data at the LA site from only June 1 to June 15 were analyzed. Later in the summer of the same year (2010) after CalNex, identical measurements were conducted in Atlanta, GA for a month from August 6 to September 7,

2010. The measurement platform was located in the rooftop laboratory of the Ford Environmental Science and Technology building on the Georgia Institute of Technology campus (33.778427 N, 84.396181 W), roughly 30-40m above ground level. All data are reported in local time (PDT for LA and EST for Atlanta) and at ambient T and p.

4.2.2 Online WSOC light absorption measurement

A Particle-Into-Liquid Sampler (PILS) that continuously transfers ambient $PM_{2.5}$ particles to an aqueous flow of purified water was coupled in series with a long optical path length (1 m) Liquid Waveguide Capillary Cell (LWCC) (World Precision Instrument, Sarasota, FL) and a Total Organic Carbon (TOC) analyzer (GE Analytical, Boulder, CO) for semi-continuous measurements of the soluble $PM_{2.5}$ light absorption spectra and water soluble organic carbon (WSOC) concentration. Light absorption spectra between wavelengths of 200 and 800 nm at a resolution of 1 nm were recorded with a UV/Vis spectrophotometer at a time resolution of 15 min for complete absorption spectra and 1 min for absorption at selected wavelengths (365 and 700 nm). Absorption data for all wavelengths were referenced to absorption at 700 nm, a wavelength where contributions from ambient brown carbon are expected to be zero, to account for any baseline drift during the study. For ease of analysis we focus on the absorption averaged between 360 and 370 nm (b_{ap365}) as an overall proxy of soluble brown carbon. Three background measurements were performed daily (3:00, 10:00 and 19:00), each for 20 min, and both absorption and WSOC data were blank-corrected by interpolation between measurements. Overall measurement uncertainty was ~8% and the limit of detection (LOD) for WSOC is ~0.1 μgC m^{-3}. Detailed information on the PILS-LWCC-TOC

system and analysis of absorption data is described elsewhere [*Hecobian et al.*, 2010]. The absorption Angström exponent ($Å_a$, where $b_{ap} \sim \lambda^{-Åa}$) as a measure of the spectral dependence of aerosol light absorption, was determined from the linear regression fit of b_{ap} for wavelengths between 300 and 600 nm on log-log plots.

4.2.3 Offline filter sampling and analysis

During CalNex, $PM_{2.5}$ and PM_1 high-volume filter samples were collected on the roof of the Keck Building located on the Caltech campus approximately 0.3 km southwest of the Pasadena ground site for offline chemical analyses. PM_1 samples from June 4 and 14, 2010 with an integration time of 3-4 hr were analyzed for carbon isotopes [*Szidat et al.,* 2004]. On June 4, 10 and 13, 2010, $PM_{2.5}$ high-volume filter samplers (Tisch Environmental) operated at a nominal flow rate of 1.13 m^3 min^{-1} were used to collect particles onto pre-baked quartz-fiber filters (Pall Life Sciences) following an intensive sampling schedule, where filters were changed every 3-6 hr. Chemical characterization of light-absorbing brown carbon constituents was performed using ultra performance liquid chromatography (UPLC) coupled with diode array detection (DAD) and high-resolution quadrupole time-of-flight mass spectrometry equipped with an electrospray ionization source (ESI-HR-Q-TOF-MS, Agilent 6500 Series) for separation, identification, and structural elucidation. Briefly, samples were flowing through the UPLC system, detected by a DAD scanning the absorbance from 200 to 800 nm, and subsequently analyzed by an on-line ESI-HR-Q-TOF mass spectrometer to acquire accurate mass data for compositional information.

A punch from the intensive filters was extracted with 30 ml of 18-MΩ Milli-Q

water and analyzed for WSOC concentration via a TOC analyzer and soluble $PM_{2.5}$ light absorption using LWCC-spectrophotometer. Another punch of the filter samples was dissolved in 30 ml of Methanol (HPLC grade, Fisher Chemical) for total $PM_{2.5}$ light absorption measurement using the same LWCC. Similar filter sampling and analysis were not performed in Riverside or Atlanta. $PM_{2.5}$ OC and EC from the intensive filter samples were analyzed using a counter-top Sunset Labs OCEC Analyzer (Sunset Laboratory Inc., Tigard, OR) following NIOSH TOT protocol [*NIOSH*, 1996].

4.3 Results and discussion

4.3.1 Light-absorbing organic aerosol in the LA Basin

4.3.1.1 Characteristic of bulk soluble brown carbon measured in the LA Basin

The water-soluble fraction of fine particle ($PM_{2.5}$) organic aerosols (OA) depends on the source and age of the aerosols. Since the biomass burning influence on OA concentration was minimum during CalNex [*Hayes et al*., 2012], the measured WSOC is expected to be mainly from SOA formation, which is also supported by the strong correlation between WSOC and AMS-OOA (r^2 = 0.74) [*Zhang et al*., 2012b]. Measurements of the major SOA components, including WSOC, AMS-OOA, and small organic acids [*Veres et al*., 2011; *Liu et al*., 2012; *Zhang et al*., 2012b], all show a similar diurnal pattern at the Pasadena ground site. The formation of these SOA components was largely driven by photochemistry as they reached their peak concentrations in mid-afternoon (14:00-15:00 PDT) following daily peak concentrations in primary pollutants, such as EC and VOCs. The major source of LA SOA is anthropogenic emissions, and a significant fraction of SOA is freshly formed within the basin [*Hersey et al*., 2011; *Zhang*

et al., 2011; *Bahreini et al*., 2012; *Hayes et al*., 2012]. Consistent with the low hygroscopicity of the LA SOA, WSOC comprised only ~ 26% of the total OC (estimated from AMS OM measurements), which is much smaller a fraction than those reported in Atlanta (58%) and Tokyo (77%) [*Kondo et al*., 2007].

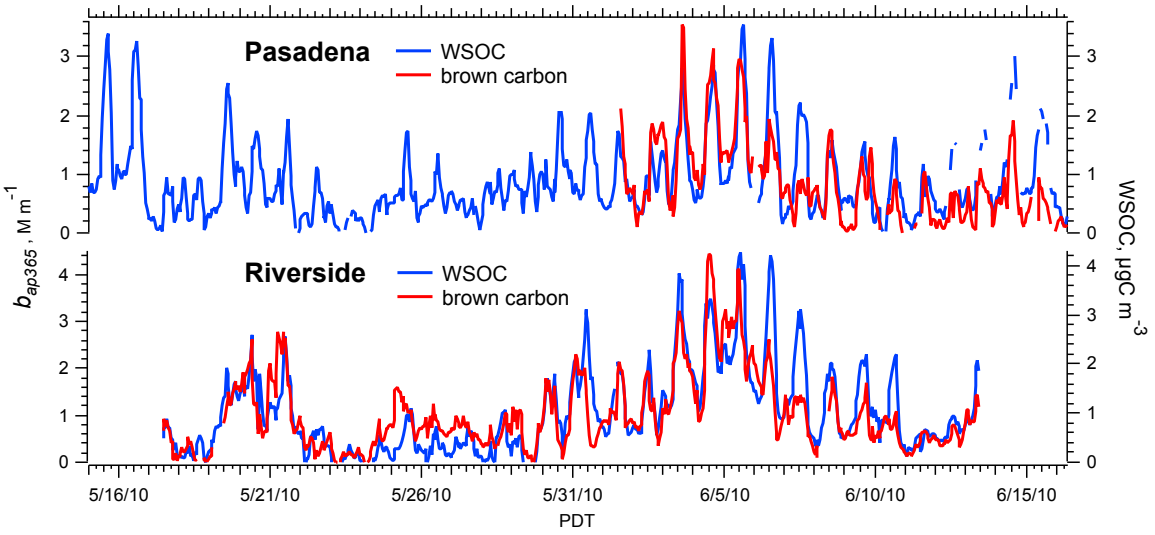

Figure 4.1 Time series of WSOC concentration and bulk (solution) WSOC light absorption at 365 nm (b_{ap365}) in Pasadena (LA) and Riverside during CalNex.

The soluble fraction of light-absorbing OA (i.e. soluble brown carbon) was measured using online PILS-LWCC technique simultaneously in Pasadena and Riverside during CalNex. Figure 4.1 shows the time series of bulk WSOC light absorption at 365 nm (b_{ap365}), a measure of soluble brown carbon, and WSOC concentration. At both sites b_{ap365} closely tracked the variations of WSOC (r^2 of b_{ap365} versus WSOC is 0.55 for Pasadena and 0.68 for Riverside), suggesting SOA formation as the major source of soluble brown carbon in LA. Riverside is located approximately 80 km to the east-southeast of Pasadena, within the eastern edge of the LA Basin. During daytime the

primary pollutants originated from the LA downtown travelled downwind to Riverside and undergo further oxidation en route. As a result, the air masses are expected to be more aged and well mixed in Riverside than Pasadena, which may explain the better correlation between b_{ap365} and WSOC in Riverside.

Scatter plots of b_{ap365} versus WSOC for Pasadena and Riverside are shown in Figure 4.2, where the regression slope represents the average mass absorption efficiency at 365 nm (MAE_{365}) of the bulk solution. MAE_{365}'s are similar at the two sites, ranging from 0.70 to 0.73 m^2 $g^{-1}C$ with an average of 0.71 m^2 $g^{-1}C$ for the overall LA soluble brown carbon. Compare to pure (i.e. uncoated) soot that has an MAE of 7.5±1.2 [*Bond and Bergstrom*, 2006], soluble organic aerosols are weak light absorbers since a significant mass fraction likely does not absorb light. Further speciation of the light-absorbing fraction of the soluble OA is discussed in Sect. 4.3.1.2.

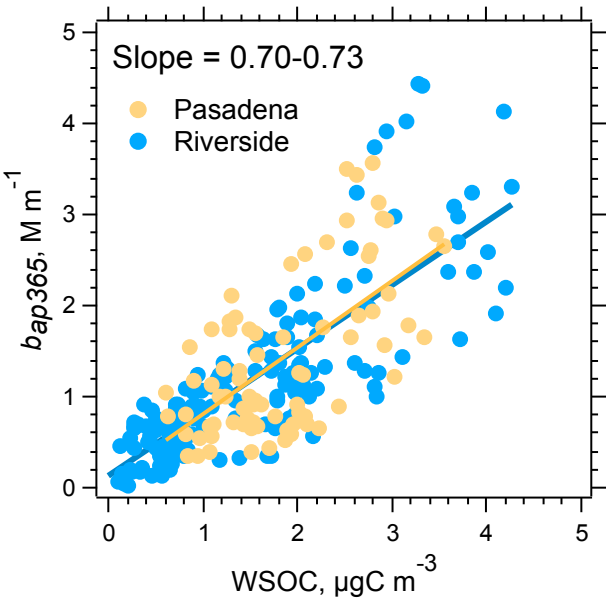

Figure 4.2 Bulk WSOC mass absorption efficiency (MAE, bulk absorption at 365 nm per soluble carbon mass) in Pasadena and Riverside.

The LA spectral dependence of soluble brown carbon, characterized by the absorption Angström exponents ($\mathring{A}_a$), varied between 1.2 and 5.4 with a study mean of 3.2 ±1.2 for curve fits over wavelengths between 300 and 600 nm. The relatively rapid decrease in absorption with increasing wavelength is the characteristic of brown carbon. As shown in Figure 4.3, there was not a strong diurnal variation of $\mathring{A}_a$ despite soluble brown carbon (b_{ap365}) concentrations changing drastically throughout the day. Thus, although the concentrations of light-absorbing WSOC (b_{ap365}) varied substantially due mainly to factors influencing SOA formation (Figure 4.1) and to a lesser extent primary emissions (discussed in Sect. 4.3.2.1), the light absorption properties of the combined chromophores in the solution were very similar, which indicates that the chemical composition of the soluble chromophores was largely similar throughout the day.

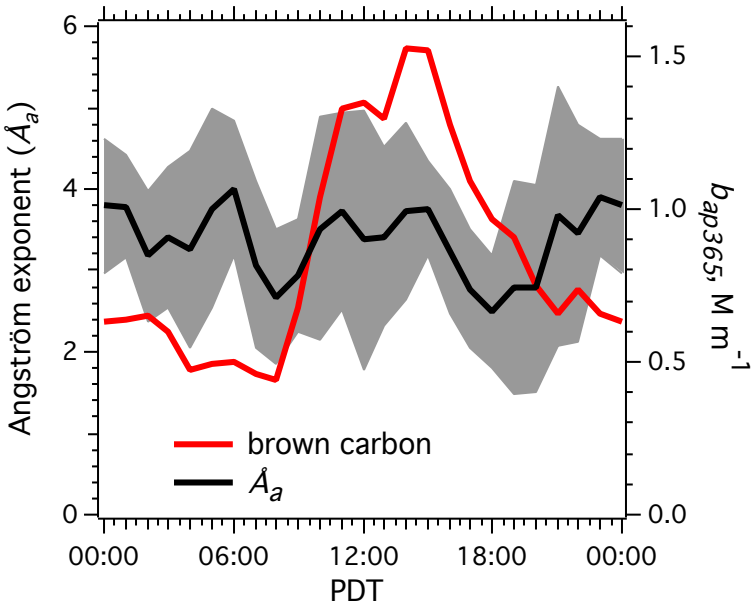

Figure 4.3 Diurnal variation of absorption coefficient (b_{ap365}) and the mean soluble brown carbon Angström exponent ($\mathring{A}_a$) (fitted between 300 and 600 nm) plus/minus one standard deviation (grey shading).

4.3.1.2 Chemical speciation of LA light-absorbing SOA constituents

PAHs emitted from anthropogenic sources are a significant class of SOA precursors in LA [*Hersey et al.*, 2011]. Environmental chamber experiments have shown that the photo-oxidation of aromatics (e.g., toluene) under high-NO_x conditions produces brown SOA [*Jaoui et al.*, 2008; *Zhong and Jang*, 2011]. Fifteen intensive filter samples collected in Pasadena during CalNex (on June 4, 10 and 13 with an integration time of 3-6 hr) were analyzed by UPLC/ESI-HR-Q-ToFMS and a number of nitrogen-containing mono- and poly- aromatic SOA constituents were identified and quantified. Measurements of standard solutions (discussed further below) of these nitro-aromatics with the LWCC-spectrophotomer showed that they absorb light over a wide range of wavelengths (i.e. between 300-500 nm), and depending on their molecular weights, had maximum absorption at different wavelengths (Figure 4.4). Table 4.1 lists the identified nitro-aromatic compounds and the correlations of their ambient concentrations with the overall bulk b_{ap365} measured from the same filter samples. Some of these nitro-aromatics were highly correlated with b_{ap365}, indicating that they likely had similar sources and/or formation processes. Other identified aromatic SOA components that do not have a nitrogen group, such as aromatic acids (e.g., benzoic acid and phthalic acid), absorb mostly below 300 nm and their ambient concentrations were not correlated with b_{ap365}.

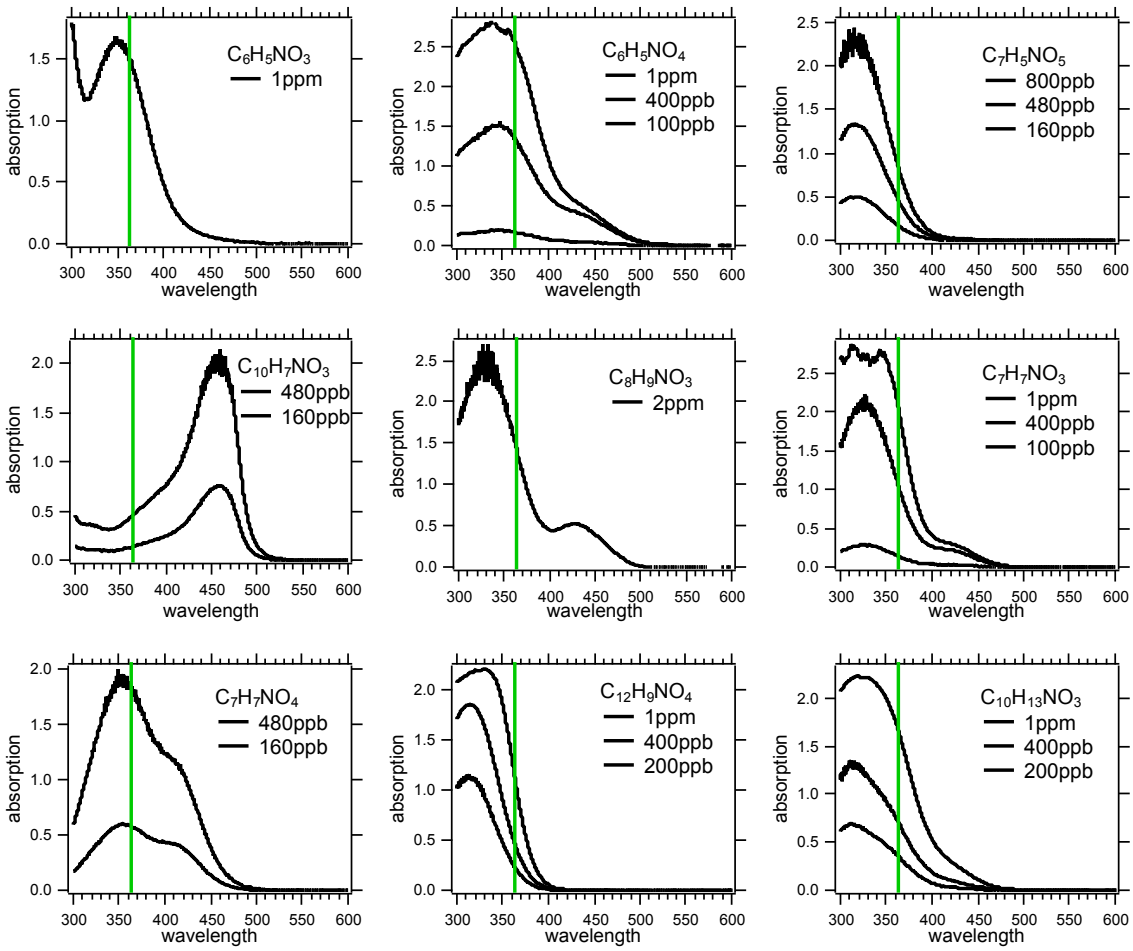

Figure 4.4 UV-Vis absorption spectra of the individual nitro-aromatic compounds identified with UPLC/ESI-Q-ToFMS, recorded with solutions of commercial standards. The example spectra of the standards were recorded at different concentration levels for some of the compounds. The green line indicates a wavelength of 365 nm.

Table 4.1 Identified nitro-aromatic compounds by UPLC/ESI-Q-ToFMS and their correlation coefficients with bulk WSOC light absorption at 365 nm (b_{ap365}).

Formula	ESI ion mode	Molecular structure	r^2 with bulk b_{ap365} (N =15)
*$C_6H_5NO_3$	Negative	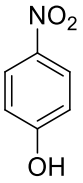	0.06
*$C_6H_5NO_4$	Negative	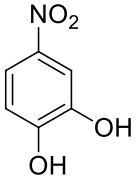	0.84
*$C_7H_5NO_5$	Negative	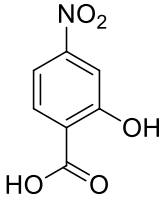	0.79
*$C_{10}H_7NO_3$	Negative	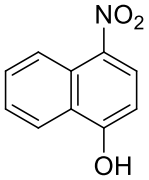	0.56
*$C_8H_9NO_3$	Negative	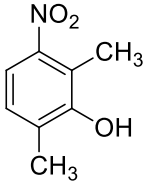	0.19
*$C_7H_7NO_3$	Negative	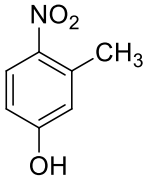	0.18
*$C_7H_7NO_4$	Negative	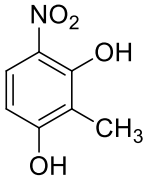	0.38

Table 4.1 Continued.

Formula	ESI ion mode	Molecular structure	r^2 with bulk b_{ap365} (N=15)
*$C_7H_6N_2O_5$	Negative	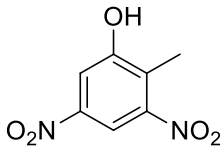	0.00
*$C_{12}H_9NO_4$	Negative	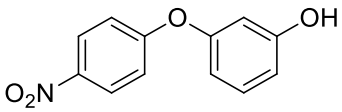	0.77
$C_9H_{11}NO_3$	Negative	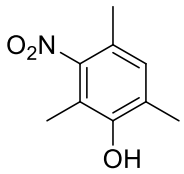	0.49
*$C_{10}H_{13}NO_3$	Negative	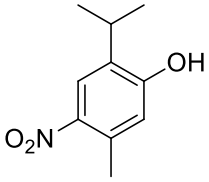	0.35
$C_{14}H_{13}NO_3$	Negative	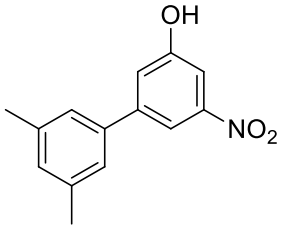	0.50
*$C_{11}H_{15}NO_3$	Negative	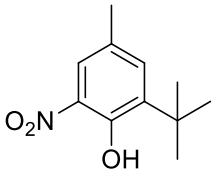	0.67
$C_{16}H_9NO_3$	Negative	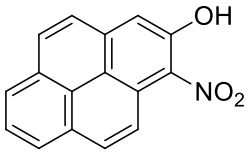	0.64

* Authentic standards available and tested via LWCC.

The contribution of the absorption by each nitro-aromatic compound to the total observed b_{ap365} was estimated from the mass absorption efficiency at 365 nm (MAE_{365}) of the individual compound. Authentic standards were commercially available for eleven of the nitro-aromatic compounds identified (labeled in Table 4.1). The standards were dissolved in 18-MΩ Milli-Q water and diluted in series to a range between 100 ppbC and 2 ppmC. The liquid solutions were then measured for WSOC concentration and light absorption. Figure 4.4 shows example absorption spectra for these standard solutions at different carbon concentration levels. Table 4.2 summarized the bulk MAE_{365} and ambient concentrations of the eight light-absorbing compounds that exhibited positive correlation ($r > 0$) with the total soluble brown carbon. The MAE_{365} of the individual compound was generally more than an order of magnitude larger than the MAE_{365} for ambient brown carbon measured in LA and Riverside (Figure 4.2), or laboratory-generated SOA, such as toluene-SOA (MAE_{350} of 0.57 m^2 g^{-1}) [*Zhong and Jang*, 2011] and aged limonene-SOA (MAE_{350} of 0.07 m^2 g^{-1}) [*Bones et al*., 2010]. The average mass concentrations of individual compounds from the filter samples were in the range of a few ng m^{-3}. As a result, the light absorption of each compound, calculated as the product of the ambient carbon mass concentration and the MAE, accounted for only a few percent of the total absorption. Among the eight compounds, 4-nitrocatechol ($C_6H_5NO_4$) is identified as the largest contributor, which also has the highest correlation coefficient (r^2 = 0.84) with the bulk b_{ap365} (Table 4.1), suggesting a similar formation process of the overall soluble brown carbon and 4-nitrocatechol. Overall, the absorption from these eight nitro-aromatic compounds comprises approximately 3.8% of the bulk b_{ap365} (Table 4.2). This small fraction is consistent with the presence of a large "unresolved complex

mixture" that is typically seen in chromatographic separation of ambient organic aerosols [*Robinson et al*., 2007]. Figure 4.5 shows the UPLC-DAD chromatographs at 365 nm of one CalNex filter sample together with mixed nitro-aromatic standards and blank filter injections. These overlaid chromatographs clearly show that besides the seven compounds identified with the UPLC/ESI-Q-ToFMS, there are many more unresolved species that contribute to the overall light absorption at 365 nm (indicated by the increased baseline between 5 and 13 min only seen in the ambient sample injection). The UPLC/ESI-Q-ToFMS operated in positive ion mode identified several more nitrogen-containing compounds that likely absorb light at 365 nm, but their molecular structures are still tentative. Table 4.3 listed these nitro-containing compounds and the correlation coefficients of their relative abundance (i.e. normalized peak area) with the bulk b_{ap365}. More work is needed to fully characterize and quantify these compounds.

Table 4.2 Contribution of light absorption from each identified nitro-aromatic compound to the total observed bulk b_{ap365}.

Formula	MAE (m^2 $g^{-1}C$)	Ambient concentration (ng m^{-3})	Predicted absorption at 365 nm (M m^{-1})	Percentage of bulk b_{ap365} (%)
$C_6H_5NO_4$	15.4	1.67	0.012	1.37
$C_7H_5NO_5$	8.1	0.92	0.0034	0.39
$C_{10}H_7NO_3$	6.4	0.14	0.00058	0.07
$C_8H_9NO_3$	9.5	0.92	0.0050	0.58
$C_7H_7NO_3$	10.1	1.24	0.0069	0.79
$C_7H_7NO_4$	19.6	0.36	0.0035	0.41
$C_{12}H_9NO_4$	2.22	0.047	0.000064	0.007
$C_{10}H_{13}NO_3$	5.52	0.50	0.0017	0.19

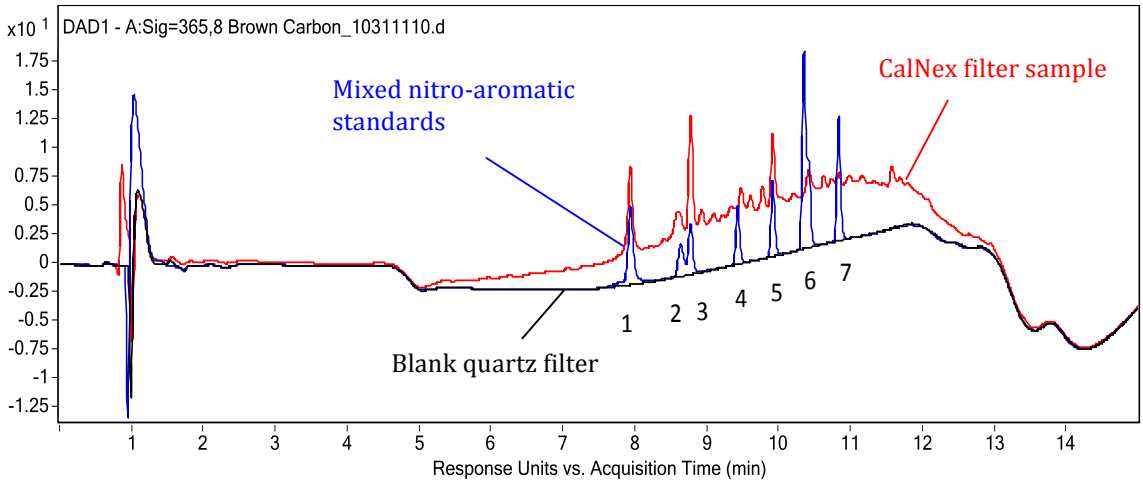

Figure 4.5 Overlaid UPLC-DAD chromatograms at 365 nm of CalNex filter sample, mixed nitro-aromatic standards and blank quartz filter injections.

Table 4.3 The nitrogen-containing compounds identified by UPLC/ESI-Q-ToFMS operated in positive ion mode and their correlation coefficients with bulk WSOC light absorption at 365 nm (b_{ap365}).

Formula	ESI ion mode	r^2 with bulk b_{ap365} (N =15)
$C_5H_5N_5O_3$	Positive	0.01
$C_7H_{10}N_4$	Positive	0.52
$C_8H_{19}N$	Positive	0.77
$C_9H_{19}NO$	Positive	0.48
$C_{10}H_{19}NO_5$	Positive	0.84
$C_{11}H_{15}N_5O$	Positive	0.83

4.3.1.3 Water-soluble fraction of the total brown carbon in LA

As discussed in Sect 4.3.1.1, since the SOA within the LA Basin is relatively fresh, the water-soluble fraction of the total OC is generally low (on the order of 25%). In this section, the soluble fraction of the nominal total brown carbon (i.e. methanol-extract)

is investigated based on intensive filter samples collected at the Pasadena site during CalNex. A punch of the high-volume filter sample was extracted in methanol, and the absorption spectrum was compared to that from the water-extract of another punch from the same sample. *Chen and Bond* [2010] found that using methanol approximately 98% of the OC can be extracted from the filters and thus the absorption by methanol-extracts is considered to represent the absorption of total brown carbon. Figure 4.6a shows the average absorption spectra of water-extracts and methanol-extracts from the 15 filters collected on June 4, 10 and 13 (with an integration time of 3-6 hr) during CalNex. The methanol-extracts have higher absorption than the water-extracts across all wavelengths between 300 and 700 nm, consistent with previous findings by *Sun et al*. [2007] and *Chen and Bond* [2010]. From our data, the absorption by total brown carbon is on average 3.2 ± 1.1 and 20.5 ± 14.1 times higher than that by soluble brown carbon at 365 and 532 nm, respectively (the absorption Angström exponents of the two extracts are compared below). Since WSOC comprised 42-82% of OC for the filter samples, the bulk MAE_{365} of the total brown carbon (absorption by the methanol-extracts per OC mass) was 2.2 times larger than the MAE_{365} for soluble brown carbon. This implies that the water-insoluble fraction of OC was highly absorbing, contributing 16-80% of the total absorption and on average was 4.2 times more absorbing than WSOC. *Chen and Bond et al*. [2010] suggested that these strongly light-absorbing components are likely large molecular PAHs such as quinones from biomass burning and fossil fuel combustion [*Sun et al*., 2007]. The total and soluble brown carbon are well correlated ($r^2 = 0.67$, Figure 4.7a), and the fraction of water-soluble brown carbon exhibited a negative relationship with the ambient EC concentrations (Figure 4.7b), suggesting that the water-insoluble

brown carbon and EC likely have similar sources.

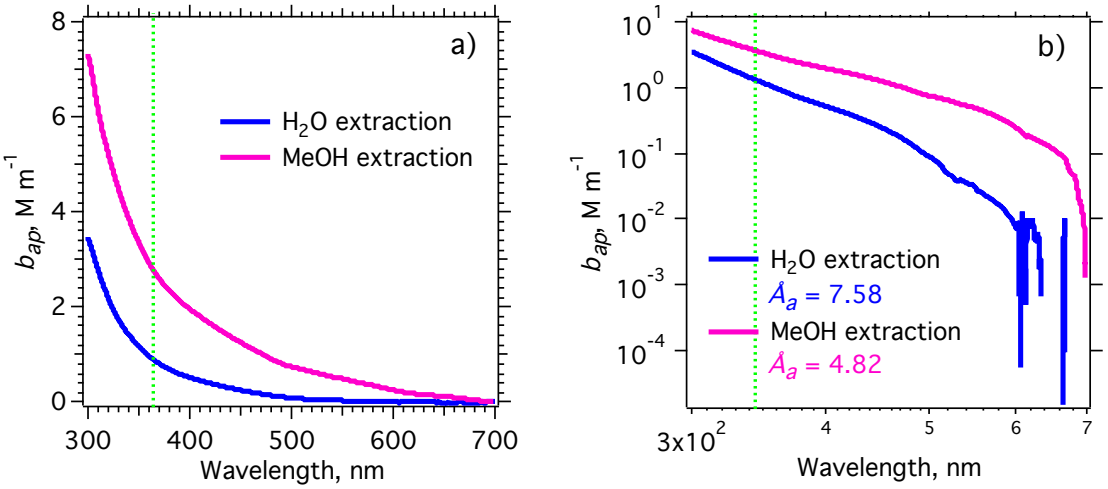

Figure 4.6 Averaged absorption spectra of water and methanol (MeOH) extracted ambient brown carbon from quartz-fiber filter samples during CalNex, plotted on a) linear scale and b) log scale. The Angström exponents ($Å_a$) are given in plot b).

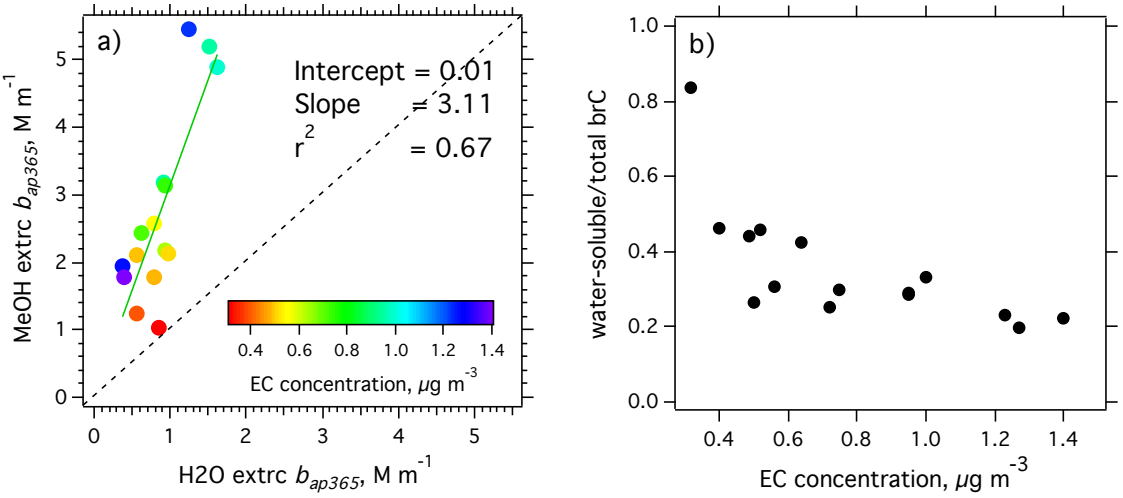

Figure 4.7 Scatter plot of a) methanol (MeOH) versus water extracted brown carbon (bulk absorption at 365 nm), color-coded by EC concentration measured from the filters, and b) the fraction of water-soluble of total brown carbon (methanol-extract) at 365 nm versus EC concentration.

It is noteworthy that the $\mathring{A}_a$ (between 300 and 600 nm) derived from the water-extracted and methanol-extracted brown carbon spectra were significantly different (Figure 4.6b). $\mathring{A}_a$ for water-soluble brown carbon from the filter samples had a mean (± one standard deviation) of 7.58 (± 0.49), in the same range as those reported for biomass burning HULIS [*Hoffer et al*., 2006] and aged SOA in the southeastern U. S. [*Hecobian* et al., 2010], but was significantly higher than the average $\mathring{A}_a$ (3.2 ± 1.2) derived from online soluble brown carbon measurements using PILS (Figure 4.3). In contrast, the total brown carbon from filters extracted in methanol had an average $\mathring{A}_a$ of 4.82 ± 0.49, closer to the online PILS $\mathring{A}_a$. As can be seen from the absorption spectra of the individual nitro-aromatics shown in Figure 4.4, compounds with higher molecular weight tend to absorb more at longer wavelengths, resulting in lower $\mathring{A}_a$, consistent with findings by *Apicella et al*. [2004] showing that more aromatic rings (i.e. a higher degree of conjugation) within the molecules make the absorption shift to longer wavelengths. These combined results suggest that the difference in $\mathring{A}_a$ from various measurements may be related to the solubility of the compounds. Large molecular PAHs that absorb more toward the visible range have a lower water-solubility compared to small organic compounds. Therefore, the absorption spectra of the methanol-extracts are expected to have a lower $\mathring{A}_a$ than those of the water-extracts. Compared to the filters extracted in water, PILS samples may produce a more soluble environment since the solutions are roughly a factor of 10 more dilute and the sample is heated (PILS is based on steam condensation collection system), which may increase the solubility. This may result in a lower $\mathring{A}_a$ of PILS extracts than aqueous filter extracts. Since the mass fraction of the chromophores to the total WSOC is small, differences in light absorption properties between the PILS and filter extracts

would not be detected in comparisons of carbon mass concentrations. More experiments on filter extraction under various conditions can help test these hypotheses, however, the results from this work suggest that measurements of bulk light absorption from aqueous filter extracts (e.g., [*Hecobian et al*., 2010]) are likely to significantly under-predict light absorption, especially at higher wavelengths.

In summary, LA SOA from anthropogenic sources had a consistent brown color and one component of the brown SOA identified is the nitro-aromatic compounds. In the next section (Sect. 4.3.2), online WSOC and light absorption data collected in Atlanta are contrasted to the measurements made in LA, and the factors contributing to the different light-absorbing properties of soluble organic aerosols in these two environments are explored.

4.3.2 Contrasting light-absorbing SOA in LA and Atlanta

4.3.2.1 LA soluble brown carbon

Figure 4.8a shows the diurnal profiles of b_{ap365}, WSOC and EC concentrations at the Pasadena site during CalNex. b_{ap365} followed a consistent diurnal trend in LA that largely tracked the formation and dispersion of SOA. Enhancement in EC near noon (average increase of 0.48 μg C m^{-3}) indicated arrival of the LA plume and was later followed by simultaneous increases in b_{ap365} and WSOC from a background of 0.5 M m^{-1} and 0.9 μg C m^{-3} at ~9:00, respectively, to a daily maximum of 1.5 M m^{-1} and 2.0 μg C m^{-3}, which occurred at 15:00. Brown carbon largely tracked WSOC and other independent measures of SOA throughout the day, indicating a strong association between the two. It is known that incomplete combustion, such as vehicle emissions, also

contributes to primary brown carbon [*Hecobian et al.*, 2010]. Pasadena is a receptor of LA emissions. The advection time from LA and photochemical SOA production in early afternoon resulted in overlapping trends in EC and WSOC (SOA), tending to merge primary and secondary sources of brown carbon. SOA formation was the strongest source, indicated by a stronger correlation of brown carbon with WSOC (r^2 of 0.55) than with EC (r^2 of 0.38) and by differences in weekend-weekday data. Reduced weekend traffic (especially diesel) would be expected to reduce primary emission levels, but have less of an influence on secondary formation (WSOC). The amount of b_{ap365} per EC mass was nearly doubled on the weekend (b_{ap365}/EC linear regression slope in Table 4.4), whereas b_{ap365} to WSOC slopes remained similar, suggesting different sources for brown carbon and EC, but similar secondary production for brown carbon and WSOC.

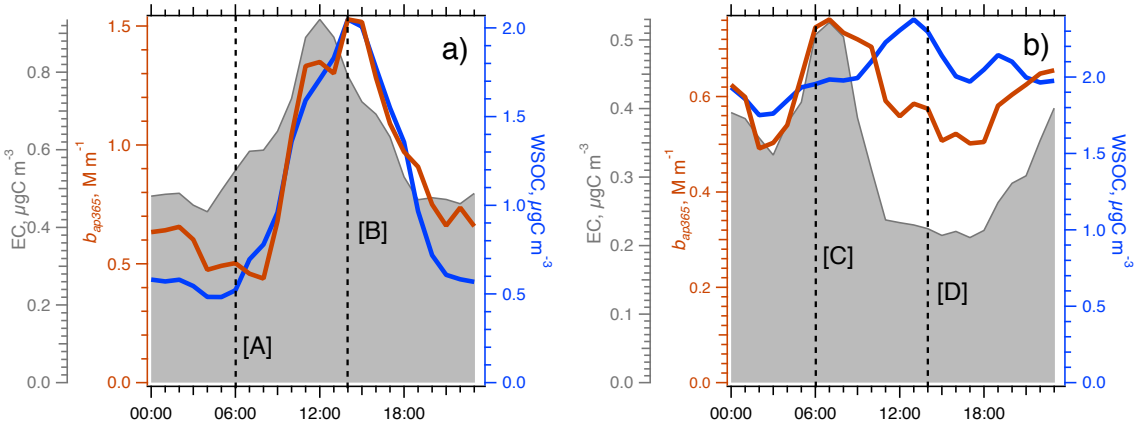

Figure 4.8 Study mean diurnal profiles of the $PM_{2.5}$ components; elemental carbon (EC) and the water-soluble extract light absorption at 365 nm (b_{ap365}) and organic carbon mass (WSOC) measured at a) Pasadena, CA (June 1 to June 15, 2010) and b) Atlanta, GA (Aug 6 to Sep 7, 2010).

Table 4.4 Comparison of mean properties for all study data and for weekday and weekend data. Pasadena and Atlanta weekend data are from 2 weekends and 5 weekends, respectively.

	Pasadena		Atlanta	
b_{ap365}, M m^{-1}	0.88 ± 0.71		0.61 ± 0.38	
WSOC, μg C m^{-3}	1.00 ± 0.72		2.03 ± 1.01	
EC, μg C m^{-3}	0.60 ± 0.33		0.33 ± 0.26	
	Weekday	Weekend	Weekday	Weekend
Slope* (r^2) b_{ap365} vs. EC	1.25 (0.41)	2.45 (0.58)	1.15 (0.44)	1.60 (0.36)
Slope* (r^2) b_{ap365} vs. WSOC	0.77 (0.48)	0.69 (0.73)	0.19 (0.21)	0.11 (0.29)

4.3.2.2 Atlanta soluble brown carbon

Example spectra of WSOC-extracts showing the wavelength dependence of brown carbon absorption for two time periods identified in Figure 4.8 are shown in Figure 4.9. Although a similar spectral dependence of absorption was observed in Atlanta (mean $\mathring{A}_a$ at 3.4 ± 0.7), the association between brown carbon and WSOC in Atlanta was different from that in LA. Variability of brown carbon in Atlanta was more associated with primary vehicle emissions; brown carbon was better correlated with EC (r^2 of 0.50) than with WSOC (r^2 of 0.25), opposite to LA. The average Atlanta diurnal trends show that brown carbon and WSOC exhibited moderate enhancements at different time periods during the day relative to a high background (Figure 4.8b). Since the site is located in the urban center, unlike Pasadena as a LA receptor, Atlanta local rush hour is evident by a strong EC enhancement between 5:00 and 8:00. The dominant brown carbon diurnal feature is that it tracks morning rush hour EC. Boundary layer expansion and reduced traffic account for the sharp EC decrease and leveling off in the afternoon to ~0.2 μgC m^{-3}, roughly a third of that recorded in Pasadena. Photochemical SOA production in urban

Atlanta is identifiable as the daytime increase in WSOC between 9:00 and 18:00, a 20-30% enhancement over the regional background observed at a rural site 55 km northwest of Atlanta (Yorkville, GA). During this period when WSOC (SOA) was photochemically produced within the city, brown carbon only exhibited minor enhancement (Figure 4.8b). Furthermore, unlike LA where the weekday and weekend b_{ap365}/WSOC slopes were similar, in Atlanta this slope was much lower on the weekend. In contrast, the b_{ap365}/EC slopes were similar in Atlanta on weekday and weekend (Table 4.4). In both cities, daily enhancements in brown SOA may be from light-absorbing compounds formed in the gas phase that partition to the particles, such as nitro-aromatics, given that they were produced rapidly. Heterogeneous reactions leading to brown SOA tend to be slower, but may also contribute to brown carbon, especially on a regional basis.

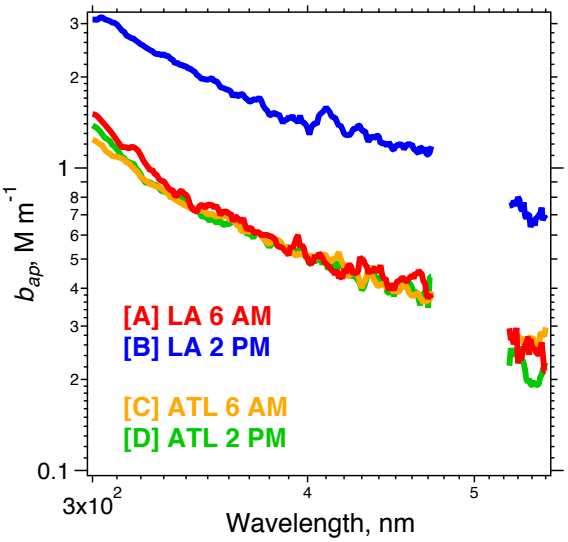

Figure 4.9 Study mean absorption spectra between wavelengths 300 and 550 nm at selected time periods (A-D are identified in Figure 4.8) in Pasadena (n = 15) and Atlanta (n = 29). The gaps in the spectra between 475 and 525 nm are due to instrumentation issues.

4.3.2.3 Regional brown carbon in the southeast

Although fresh Atlanta WSOC is less light absorbing than LA WSOC, our measurements of light-absorbing properties of WSOC throughout the southeastern U.S. show that brown carbon is a ubiquitous component of WSOC [*Hecobian et al.*, 2010]. Similar analytical measurements of brown carbon (b_{ap365}) and WSOC made off-line on aqueous extracts from $PM_{2.5}$ 24-h integrated filters collected at various sites throughout the southeast showed that b_{ap365} and WSOC were correlated at all sites (for rural sites r = 0.5 to 0.7; for urban sites r = 0.7 to 0.9). A factor analysis indicated that in summer the variability of b_{ap365} was linked with aerosol oxalate concentrations [*Hecobian et al.*, 2010]. Although further analysis is needed to understand the source of this brown WSOC and oxalate, the results are consistent with laboratory studies that show water-soluble dicarbonyls, such as glyoxal and methylglyoxal, produced from isoprene oxidation can form brown SOA via aqueous phase reactions, when mixed with a source of nitrogen (e.g. ammonium, amines) [*Shapiro et al*., 2009; *Sareen et al*., 2010]. Aqueous reactions are also a known source of oxalate (e.g., [*Sorooshian et al.*, 2006]). However, given the relatively slow rate of these brown carbon-forming reactions in the aqueous phase (from several hours to ~day) [*Sareen et al.,* 2010], and that no concurrent increase in oxalate was observed between 9:00 and 18:00 within Atlanta (not plotted), it appears that this regional formation process differs from the urban brown carbon source that we associate with the fresh daily WSOC production discussed above.

4.3.2.4 Why is fresh Atlanta WSOC (SOA) less light-absorbing than LA?

Fresh LA WSOC is 4 to 6 times more absorbing per WSOC mass than the fresh

Atlanta WSOC. The slope of b_{ap365}/WSOC in LA ranged from 0.69 (weekdays) to 0.77 $m^2\ g^{-1}C$ (weekends), whereas in Atlanta b_{ap365}/WSOC was only between 0.11 (weekends) and 0.19 $m^2\ g^{-1}C$ (weekdays) (Table 4.4).

Differences in light-absorbing properties of fresh SOA between LA and Atlanta may be attributed to different SOA precursors within the two urban environments, resulting in different types of SOA, and possibly SOA formation mechanisms. Radiocarbon analysis of CalNex PM_1 filters show a significant afternoon enhancement of only fossil carbon; the increase of fossil carbon between 12:00 and 18:00, relative to other times of day, was ~4.5 times larger than that of modern carbon. Our observed linkage between aromatic photo-oxidation products in a high-NO_x environment and brown SOA (b_{ap365}), and overall correlation of b_{ap365} with LA WSOC, suggest brown SOA may be a general characteristic of fresh anthropogenic SOA in urban (high NO_x) environments. Radiocarbon analysis of Atlanta summertime WSOC has shown that it is largely modern [*Weber et al.*, 2007], consistent with high isoprene emissions in the southeast [*Müller et al.*, 2008]. Thus, one possible reason why urban Atlanta produces less light-absorbing SOA within the city is that biogenic VOCs play a more dominant role.

Chamber experiments have investigated the optical properties of SOA produced from anthropogenic and biogenic VOCs and found greater light absorption from anthropogenic (aromatic) components [*Zhong and Jang*, 2011; *Nakayama et al*., 2010]. *Jaoui et al.* [2008] found that a significant mass of light-absorbing compounds were formed from irradiation of toluene/α-pinene mixture in the presence of NO_x; however, when isoprene was introduced to the mixture, the SOA became whiter due to faster

isoprene oxidation reactions than aromatics, which sequestered NO_x and consumed the limited oxidants within the chamber. The *Jaoui et al.* [2008] results are curiously similar to our LA-Atlanta comparison in that fresh SOA formed in an anthropogenic (aromatics)-dominated environment is much more light-absorbing than one involving a mix of anthropogenic and biogenic (isoprene) VOCs. However, the *Jaoui et al.* [2008] experiments were performed under dry (30% RH) conditions, and it is known that isoprene and aromatic oxidation in high-NO_x regimes preferentially leads to low molecular weight (higher vapor pressure) water-soluble carbonyls that can partition to water and form SOA [*Ervens et al.*, 2011]. Thus, if sufficient aerosol water is present, an aqueous SOA route may be important in a high-NO_x/isoprene environment. Evidence for enhanced partitioning of WSOC to the particle phase has been observed in Atlanta [*Hennigan et al.*, 2009] but not in LA; an analysis of CalNex data suggests the partitioning preference in LA was to the pre-existing organic phase [*Ervens et al.*, 2011]. Other ambient studies have also reported preferential formation of modern (biogenic) SOA in polluted environments [*de Gouw et al.*, 2005; *Weber et al.*, 2007; *Hoyle et al.*, 2011].

4.3.3 Optical importance of brown carbon

Due to its high spectral dependence, the brown carbon absorption in the UV range is significant, and thereby may influence photochemistry and thus reduce tropospheric ozone concentration [*Jacobson*, 1998]. Compared to black carbon or soot, organic compounds are weak absorbers in the visible range and their overall contribution to the direct radiative forcing is considered minor, especially in the urban environments where

BC emissions from motor vehicles are large [*Andreae and Gelencsér*, 2006]. An analysis of the LA aerosol optical properties during CalNex suggested that soluble brown carbon contributed less than 25% to the overall measured absorption in the mid-visible range [*Thompson et al*., 2012], contributions from the total brown carbon (methanol-extract) would be significantly larger. However, in rural regions where BC level is low and SOA from biogenic emissions are prevalent, the absorption by brown carbon may play a larger role. For example, based on filter measurements throughout 2007 at Yorkville, a rural site in Georgia, WSOC on average had an MAE of 0.12 m^2 g^{-1} at 365nm [*Hecobian et al*., 2010]. Given that the typical WSOC mass concentration in the summer was approximately 6 μgC m^{-3} [*Weber et al*., 2007], the expected absorption by WSOC at 365 nm in Yorkville was 0.72 M m^{-1}. Although pure BC has a much higher MAE (7.5 m^2 g^{-1}) compared to WSOC [*Bond and Bergstrom*, 2006], in rural areas like Yorkville the EC concentration are generally very low (~0.15 μgC m^{-3}) [*Weber et al*., 2007]. Therefore, the absorption by soluble brown carbon and BC are comparable near the UV range. Depending on the $\mathring{A}_a$ of soluble brown carbon (~7.0 from filter extracts and ~3.5 based on online PILS data), the absorption coefficient at mid-visible wavelengths (e.g., 532 nm) would fall to 0.25 ($\mathring{A}_a$ = 3.5) to 0.07 M m^{-1} ($\mathring{A}_a$ = 7.0), contributing roughly 10 to 33% to the total absorption, which is still significant. It is noteworthy that these estimates are based on bulk light absorption measurements and do not consider particle size. Recent work on size-resolved measurements of soluble brown carbon and application of simple Mie theory indicates that the estimated absorption by brown carbon would be even higher (Jiumeng Liu, personal communication). A detailed radiative transfer model that includes information on the concentration and distribution of brown carbon aerosols and possible

BC coatings effects is needed to fully address the optical impacts of brown carbon.

4.4 Conclusions and implication

Online and offline measurements of brown carbon were carried out in the spring-summer of 2010 in the LA Basin and Atlanta to study the optical and chemical properties of light-absorbing organic aerosols. The major source of LA soluble brown carbon was secondary organic aerosol (SOA) formation. Radiocarbon measurements of filter samples show that LA SOA was mainly from fossil carbon and chemical analysis of aqueous filter extracts identified nitro-aromatic compounds as one component of LA brown SOA, but the contribution of individual compound to the total observed light absorption was small (on the order of several percent). The absorption by total brown carbon extracted in methanol was on average 3.2 ± 1.1 and 20.5 ± 14.1 times higher than that by soluble brown carbon at 365 and 532 nm, respectively, suggesting that the water-insoluble organic aerosol was much more absorbing than the soluble fraction in LA.

The WSOC mass absorption efficiency (MAE) of the freshly-formed WSOC, defined as the bulk absorption per soluble carbon mass at 365 nm, was 4 to 6 times higher in LA than in Atlanta. Interpreting soluble brown carbon as a property of fresh anthropogenic SOA, the difference in the MAE between these two cities suggests most fresh secondary WSOC formed within Atlanta is not from an anthropogenic process similar to LA. Contrasting emissions of biogenic volatile organic compounds may account for these differences. The results between LA and Atlanta suggest that water-soluble brown carbon can be a prevalent component of SOA freshly produced from anthropogenic compounds and a useful tool to investigate SOA formation processes.

Applied to a LA-Atlanta comparison, it supports other studies that suggest SOA formed in an anthropogenic/biogenic VOC mixture under high-NO_x conditions would preferentially generate SOA from the biogenic emissions and alter the SOA properties (e.g., optical) and possibly formation mechanism (e.g., partitioning preference, discussed in Chapter 5).

CHAPTER 5

GAS-PARTICLE PARTITIONING OF WSOC IN LOS ANGELES AND ATLANTA

5.1 Background

How semi-volatile compounds partition between the gas and particle phase influences the mass, size and chemical composition of the secondary organic aerosols formed. Despite its fundamental importance to SOA formation, few studies have reported gas-particle partitioning in the ambient atmosphere. Previous studies of SVOC partitioning have been limited to a few alkanes and alkanoic acids [*Williams et al*., 2009], carbonyls [*Matsunaga et al.,* 2005], carboxylic acids [*Fisseha et al.,* 2006; *Liu et al*., 2012], and PAHs [*Terzi and Samara*, 2004]. Instead of investigating single compounds, an alternative approach for studying partitioning is to measure a group of compounds with similar properties, such as water-soluble organic carbon in both gas ($WSOC_g$) and particle phase ($WSOC_p$) [*Hennigan et al.,* 2008a, 2009]. This approach allows for the examination of integrated gas-particle partitioning behaviors of a large class of SVOC compounds and a substantial fraction of SOA mass. An analysis by *Hennigan et al.* [2008a] found that in Atlanta WSOC partitioning was related to ambient relative humidity (RH), and hence aerosol water content, highlighting the importance of uptake of soluble VOCs by dissolution as a source of SOA mass and the potential for some of those compounds to remain in the aerosol phase through multiphase reactions that produce lower volatility products. The reversibility of the observed WSOC partitioning, especially when RH decreases, may be significant, but cannot be obtained from this data set.

Previous study in Mexico City has found that roughly 25% the WSOC may re-partition when RH was reduced [*Hennigan et al.*, 2008b].

In this chapter, we contrast the partitioning of WSOC in LA and Atlanta based on data obtained from a suite of instruments deployed during the spring/summer of 2010. We find that gas-particle partitioning of WSOC differs between Atlanta and LA, providing important insight on SOA formation pathways in these two urban environments. The findings are consistent with additional contrasts in the partitioning behaviors of formic acid [*Liu et al*., 2012], concentrations and trends of specific aerosol components (oxalate), as well as some physical properties of SOA (WSOC light absorption, detailed in Chapter 4) between the two cities.

5.2 Experimental methods

5.2.1 Field sites

Ambient gas and particle measurements were carried out in Pasadena, CA and Atlanta, GA in the spring and summer of 2010, respectively; each study was one month in duration. Measurements at the Pasadena ground site were conducted on the campus of the California Institute of Technology from May 15 to June 15, 2010 as a part of the CalNex-LA field campaign. The site (34.140582 N, 118.122455 W) was located ~16 km downwind of downtown LA, and was regularly impacted by urban plumes advected from LA [*Veres et al*., 2011]. General details of the sampling location and spring/summer climatology were provided by *Hersey et al*. [2011] and *Washenfelder et al*. [2011]. Atlanta measurements were made from August 6 to September 7, 2010 in the rooftop laboratory of the Ford Environmental Science and Technology building on the Georgia Institute of Technology (GIT) campus (33.778427 N, 84.396181 W) located in central

Atlanta. The measurement platform was 30-40m above the ground, situated ~400 m from a heavily traveled interstate highway. A number of studies have reported ambient data collected from this site [*Hennigan et al*., 2008a; 2009; *Hecobian et al*., 2010; *Zhang et al*., 2011].

5.2.2 Instrumentation

5.2.2.1 Gas and particle phase WSOC measurements

Gaseous and particulate WSOC (i.e. $WSOC_g$, $WSOC_p$) concentrations were determined with a Mist Chamber/Particle-Into-Liquid Sampler–Total Organic Carbon Analyzer (MC/PILS-TOC) system [*Hennigan et al*., 2009]. During CalNex, the instruments were situated inside a trailer where the temperature was kept at ~25 °C. The sample inlet was ~7 m above the ground and 8.8 m long, and were insulated to minimize the temperature and RH changes of the sampled air before entering the instruments. Gas-phase samples were collected in a five-minute batch using a glass MC fitted with a Teflon filter (47 mm dia., 2.0 μm pore size, Pall Life Sciences) upstream to remove particles in the sampled air. Aerosol samples were collected continuously via a PILS with a $PM_{2.5}$ cut size cyclone and a *parallel* plate carbon *denuder [Eatough, 1993]*. Both gaseous and particulate samples in the aqueous stream were transferred through a 0.45 μm pore PTFE syringe filter (Fisher Scientific) alternatively to a single TOC analyzer (GE Analytical) to quantify the carbon content in the solution. For the PILS channel, $PM_{2.5}$ light absorption spectra of soluble aerosol components were measured using a UV-Vis spectrophotometer with 1-m liquid-waveguide capillary absorption cell (World Precision Instruments) placed upstream of the TOC analyzer [*Zhang et al*., 2011].

5.2.2.2 Other co-located aerosol measurements

$PM_{2.5}$ organic carbon (OC) and elemental carbon (EC) were quantified semi-continuously with a Sunset Labs OCEC Analyzer (Sunset Laboratory Inc., Tigard, OR). The measurements consisted of a 45-min sampling period followed by 15-min of analysis. A parallel plate carbon denuder was placed inline to remove volatile gases [*Eatough et al*., 1993]. Periodic blank measurements were made throughout the study by placing a Teflon filter (47 mm dia., 2.0 μm pore size, Pall Life Sciences) on the $PM_{2.5}$ inlet. Blank-corrected optical EC and OC data are reported in this paper. $PM_{2.5}$ soluble organic acids (e.g., formate and oxalate) and inorganic anions (e.g., NO_3^-) were measured with a PILS coupled to a Dionex Ion Chromatograph with conductivity detection (PILS-IC) [*Liu et al*., 2012].

Exclusive to the CalNex study, non-refractory PM_1 (NR-PM_1) components were measured with a high-resolution time-of-flight aerosol mass spectrometer (AMS, Aerodyne Research Inc.) [*DeCarlo et al*., 2006; *Hayes et al*., 2012]. Further separation of AMS OA spectra was achieved using Positive Matrix Factorization (PMF) [*Ulbrich et al*., 2009]. In the following analysis of the CalNex data, AMS NR-PM_1 NO_3- is reported since PILS-IC soluble $PM_{2.5}$ NO_3- is shown to be significantly higher due to contributions from $NaNO_3$ [*Liu et al*., 2012; *Hayes et al*., 2012]. In Atlanta where NaCl is negligible [*Zhang et al*., 2010], PILS-IC $PM_{2.5}$ NO_3- is reported. AMS OA mass (OM) and Sunset Labs OC were highly correlated (for complete study r2 = 0.76), but OM/OC ratios were significantly higher than expected (regression slope of 3.3 compared to 1.4–2.3 expected for typical urban environments [*Turpin and Lim*, 2001]) [*Hayes et al.,* 2012]. This difference was likely attributed to the loss of semi-volatile compounds from the inline

carbon denuder or the collection filter media within the OCEC analyzer [*Grover et al.,* 2008]. Recent measurements (unpublished) in Atlanta for two weeks in the fall of 2011 comparing an Aerosol Chemical Speciation Monitor (ACSM, Aerodyne Research Inc. [*Ng et al*., 2011]) with the same Sunset Labs OCEC instrument, operated identically to the CalNex study, showed excellent agreement (OM/OC regression slope of 1.7, r2 = 0.92) between the two instruments, which is consistent with substantially lower contributions of semi-volatile SOA in Atlanta [*Peltier et al*., 2007]. In the following analysis, we focused on the qualitative relationship between WSOC gas-particle partitioning and OC mass since only OC data were available in both LA and Atlanta. LA data are reported in PDT and Atlanta data in EST. All data are reported at ambient temperature and pressure.

5.3 Results

5.3.1 General diurnal trends of gaseous and particulate pollutants

LA Diurnal Profiles. Regular and distinct diurnal trends in primary and secondary gas and particle phase species were observed at the LA site throughout the measurement period (Figure 5.1a). Primary emissions from local sources were identified by the morning rush hour peak of EC and other primary VOCs (not plotted) between 5:00 and 8:00, which were then followed by a substantially larger enhancement of EC (ΔEC of 0.48 μgC m^{-3}) at 12:00 as air masses were transported from downtown LA to the site after 3-5 hours advection time [*Veres et al*., 2011]. Both $WSOC_g$ and $WSOC_p$ reached their daily maximum concentrations following EC peak abundance in the early afternoon when solar radiation was most intense, indicating photochemical production as a major source. On a diurnal basis, $WSOC_g$ steadily increased from a morning minimum of 5.2

µgC m^{-3} at 5:00 to a daily maximum of 9.6 µgC m^{-3} at 13:00. The variation of $WSOC_p$ concentration closely tracked that of AMS OOA (oxygenated organic aerosol) component, showing substantial enhancement from a background of 0.6 µgC m^{-3} in the late evening and early morning to a peak value of 1.7 µgC m^{-3} at 14:00. The correlations of $WSOC_p$ with OOA and SV-OOA (semi-volatile OOA) were both reasonably good (r^2 = 0.74 and 0.67, respectively), suggesting that the WSOC mass formed in the afternoon was mainly less aged, semi-volatile oxygenated organic species.

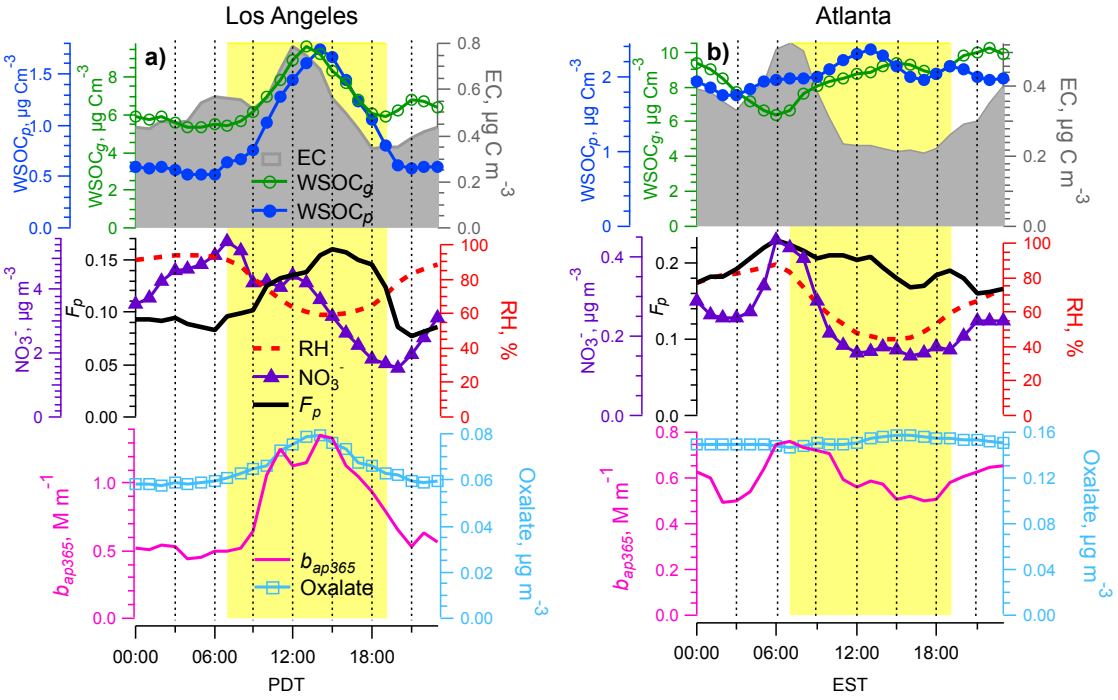

Figure 5.1 Average diurnal variations of $WSOC_g$, $WSOC_p$ and EC (top panel), WSOC partitioning coefficient (F_p), NO_3^- and RH (middle panel), oxalate and soluble brown carbon (indicated by b_{ap365}) (bottom panel) in a) LA and b) Atlanta. The yellow shadings in both plots indicate daytime periods when solar radiation is above zero.

Table 5.1 Summary of statistics of VOC emissions and measured species in Pasadena (LA) and Atlanta during the sampling periods. Anthropogenic VOC emissions are from EPA National Emissions Inventory (NEI). Isoprene emission data are from MEGAN-ECMWF [*Müller et al*., 2008].

Sampling period		Pasadena, CA May 15 - Jun 15, 2010	Atlanta, GA Aug 6 - Sep 7, 2010
VOC emission (Molecule Carbon/cm^2/s)	Anthropogenic	3.27×10^{13}	1.94×10^{13}
	Isoprene	8.06×10^{11}	3.85×10^{12}
$WSOC_g$ ($\mu gC\ m^{-3}$)	Mean ± std.	6.69 ± 3.10	8.64 ± 3.34
	Max	18.52	25.27
	Min	1.10	2.96
$WSOC_p$ ($\mu gC\ m^{-3}$)	Mean ± std.	0.90 ± 0.66	2.04 ± 1.00
	Max	3.68	5.04
	Min	0.01	0.16
F_p	Mean ± std.	0.11 ± 0.05	0.19 ± 0.07
	Max	0.23	0.40
	Min	0.002	0.018
Oxalate ($\mu g\ m^{-3}$)	Mean ± std.	0.065 ± 0.023	0.152 ± 0.019
	Max	0.148	0.217
	Min	0.015	0.127

Atlanta Diurnal Profiles. Diurnal trends of EC, $WSOC_g$ and $WSOC_p$ observed in central Atlanta were distinctly different from those in LA (Figure 5.1b). Unlike the CalNex measurement site, the Atlanta site was located in the urban center and therefore was immediately impacted by local emissions, identified from the diurnal variation of EC. EC exhibited a clear morning rush hour enhancement of 0.19 $\mu gC\ m^{-3}$ (from 0.34 $\mu gC\ m^{-3}$ to 0.53 $\mu gC\ m^{-3}$) between 4:00 and 7:00 from primary vehicle emissions, and decreased sharply afterwards to a daily minimum of 0.21 $\mu gC\ m^{-3}$ in the afternoon as the boundary layer expanded. The average EC concentration in Atlanta (0.33 ± 0.26 $\mu gC\ m^{-3}$) was ~65% of that in LA (0.51 ± 0.30 $\mu gC\ m^{-3}$) during the sampling periods, in good

agreement with anthropogenic VOC emissions in Atlanta being ~60% of those in LA based on emission inventories (Table 5.1). However, while $WSOC_g$ concentrations tended to be in the same range at the two sites, the mean $WSOC_p$ concentration was significantly higher in Atlanta (Table 5.1).

Unlike LA where $WSOC_g$ and $WSOC_p$ exhibited regular and similar diurnal patterns, in Atlanta both had only moderate enhancements relative to a high background and reached their maximum concentrations at different times of the day. As shown in Figure 5.1b, photochemical production led to an increase in $WSOC_p$ concentration between 9:00 and 16:00, whereas $WSOC_g$, representative of the overall water-soluble SVOC trend, continued to build up throughout the day and reached a daily maximum of 10.0 μgC m^{-3} at 23:00. This nighttime enhancement in $WSOC_g$ has been observed in Atlanta during previous summer studies and is thought to be associated with O_3 and NO_3 radical oxidation of biogenic VOCs that persist late into the evening [*Hennigan et al*., 2009]. $WSOC_p$ concentrations at night returned to a regional background level of ~2.0 μgC m^{-3}, suggesting SVOC formed through dark reaction mechanisms did not contribute significantly to the SOA mass relative to daytime production, as has been reported in other studies [*Hennigan et al*., 2009].

5.3.2 WSOC gas-particle partitioning

5.3.2.1 RH and particle liquid water content (LWC)

Particle liquid water content (LWC) was predicted with the ISORROPIA-II thermodynamic equilibrium model [*Fountoukis and Nenes*, 2007] for the NH_4^+-SO_4^{2-}-NO_3^- system, using AMS NR-PM_1 data during CalNex (which ignores the influence of

supermicron particles that tend to contain most of the sea-salt related species such as NaCl and $NaNO_3$ [*Murphy et al*., 2006]) and PILS-IC $PM_{2.5}$ data in Atlanta (where salts are not prevalent [*Zhang et al*., 2010]). Local meteorological data (i.e. RH and temperature) were used for both cities. The model results are summarized in Table 5.2. As expected, in both cities LWC exhibited a positive relationship with ambient RH, and LWC increased rapidly at RH levels above 80%, indicating substantial water uptake by the inorganic components when ambient RH reached the deliquescence point of the particles in the modeled system. Due to the limitations with model-predicted LWC and the fact that the predicted LWC was highly sensitive to RH (especially for RH above 90%), for simplicity in the following analyses, ambient RH was used as a proxy of LWC and hence the aerosol hygroscopicity.

Table 5.2 Mean particle liquid water content (LWC) predicted by ISORROPIA-II and the average F_p values for each RH bin in LA and Atlanta.

	Los Angeles		Atlanta	
RH bin (%)	LWC (μg m^{-3})	F_p	LWC (μg m^{-3})	F_p
20-30	0.30 ± 0.12	0.102 ± 0.021	0.29 ± 0.21	0.159 ± 0.053
30-40	0.59 ± 0.41	0.094 ± 0.041	0.86 ± 0.57	0.175 ± 0.063
40-50	1.11 ± 0.61	0.127 ± 0.040	1.34 ± 0.72	0.168 ± 0.066
50-60	3.31 ± 2.59	0.149 ± 0.042	1.77 ± 0.98	0.175 ± 0.064
60-70	5.80 ± 3.03	0.145 ± 0.045	2.51 ± 1.46	0.188 ± 0.061
70-80	7.35 ± 4.53	0.123 ± 0.052	3.41 ± 1.94	0.204 ± 0.064
80-90	11.80 ± 9.12	0.096 ± 0.040	5.61 ± 3.00	0.225 ± 0.062
90-100	151.26 ± 208.56	0.095 ± 0.035	56.37 ± 96.90	0.264 ± 0.050

5.3.2.2 Diurnal variation of WSOC partitioning coefficient (F_p)

Partitioning behavior of WSOC in Atlanta has been investigated by exploring the

dependence of F_p on possible absorbing aerosol components, where F_p is defined as the fraction of total WSOC ($WSOC_g$ + $WSOC_p$) in the particle phase ($WSOC_p$) [*Hennigan et al*., 2008a; 2009]. Figure 5.1 (middle panel) shows the diurnal variations of F_p in LA and Atlanta, together with the diurnal profiles of nitrate aerosol concentrations and ambient RH. NO_3^- is formed by partitioning of HNO_3 to the particle phase and is enhanced by high LWC, low temperature, and the presence of NH_3 due to sensitivity to particle pH. During CalNex, non-refractory NO_3^- was the dominant inorganic anion in the fine aerosol mode, mainly in the form of NH_4NO_3 [*Hayes et al*., 2012]. *Liu et al.* [2012] examined CalNex nitrate partitioning and found a strong dependence of NO_3^-/HNO_3 ratio on ambient RH. Since the diurnal variability of NO_3^- during CalNex resembled that of the NO_3^-/HNO_3 ratio [*Liu et al*., 2012] and no HNO_3 measurement was made in Atlanta, only the NO_3^- trend was plotted in Figure 5.1 to represent the partitioning behavior of nitrate aerosol. As expected, in both LA and Atlanta, NO_3^- exhibited a daily maximum concentration in early morning, coinciding with higher RH and lower T, similar to previous observations in Mexico City by *Hennigan et al*. [2008b] where they have shown that comparisons of NO_3^- and $WSOC_p$ can provide unique insights on secondary aerosol formation processes.

F_p of WSOC had different diurnal patterns and correlations with aerosol water in LA and Atlanta. In Atlanta, peak F_p coincided with NO_3^- at 6:00 when RH was also the highest of the day. Shortly after sunrise, NO_3^- concentration started to decrease as the particles began to dry out, and F_p did not follow the sharp decrease of NO_3^-, but instead remained at ~0.20 until the late afternoon, then decreased as $WSOC_p$ was approaching background levels. In contrast, during CalNex, F_p largely tracked photochemically

produced $WSOC_p$ and thus followed an opposite diurnal trend to NO_3^- and RH. These different diurnal F_p patterns are apparently related to the different gas-particle partitioning behaviors of WSOC in these two contrasting cities, which will be discussed next.

5.3.2.3 Partitioning preference of WSOC in LA and Atlanta

The partitioning of a species between the gas and particle phase in environmental chamber experiments can be predicted by the gas-particle absorptive partitioning theory by introducing the temperature-dependent partitioning coefficient (K_p). At a given temperature, the partitioning of SVOCs is highly dependent upon the mass loading of the absorptive organic aerosols [*Pankow*, 1994; *Odum et al*., 1996]. However, recent laboratory studies have revealed the importance of an additional SOA formation route, involving dissolution of water-soluble VOCs and SVOCs (e.g., small carbonyls) into particle water followed by hydration and possibly further oxidation to lower volatility products [*Ervens et al*., 2011 and references therein]. Absorption to water has been indirectly observed in the ambient atmosphere through the relationship of F_p with RH (and hence particle liquid water content) in Atlanta [*Hennigan et al*. 2008a; 2009] and the positive relationship between RH and the fraction of organic acids in the total organic aerosols during airborne studies off the Pacific coast and over the continental U. S. [*Sorooshian et al*., 2010].

The F_p–RH relationship: Figure 5.2 shows the contrasting WSOC partitioning behaviors relative to ambient RH in LA and Atlanta. As expected from the diurnal trends, there is no well-defined relationship between F_p and RH (r = -0.36) in LA. The highest median F_p values occur at RHs between 50-70%, generally in the middle of the day when

most SOA was photochemically produced. However, despite on average a 13% lower RH in Atlanta than in LA during the sampling periods (Figure 5.1, middle panel), the F_p observed in Atlanta exhibited a strong dependence on RH, consistent with findings by *Hennigan et al*. [2008a] in the summer (May through September) of 2007. Atlanta F_p showed little variation with an average median value of 0.17 ± 0.01 between 20–70% RH, and increased sharply with RH when RH was greater than 70%. F_p reached a maximum median value of 0.26 at RH greater than 90%, translating to a mass increase of $WSOC_p$ due to uptake by water of ~0.51 μgC m^{-3}.

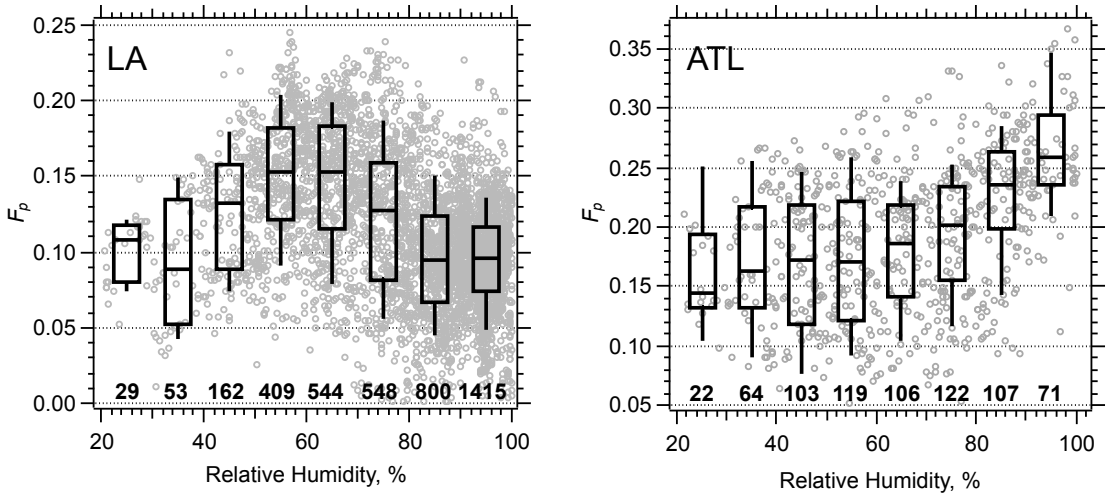

Figure 5.2 Box plots of F_p versus RH in LA and Atlanta. Data points shown as grey open circles are binned by RH. Median values (horizontal bars), 25th and 75th percentiles (lower and upper box bounds, respectively), and 10th and 90th percentiles (lower and upper whiskers, respectively) are shown in the plots. Numbers under each box indicate the number of data points in each RH bin.

The F_p–OC relationship: The dependence of F_p on OC mass also differed between the two cities (Figure 5.3). For LA aerosols there was an overall correlation

between F_p and OC (r^2 = 0.35) (for F_p and AMS OM correlation, r^2 = 0.28), and the median F_p from the binned data is strongly correlated with binned OC (r^2 = 0.99) (for binned F_p and AMS OM correlation, r^2 = 0.96), suggesting that the water-soluble SVOC partitioning was dependent on the mass concentration of the organic phase (OA). Although the characteristics of the absorbing organic phase are somewhat ambiguous [*Song et al.,* 2007; *Hallquist et al.,* 2009], in LA the absorbing medium is probably secondary organic aerosols since the dependence of F_p on AMS OOA mass was much stronger (r^2 = 0.97 for binned data) than on HOA (hydrocarbon-like organic aerosol) mass (r^2 = 0.63 for binned data). The correlation between F_p and OA was also consistent with the diurnal trends, where the daily peak of F_p coincided with the peaks of major SOA components such as $WSOC_p$ (Figure 5.1a) and SV-OOA. We note that the correlation between F_p and OC in LA might be partly due to the strong correlation between $WSOC_p$ and OC (r^2 = 0.73) since the sampled air masses were advected from downtown LA, which tended to merge primary emissions and secondary formation processes and resulted in highly correlated air masses. However, the F_p dependence on OC is not likely to be solely driven by the correlated air masses since a tighter correlation between $WSOC_p$ and OC was found in Atlanta (r^2 = 0.79), where a similar dependence of F_p on OC mass was not observed. In Atlanta the F_p-OC relationship appeared to be more scattered and complex. There was only a weak dependence of F_p on OC at lower OC concentrations. At higher OC concentrations, F_p leveled off at a median value of ~0.21.

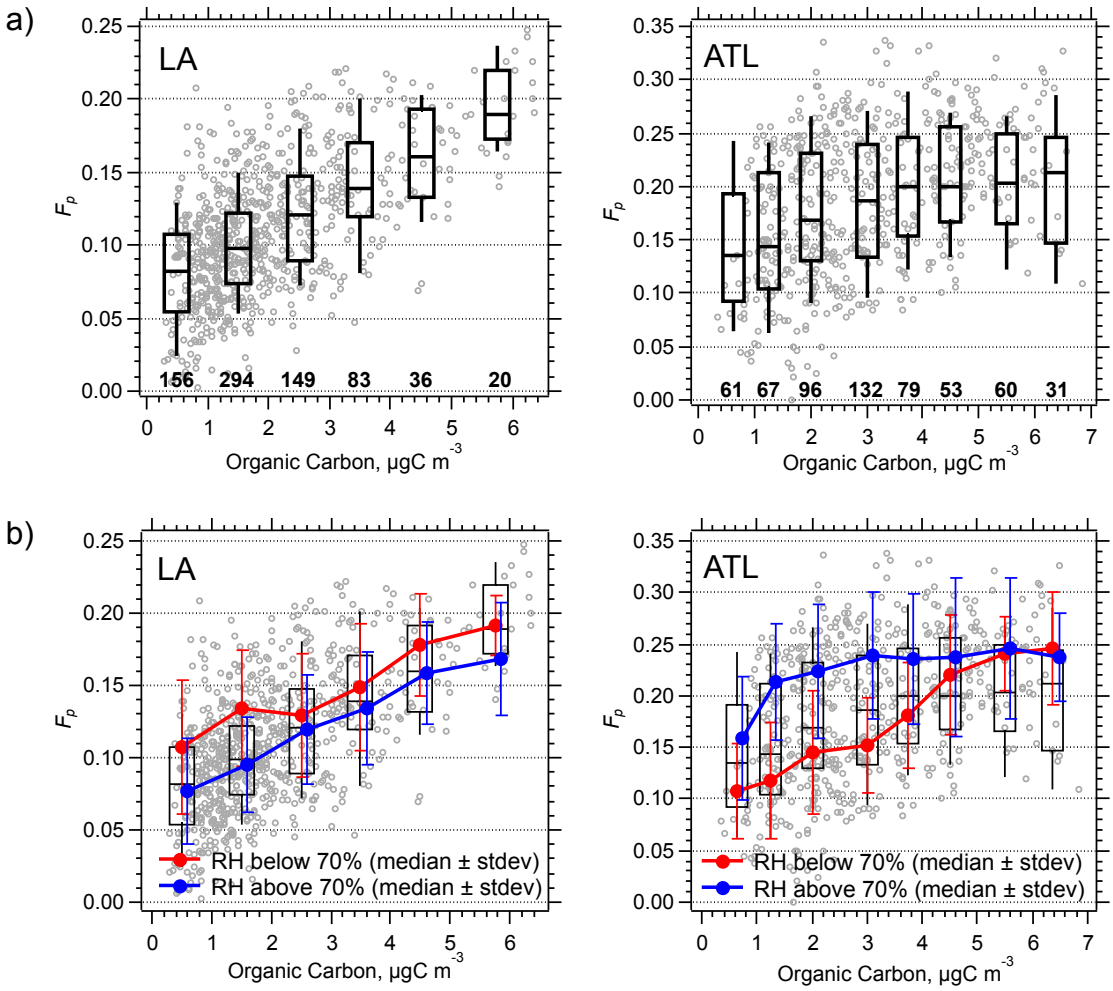

Figure 5.3 F_p versus organic carbon (OC) mass in LA and Atlanta a) for the whole data sets as those presented in Figure 5.2, and b) for the two sub data sets where data are segregated for high and low RH levels (blue and red markers and lines, respectively).

To better understand if some of the scatter in the F_p-OC relationship in both cities can be attributed to a RH effect on WSOC partitioning, the data were segregated into two sub data sets by high (above 70%) and low (below 70%) RH levels. Figure 5.3b shows that for the LA data, similar trends in the F_p-OC relationship for the two sub data sets, which followed the trend for all the data, were observed. The F_p values for the high RH (> 70%) group were consistently lower, possibly due to less WSOC partitioning in the

particle phase at night when RH was generally higher. *Hennigan et al*. [2008a] also observed lower F_p values during nighttime relative to daytime, and attributed this difference in part to the diurnal variability of ambient oxidant or NO_x levels. In Atlanta, however, the F_p-OC trends for the two sub data sets were distinctly different (Figure 5.3b). For data with higher RH, there was no well-defined F_p-OC relationship, indicating the dominant role of liquid water in WSOC partitioning when ambient RH was sufficiently high. For data with lower RH, when no F_p-RH relationship was observed, there was nearly a linear dependence of F_p on OC ($r^2 = 0.94$ for binned data), which was very similar to the trend observed in LA, suggesting that the absorbing phase for WSOC partitioning in Atlanta could shift from particle water, when sufficient LWC was present, to organic aerosols when the particles were generally drier. In the atmosphere, these two types of partitioning processes may occur simultaneously and shift in importance as the ambient RH changes dramatically throughout a diurnal cycle at the ground, or as particles experience increasing humidity as they are mixed towards the top of the boundary layer. For example, between 8:00 and 9:00 for 22 out of 36 days during the Atlanta sampling period, the hourly RH was above 70%, compared to zero days with an RH above 70% between the times of 14:00 and 15:00. However, despite lower RH during these afternoon periods (between 12:00 to 18:00), a similar dependence of F_p on RH as that seen for the whole data set was still observed (not plotted). In the previous study by *Hennigan et al.* [2009] that was conducted over 5 months (May to September 2007) in Atlanta, a clear F_p-RH relationship was also found at any time during the day. In summary, our August data set suggests that during afternoon lower RH periods, partitioning to liquid water could still occur, but not likely as important an absorbing phase as OA.

5.3.2.4 Partitioning and WSOC production; optimal conditions for partitioning to water

The comparison between LA and Atlanta F_p not only showed a difference in their diurnal trends and relationships with RH and OC, but also a significant difference in F_p magnitude. In Atlanta where the absorbing phase included particle water, the F_p levels were always measurably larger than those in LA (Table 5.2). On average, F_p in Atlanta (0.19 ± 0.07) was roughly twice that of LA (0.11 ± 0.05) (Table 5.1). The highest F_p correlates with highest RH, suggesting greater uptake of water-soluble SVOCs by dissolution to water compared to absorption by OA.

For absorptive partitioning to particle water of the freshly formed SVOCs ($WSOC_g$) to be an effective pathway to form SOA, both wet particles and sufficient oxidants are required. Although RH is the highest at night, all our analyses have shown that most $WSOC_p$ production in Atlanta is during daytime and hence driven by photochemical oxidation processes [*Hennigan et al.,* 2009; *Zhang et al.,* 2012a]. The optimal period for multiphase SOA formation is then before noon when aerosols are drying from the high RH period before sunrise, but could still remain wet due to their low efflorescence RH [*Bertram et al*., 2011]. As discussed in Sect. 5.3.2.2, there is evidence for this mechanism from the NO_3^- diurnal trend in LA (Figure 5.1) and the NO_3^- formation in the morning hours in Mexico City during a wet period (3/27 to 3/30/2006) [*Hennigan et al*, 2008b]. In Mexico City, NO_3^- and $WSOC_p$ were strongly correlated between 8:00 and 12:45, suggesting very similar atmospheric processes affecting the formation and loss of both species. Thus, it appears possible that some of the Mexico City morning $WSOC_p$ formation was related to partitioning to liquid water. However, as

noted above, in Atlanta F_p remained high for a period extending into the early afternoon, when aerosols were most likely dry, allowing partitioning to shift to absorption by organic components. The data suggest that for the month of August, the increase in $WSOC_p$ within Atlanta likely involves a combination of partitioning to water and absorption to OA, with the former being most prevalent in the morning hours and the latter in the afternoon when $WSOC_p$ concentrations were highest. Recent laboratory studies, generally performed at low RH (~30%), have suggested the possibility of "glassy" SOA formation, a process that does not follow the equilibrium partitioning theory due to the slow diffusivity within the formed particles [*Virtanen et al*., 2010; *Cappa and Wilson*, 2011; *Perraud et al*., 2012]. Our ambient observations in this study do not show evidence for this process, but instead appear to confirm the importance of absorptive partitioning to OA as a source of $WSOC_p$ production in both LA and Atlanta.

Contrasts between F_p-RH and F_p-OC relationships in LA and Atlanta are consistent with differences observed for other SOA components and properties, including partitioning of formic acid, oxalate formation pathways, and $WSOC_p$ light absorption properties (i.e. brown carbon). These additional contrasts discussed below support the differences in observed partitioning of bulk WSOC.

5.3.3 Additional differences between LA and Atlanta

5.3.3.1 Formic acid partitioning

Liu et al. [2012] presents a detailed analysis of formic acid partitioning in LA and Atlanta based on the same studies discussed in this work. As a low molecular weight carboxylic acid, formic acid is volatile and is expected to be predominately in the gas phase. Formic acid particle/gas (p/g) ratios in both LA and Atlanta were typically only a

few percent (~1-2%), yet the relationship of formic acid with RH differed in the two cities. In LA, formic acid p/g ratios generally showed limited correlation with RH, with the exception of a few episodes of overcast periods when photochemistry was suppressed. During these three brief 1 to 2 day periods formic acid p/g ratios on average followed increasing RH, providing evidence for gas-phase formic acid partitioning to liquid water, and the p/g ratios were the largest at these times (up to 10% when RH > 90%). In contrast to LA, Atlanta formic acid p/g ratios behaved in a similar way as WSOC F_p, with higher p/g ratios at higher RH. Overall, the contrasts in formic acid partitioning between LA and Atlanta are similar to those in bulk WSOC.

5.3.3.2 Contrasts in $PM_{2.5}$ oxalate formation pathways

Oxalate is one of the most ubiquitous carboxylic acids in tropospheric aerosols, contributing to a few percent of the total organic mass in the continental atmosphere [*Kawamura and Ikushima*, 1993; *Huang et al*., 2006; *Sorooshian et al*., 2007], and up to 21% in the coastal Pacific atmosphere [*Sorooshian et al*., 2010]. In this study, oxalate ranged from 0.015 to 0.148 μg m^{-3} in LA and between 0.127 and 0.217 μg m^{-3} in Atlanta, comprising on average 2.0 % and 2.7 % of the total $WSOC_p$ on a carbon mass basis in LA and Atlanta, respectively (Table 5.1).

Oxalate is mostly a product of secondary production processes with minor contributions from primary emissions such as biomass burning and fossil fuel combustion [*Huang and Yu*, 2007; *Schmidl et al*., 2008; *Zhang et al*., 2010; *Myriokefalitakis et al*., 2011], and is often detected in the accumulation mode internally mixed with sulfate [*Huang et al*., 2006; *Sorooshian et al*., 2006], suggesting significant contribution from

multiphase reactions. Laboratory studies have shown that oxalate can be formed from small aldehydes reacting with OH radical in the aqueous phase [e.g., *Lim et al*., 2010; *Tan et al*., 2010]. Gas-phase oxidation of parent organic species leading to oxalate is not well established [*Warneck*, 2003], but has been speculated based on ambient observations [*Chebbi and Carlier*, 1996; *Sorooshian et al*., 2006]. Since oxalate can be formed by condensation of gas-phase oxalic acid, as well as from multiphase reactions in the aqueous phase, differences in oxalate sources and formation mechanisms in LA and Atlanta provide insight on SOA formation pathways between these two urban environments.

In LA and Atlanta we observed different oxalate diurnal trends and their association with $WSOC_p$ (Figure 5.1). In LA, the diurnal profile of oxalate was nearly identical to that of $WSOC_p$, showing maximum concentration in the early afternoon tracking most SOA components. Oxalate was well correlated with $WSOC_p$ and OOA (r^2 = 0.68 and 0.73, respectively). Furthermore, as shown in Figure 5.4a, oxalate and $WSOC_p$ evolved together with increasing photochemical age, indicated by $-\log(NO_x/NO_y)$ [*Kleinman et al*., 2008], suggesting their common sources and formation mechanisms. Two branches (y-intercepts) are evident in Figure 5.4a and are attributed to different air mass histories. During CalNex sampling between May 29 and June 6, a general stagnation event in the LA basin led to a substantial increase in background levels for several species, including oxalate and LV-OOA (low-volatility OOA). The average nighttime concentration of oxalate increased substantially from 0.28 μg m^{-3} prior to the stagnation event (before May 29) to 0.63 μg m^{-3} during the event (after May 29), resulting in the two branches of Figure 5.4a. However, similar oxalate/$WSOC_p$ ratios

(0.020 and 0.026 µg/µgC) were obtained for these two periods.

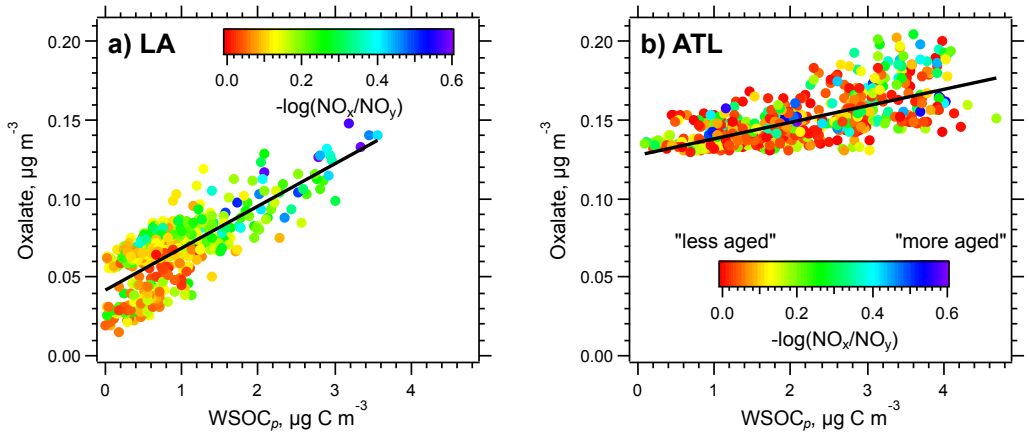

Figure 5.4 Oxalate versus $WSOC_p$ as a function of photochemical age (indicated by $-\log(NO_x/NO_y)$ in a) LA and b) Atlanta.

Veres et al. [2011] measured several gas-phase organic acids during CalNex, such as formic, pyruvic/butyric and propionic acids, and concluded they were formed through rapid photochemical production within the urban plume. Oxalic acid appeared to be produced in a similar fashion as other measured organic acids; in the gas phase and partitioning to the condensed phase to form aerosol oxalate (note, no gas-phase oxalic acid data were available during CalNex).

Higher average aerosol oxalate concentrations, as well as a larger fraction of oxalate in the total $WSOC_p$, were found in Atlanta than in LA (Table 5.1). The larger y-intercept value of oxalate versus $WSOC_p$ (Figure 5.4b) corresponds to a substantially higher background level of oxalate in Atlanta and is indicative of significant regional contribution, as has been observed for $WSOC_p$ [*Zhang et al.*, 2012a] and other $WSOC_p$ components (soluble brown carbon) [*Zhang et al.*, 2011]. Despite the much higher background level, the daytime enhancement of oxalate was only ~5% relative to the

average nighttime concentration, roughly 1/6 of that observed in LA. Unlike LA where the diurnal trend of oxalate tracked $WSOC_p$, in Atlanta oxalate peaked 2-3 hours later than $WSOC_p$ (Figure 5.1b), suggesting rapid formation through gas phase oxidation of parent VOCs followed by condensation was not an important source for Atlanta oxalate. The correlation between oxalate and $WSOC_p$ in Atlanta was weaker ($r^2 = 0.45$) than in LA and was not related to photochemical age (Figure 5.4b), which further suggested that daytime $WSOC_p$ and oxalate were not formed by similar mechanisms. Instead, unlike LA where oxalate appeared to form in the gas phase and partition to the particle phase, in Atlanta oxalate trends appeared to be driven more by a regional contribution and possibly slower production through a multiphase reaction pathway.

5.3.3.3 Contrasts in $PM_{2.5}$ soluble brown carbon

As discussed in Chapter 4, soluble light-absorbing organic aerosol (brown carbon) concentrations and their associations with $WSOC_p$ were substantially different between LA and Atlanta (Figure 5.1, bottom panel). *Zhang et al*. [2011] showed that in LA soluble brown carbon was correlated with $WSOC_p$, and a detailed chemical analysis identified nitro-aromatics as one source for the colored organics. These two findings are consistent, as many chromophores associated with SOA are expected to contain aromatic moieties, and much of the SOA formed in the LA basin is linked to these similar anthropogenic precursors (i.e. aromatics) [*Hersey et al*., 2011; *Zhang et al*., 2011; *Bahreini et al*., 2012]. Focusing on the $WSOC_p$ that was freshly formed within each urban environment, the mass absorption efficiency at the wavelength of 365 nm (bulk absorption at 365 nm per $WSOC_p$ mass) was found to be 4-6 times higher in LA, indicating that much of the soluble organic aerosols formed within Atlanta were

chemically different from those in LA.

5.4 Discussion

Differences in WSOC and formic acid partitioning preferences, oxalate formation pathways, and the extent to which brown carbon was present in the freshly formed SOA between LA and Atlanta, all point to differences in SOA compositions and formation mechanisms within these two urban environments. Particle composition can affect what acts as the main absorbing phase. Our results suggest that absorption to aerosol water plays an important role in SOA formation within Atlanta, but not in LA. This difference could be caused by: 1) contrasting particle hygroscopicity, which determines the amount of water uptake by particles, affecting gas-particle partitioning and the extent of any subsequent condensed phase reactions; 2) different types of SVOCs that partition to the particle phase; and 3) other properties of the particle water, such as pH, which could influence the uptake of weak organic acids, a significant fraction (~40%) of the summer $WSOC_p$ in Atlanta [*Sullivan and Weber*, 2006]. A detailed discussion regarding the influence of particle pH on organic acid partitioning is reported by *Liu et al*. [2012] with respect to formic acid partitioning. The first two hypotheses are explored next.

Particle hygroscopicity: Despite higher RHs in LA, differences in the actual amount of particle water could be a hypothesis to explain the greater propensity of Atlanta $WSOC_g$ to partition to particle water. However, the results from ISORROPIA-II model, summarized in Table 5.2, show that for RH ranging between 20-50%, the modeled LWC were comparable in LA and Atlanta, and for RH higher than 50%, LWC was predicted to be 2-3 times higher in LA than in Atlanta. The model does not consider the effect of organic components on particle hygroscopicity, which has generally been

thought to be minor given the much lower hygroscopicity of the organics relative to the inorganic components, such as $(NH_4)_2SO_4$ [*Jimenez et al*., 2009]. Previous field studies conducted in similar locations and time periods as the present study have derived the hygroscopicity parameter κ. κ values ranged between 0.15 and 0.51, with an average of 0.31 in LA (Pasadena) during spring-summer of 2009 [*Hersey et al*., 2011], and ranged between 0.05 and 0.52, with an average of 0.21 at an urban Atlanta site 2 km from the GIT campus in the summer of 2008 during the AMIGAS study [*Padró et al*., 2011]. The average RH levels during these two past studies and those in the current study were within ± 5%.

Both thermodynamic calculations and field measurements suggest that the overall aerosol water contents were similar in the two urban environments during the study periods discussed here (LA: May-June, Atlanta: August) and may not have a major impact on the different SOA partitioning pathways. However, since the actual concentrations of the particle water that the SVOCs partitioned to were not explicitly measured in these studies, some uncertainty remains. For example, one could expect that the organic fraction of fine particles in the southeast to be more hygroscopic since it was composed of a significant fraction of regional, aged aerosols, relative to the large fraction of freshly-formed SOA that were more hydrophobic in LA [*Zhang et al*., 2011; *Zhang et al*., 2012a]. This hypothesis is also supported by, as discussed in Sect. 3.3.2, the much higher fraction of oxalate aerosol in the total $WSOC_p$ in Atlanta than LA. Although the organic fraction may not greatly affect the amount of particle water present in these regions, it could have an important impact on the actual uptake of various gaseous species by affecting phase separations within the particle and the formation of

hydrophobic or hydrophilic surface layers [*Bertram et al*., 2011; *You et al*., 2012]. *You et al*. [2012] have shown clear evidence that Atlanta ambient particles could undergo liquid-liquid phase separation below 70% RH with an inner phase of ammonium sulfate and an outer phase of secondary organic material, which may explain the dependence of F_p on OC mass in Atlanta when RH was low. *Zuend and Seinfeld* [2012] also suggest that WSOC does not necessarily partition to the aqueous phase but rather to the hydrophilic organic phase due to liquid-liquid phase separation and salting-out effects at lower RH range. More information on the behavior of aerosol liquid phases as a function of RH in both Atlanta and LA is needed to better understand the role that phase separation plays in WSOC uptake by particles.

VOC emissions: Although the exact role that the organic aerosol composition plays in WSOC partitioning is not clear, the type of SVOCs that partition may partially determine what the dominant absorbing phase is. LA and Atlanta have large differences in the mix of VOCs that could lead to SOA. Anthropogenic VOCs and isoprene emission fluxes from emission inventories are summarized in Table 5.1. In LA, anthropogenic hydrocarbons are the dominant VOCs emitted and the likely SOA precursors [*Hersey et al.*, 2011; *Williams et al.*, 2010], which have been confirmed by radiocarbon analysis on CalNex PM_1 filters [*Zhang et al*., 2011]. In Atlanta, the emissions of anthropogenic VOCs are significantly less, approximately half of that in LA, consistent with a lower urban population density. In contrast, the emission of isoprene is predicted to be 5 times higher in Atlanta due largely to the greater presence of isoprene-emitting vegetation. Other biogenic VOC emissions, such as monoterpenes emission, are also substantially higher in the southeast [*Guenther*, 1997]. Radiocarbon analysis has shown that the

secondary $WSOC_p$ in Atlanta in the summer is largely modern (~70 to 80%) [*Weber et al*., 2007]. Based on the brown carbon data, *Zhang et al*. [2011] concluded that the daily freshly-formed $WSOC_p$ within the city of Atlanta was most likely biogenic SOA. A number of other ambient studies have also shown preferential formation of biogenic SOA in polluted environments [*Goldstein et al*., 2009; *Spracklen et al*., 2011; *Worton et al*., 2011; *Setyan et al*., 2012].

The effect of biogenic VOCs may be that it not only influences the absorbing phase, but also results in oxidized VOCs and SVOCs that are more likely to partition to water. Laboratory studies have shown that isoprene is highly reactive with OH radical and in the presence of high NO_x concentrations, the isoprene oxidation produces low molecular weight products (e.g., glyoxal and methylglyoxal) that could undergo reactive uptake by wet aerosols, and given sufficient time, transform to stable products [*Liggio et al*., 2005a, 2005b; *Lim et al.*, 2010]. Satellite observations of glyoxal columns indicate significantly higher amounts of glyoxal in the southeastern U.S. than along the west coast [*Myriokefalitakis et al*., 2008], likely due to a greater abundance of vegetation that emits the glyoxal precursor. Contrasting VOC emissions are consistent with differences in observed WSOC characteristics (color) and trends in specific aerosol components (oxalate).

5.5 Conclusions

Ambient measurements of gas and particle phase water-soluble organic aerosols were conducted in Pasadena, CA (as part of the CalNex-LA campaign) and Atlanta, GA in the spring-summer of 2010. WSOC gas-particle partitioning, analyzed through the

fraction of total WSOC in the particle phase, F_p, exhibited differing relationships with ambient RH and organic carbon mass in the two urban environments. Consistent with previous studies, in Altanta F_p was correlated with RH and inferred particle water content from a thermodynamic model. The correlation was observed throughout the day and was especially prevalent in the morning, when RH was higher. During the drier period (RH below 70%), F_p was found to have a dependence on OC mass, suggesting that in Atlanta during August, both particle water and organic components could serve as the partitioning absorbing phase, depending on ambient conditions. In contrast, in LA the diurnal variation of F_p did not track RH. As a result, no correlation was found between F_p and RH, despite a much higher average RH and predicted particle water content in LA relative to Atlanta. Instead, F_p scaled well with OC mass, consistent with SVOCs partitioning to the organic phase, as observed in environmental chamber studies.

Besides the contrast in WSOC partitioning behavior between LA and Atlanta, a number of other differences, including oxalate formation pathways (discussed in this paper), WSOC light-absorbing properties [*Zhang et al*., 2011], and partitioning of formic acid [*Liu et al*., 2012], were observed between these two urban environments. Many of the differences may be attributed to different SOA precursors within the two urban environments, resulting in different types of SOA, and possibly SOA formation mechanisms. Both cities have abundant anthropogenic VOC emissions from fossil fuel combustion, with Atlanta having an additional large source of biogenic VOCs in the summer. These ambient observations show direct evidence for different gas-particle partitioning behaviors and provide insights on SOA formation mechanisms that vary with location.

CHAPTER 6

CONCLUSIONS AND FUTURE WORK

6.1 Summary of the major findings

6.1.1 Sources of $PM_{2.5}$ and WSOC in the southeastern United States

The first part of the dissertation (Chapter 2 and 3) is devoted to a detailed analysis of chemical composition of ~900 24-hr integrated FRM Teflon filters, in conjunction of other data sets that include remotely sensed fire counts and online measurements of WSOC at an urban/rural pair. The objective is to better understand the sources and formation processes of $PM_{2.5}$ and WSOC in the southeastern U.S., a region featuring outstanding biogenic emissions of SOA precursors, moderate extent of anthropogenic pollution, and seasonally varied impact from biomass burning emissions.

First, through a comparative examination of two biomass burning tracers, i.e. levoglucosan and K^+ from the FRM $PM_{2.5}$ samples, it is found that the abundance of levoglucosan exhibits a distinct seasonal pattern characterized by a maximum in winter and a minimum in summer, which corresponds to the seasonally varied biomass burning emission activities as indicated by MODIS fire counts. By contrast, K^+ is evidently subject to impact from multiple sources including biomass burning and mineral dust. It is concluded that **levoglucosan could serve as a robust tracer of biomass burning emission contributions to ambient $PM_{2.5}$**.

Through covariance analysis of major $PM_{2.5}$ components using PMF, factors that are linked to different sources, i.e. biomass burning, secondary formation processes and refractory component are identified, and their contributions to $PM_{2.5}$ mass concentrations

are estimated. **Secondary formation processes leading to sulfate and SOA are found to be the largest source of $PM_{2.5}$ in all seasons**. WSOM (2.0 times WSOC) and ammonium sulfate together contributed up to 71% at urban and 78% at rural sites of the total $PM_{2.5}$ mass. **Biomass burning contribution varies with season, reaching up to 27% of the total $PM_{2.5}$ mass in winter, and is almost negligible during summer (2%).**

Next, utilizing the ambient concentration of the validated biomass burning tracer, levoglucosan, as a criteria, FRM samples with negligible influence (levoglucosan<50 ng m^{-3}) from biomass burning are segregated and further analyzed to investigate the sources and formation of secondary WSOC in the southeast. The spatiotemporal variations of WSOC are examined together with those of sulfate as a reference, of which the formation process is better understood. WSOC shows very similar seasonality as sulfate, characterized by a maximum in summer, apparently corresponding to enhanced photochemistry, temperature, and biogenic VOC emissions, but the links between WSOC and biogenic emissions are not yet clear given the same behavior of sulfate. Spatially, sulfate and WSOC are fairly uniform across the 15 FRM sampling sites in the southeast, suggesting **a relatively well-mixed and slowly ventilated atmosphere over this region that facilitates secondary processing** of gas precursors and aerosol components. As a result of the unique meteorology and topography, the aerosols in the southeast are generally much more aged than those in other regions, e.g., the west coast. The two PMF factors that explained most of the variability of FRM WSOC in the summer may be attributed to **two differed SOA formation routes, i.e. condensed phase reactions that lead to the formation of WSOC, aerosol oxalate and brown carbon, and the other representing the regional aged SOA and/or an acid-catalyzed route that is**

associated with sulfate.

On the smaller spatial scale, while a broad consistency is found for the inter-site gradients of isoprene emission and WSOC concentration, likely due to the considerable contribution from biogenic precursors to SOA formation, **a marked urban/rural gradient is observed from both FRM filter data and online WSOC measurements at an urban/rural pair (Atlanta/Yorkville), highlighting the importance of anthropogenic contribution to SOA formation in urban areas.** While an anthropogenic enhancement effect (by 31%) of WSOC that is evidenced by concurrent increases of CO and NO_x is found from the online measurements, such effect is found larger than that manifested by FRM samples (only 10% difference between Atlanta and Yorkville), which could be attributed to the loss of semi-volatile organic species which are enriched in urban atmosphere. Using the difference between the urban-rural WSOC and estimated boundary layer height, **an average urban Atlanta WSOC production rate in August from morning to mid-afternoon was calculated to be 0.55 mgC m^{-2} hr^{-1}.**

Overall, this study characterizes **the regional nature of fine aerosols in the southeastern U.S., confirming the importance of secondary organic aerosol and the roles of both biogenic and anthropogenic emissions.**

6.1.2 Comparative investigation of SOA formation pathways and optical properties in Atlanta and LA

Analyses of the FRM filter samples and online WSOC measurements suggest that SOA formation in summer is prevalent in the southeast, driven by multiple physio-

chemical processes with input from the substantial biogenic emissions over the region and is enhanced by anthropogenic emissions primarily in urban areas. As the second half part of the dissertation (Chapter 4 and 5), summertime online measurements of WSOC gas-particle partitioning and light absorption from Atlanta are analyzed to investigate the relative importance of the different chemical processes and the roles of anthropogenic and biogenic emissions in SOA formation. Given the unique VOC mixture resulted from both natural and anthropogenic emissions in Atlanta atmosphere, another urban area, i.e. LA that is a typical urban environment predominantly impacted by anthropogenic pollution with much less biogenic emissions, is chosen for comparison purpose, in light of the presumably differed SOA formation routes and chemical composition in these two cities. The concurrent measurements of chemical species in both gas and aerosol phases during the CalNex 2010 campaign provide valuable opportunity for comprehensive examination of SOA sources and formation in the LA area.

A number of differences with respect to SOA formation and properties are found between these two urban environments. First, **WSOC gas-particle partitioning**, analyzed through the fraction of total WSOC in the particle phase, F_p, **is found to exhibit differing relationships with ambient RH and organic aerosol mass in Atlanta and LA**. Consistent with previous studies, in Atlanta F_p was well correlated with RH, suggesting the importance of water uptake and subsequent condensed phase chemistry leading to aqueous SOA; whereas in LA, F_p is well correlated with OC mass, consistent with partitioning of SVOC to the organic phase as observed in environmental chamber studies. In addition, WSOC light absorption is also different in these two urban environments. **The mass absorption efficiency (MAE) of the freshly-formed WSOC,**

defined as the bulk absorption per soluble carbon mass at 365 nm, was found to be 4 to 6 times higher in LA than in Atlanta. Interpreting soluble brown carbon as a property of fresh anthropogenic SOA, the difference in the MAE between these two cities suggests **most fresh secondary WSOC formed within Atlanta is not from an anthropogenic process similar to LA**. The results between LA and Atlanta suggest that water-soluble brown carbon can be a prevalent component of SOA freshly produced from anthropogenic compounds and a useful tool to investigate SOA formation processes.

Overall, **many of these ambient observations in the southeastern United States, as well as the distinct differences observed between Atlanta and LA, may be attributed to different SOA precursors within the two urban environments**, resulting in different types of SOA, and possibly SOA formation pathways. Both cities have abundant anthropogenic VOC emissions from fossil fuel combustion, with Atlanta having an additional large source of biogenic VOCs in the summer. These contrasting results in the two urban environments show direct evidence for different SOA chemical composition and partitioning behaviors and provide insights on SOA formation mechanisms that vary with location.

6.2 Recommendations for future work

The scientific findings resulted from this thesis are important for better understanding SOA sources, formation pathways and properties. In particular, this work provides context and reference for future field studies with a focus on characterizing the aerosols in the southeastern U.S., such as the forthcoming 2013 The Southern Oxidant and Aerosol Study (SOAS). A full suite of novel gas and aerosol measurements in

conjunction with the measurements utilized in this study would provide valuable insights and help address the subsequent questions coming out of this work. Some recommendations for future research are summarized below.

6.2.1 Chemical characterization of brown SOA

Our results presented in Chapter 4 show that most of the speciated organic compounds exhibited a positive relationship with bulk absorption at 365 nm (b_{ap365}), yet the absorption from individual compound accounted for only a few percent of the total absorption. The sample chromatograph from the UPLC-DAD showed the presence of a large "unresolved complex mixture", which urges the further effort in chemical speciation of brown SOA. While nitro-aromatic compounds are identified as one important component of brown SOA from anthropogenic sources, little is known about the chemical composition of ambient light-absorbing biogenic SOA. Using UPLC/ESI-Q-ToFMS operated in positive ion mode, a few nitrogen-containing compounds, likely amines, imines and amides, are identified, yet their molecular structures and ambient abundance have not been fully determined. The light-absorbing organic aerosol is a ubiquitous component of regional SOA in the southeastern U.S. [*Hecobian et al*., 2010; *Zhang et al*., 2011], likely resulting from slow ageing processes of biogenic SOA as suggested by laboratory studies [*Shapiro et al., 2009*; *Sareen et al*., 2010]. Thus, it would be informative to perform chemical speciation on samples collected from rural sites and compare the results with brown SOA constituents produced in urban environments.

In addition, *Hecobian et al*. [2010] have shown that biomass-burning aerosols are highly absorbing, on average three times more absorbing than samples with minimum biomass burning influence based on measurements of soluble brown carbon from filter

samples collected throughout the southeast. It would be useful to compare the contribution of those identified nitro-aromatic species to the bulk absorption at 365 nm for biomass burning sample and non-biomass burning sample. It is found that 4-nitrocatechol ($C_6H_5NO_4$) contributes more than 40% of the total light absorption in cloud water that is influenced by biomass burning (Yury Desyaterik, personal communication), whereas from our results, 4-nitrocatechol as the largest single contributor among the six identified nitro-aromatics, contributed only 1.4% of the total bulk WSOC absorption (Table 4.2).

6.2.2 Understanding the optical importance of brown carbon

An important question that remains to be answered is how optically important is brown carbon with respect to black carbon (BC). Simultaneous optical measurements using PSAP or multi-wavelength aethalometer to quantify the total absorption together with bulk measurement of soluble and total brown carbon would make absorption closure analysis possible. The mass absorption efficiency (MAE) of soluble and total brown carbon can be compared with that of BC at different wavelengths (e.g., 365 nm and 532 nm), and the extent of absorption enhancement due to the presence of brown carbon can be inferred. It would be useful to make such measurements in different locations (i.e. urban and rural areas) to examine the relative importance of brown carbon absorption at UV and visible ranges. Furthermore, since so far the brown carbon measurements were made from bulk aqueous and methanol extracts, no direct information can be provided to estimate direct radiative forcing of brown carbon. Therefore, characterization of the size distribution of ambient brown carbon aerosols is required to better model their climate impact.

6.2.3 Investigating the gas-particle partitioning of single organic compound

While the gas-particle partitioning of bulk WSOC provides valuable information of the partitioning behavior between the overall SVOCs and SOA, studying the partitioning of individual organic compounds would provide additional insights. During the spring-summer of 2010 in LA and Atlanta, gas and particle phase formic acid was measured concurrently with measurements of $WSOC_g$ and $WSOC_p$. The partitioning preference of formic acid in the two cities differed, consistent with the partitioning behavior of bulk WSOC, providing additional contrast between the two environments. Formic acid is the most abundant organic acid in the gas phase, whereas oxalic acid is the most ubiquitous carboxylic acid condensed phase component, comprising 2.0% of the total $WSOC_p$ in LA and 2.7% in Atlanta on a carbon mass basis. Furthermore, oxalate is a product of aqueous phase chemistry and often used as a tracer compound for such reactions [*Zhang et al*., 2012a]. It is speculated that oxalate aerosol would form in the aerosol water and thus the oxalic acid particle/gas ratio would have a positive relationship with ambient RH. For these reasons, studying the partitioning of oxalic acid and comparing it with the partitioning of bulk WSOC would help characterize the chemical nature of $WSOC_p$ and enhance the overall understanding of WSOC partitioning. Specifically, a modified Chemical Ionization Mass Spectrometer (CIMS) that can alternatively quantify oxalic acid and other organic acids in both gas and particle phases with a high time-resolution would be a useful tool to study the partitioning behavior of single organic compound under various conditions.

REFERENCES

Aiken, A. C., P. F. Decarlo, J. H. Kroll, D. R. Worsnop, J. A. Huffman, K. S. Docherty, I. M. Ulbrich, C. Mohr, J. R. Kimmel, D. Sueper, Y. Sun, Q. Zhang, A. Trimborn, M. Northway, P. J. Ziemann, M. R. Canagaratna, T. B. Onasch, M. R. Alfarra, A. S. H. Prevot, J. Dommen, J. Duplissy, A. Metzger, U. Baltensperger, and J. L. Jimenez (2008), O/C and OM/OC ratios of primary, secondary, and ambient organic aerosols with high-resolution time-of-flight aerosol mass spectrometry, *Environ. Sci. Technol*., *42*, 4478–4485, doi:10.1021/ES703009q.

Aiken, A. C., D. Salcedo, M. J. Cubison, J. A. Huffman, P. F. DeCarlo, I. M. Ulbrich, K. S. Docherty, D. Sueper, J. R. Kimmel, D. R. Worsnop, A. Trimborn, M. Northway, E. A. Stone, J. J. Schauer, R. M. Volkamer, E. Fortner, B. de Foy, J. Wang, A. Laskin, V. Shutthanandan, J. Zheng, R. Zhang, J. Gaffney, N. A. Marley, G. Paredes-Miranda, W. P. Arnott, L. T. Molina, G. Sosa, and J. L. Jimenez (2009), Mexico City aerosol analysis during MILAGRO using high resolution aerosol mass spectrometry at the urban supersite (T0) – Part 1: Fine particle composition and organic source apportionment, *Atmos. Chem. Phys*., *9*, 6633–6653, doi:10.5194/acp-9-6633-2009.

Andreae, M., and A. Gelencser (2006), Black carbon or brown carbon? The nature of light-absorbing carbonaceous aerosols, *Atmos. Chem. Phys.*, *6*, 3131-3148.

Apicella, B., M. Alfe, R. Barbella, A. Tegrossi, and A. Ciajolo (2004), Aromatic structures of carbonaceous materials and soot inferred by spectroscopic analysis, *Carbon*, *42*, 1583-1589.

Bahreini, R., A. M. Middlebrook, J. A. de Gouw, C. Warneke, M. Trainer, C. A. Brock, S. S. Brown, W. P. Dube, J. B. Gilman, K. Hall, J. S. Holloway, W. C. Kuster, A. E. Perring, A. S. H. Prévôt, J. P. Schwarz, J. R. Spackman, H. Stark, S. Szidat, N. L. Wagner, R. J. Weber, P. Zotter and D. D. Parrish (2012), Major contribution from gasoline emissions to secondary organic aerosol mass in the Los Angeles Basin, *Geophys. Res. Lett*., *39*, L06805, doi:10.1029/2011GL050718.

Bauer, H., M. Claeys, R. Vermeylen, E. Schueller, G. Weinke, A. Berger, and H. Puxbaum (2008), Arabitol and mannitol as tracers for the quantification of airborne fungal spores, *Atmos. Environ*., *42*, 588-593.

Bench, G., S. Fallon, B. Schichtel, W. Malm, and C. McDade (2007), Relative contribution of fossil and contemporary carbon sources to $PM_{2.5}$ aerosol in nine

Interagency Monitoring for Protected Visual Environments (IMPROVE) network sites, *J. Geophys. Res*., *112*, D10205, doi:10.1029/2006JD007708.

Bertram, A. K., S. T. Martin, S. J. Hanna, M. L. Smith, A. Bodsworth, Q. Chen, M. Kuwata, A. Liu, Y. You, and S. R. Zorn (2011), Predicting the relative humidities of liquid-liquid phase separation, efflorescence, and deliquescence of mixed particles of ammonium sulfate, organic material, and water using the organic-to-sulfate mass ratio of the particle and the oxygen-to-carbon elemental ratio of the organic component, *Atmos. Chem. Phys*., *11*, 10995–11006.

Blanchard, C. L., G. M. Hidy, S. Tanenbaum, and E. S. Edgerton (2011), NMOC, ozone, and organic aerosol in the southeastern United States, 1999-2007: 3. Origins of organic aerosol in Atlanta, Georgia, and surrounding areas, *Atmos. Environ*., *45*, 1291-1302.

Blando, J. D., and B. J. Turpin (2000), Secondary organic aerosol formation in cloud and fog droplets: a literature evaluation of plausibilty, *Atmos. Environ*., *34*, 1623-1632.

Bond, T. C., and R. W. Bergstrom (2006), Light absorption by carbonaceous particles: An investigation review, *Aerosol Sci. Technol.*, *40*, 27-67.

Bones, D. L., D. K. Henricksen, S. A. Mang, M. Gonsior, A. P. Bateman, T. B. Nguyen, W. J. Cooper, and S. A. Nizkorodov (2010), Appearance of strong absorbers and fluorophores in limonene- O3 secondary organic aerosol due to $NH4^{+}$-mediated chemical aging over long time scales, *J. Geophys. Res.*, *115*, D05203, doi:10.1029/2009JD012864.

Brown, S. S., J. A. de Gouw, C. Warneke, T. B. Ryerson, W. P. Dubé, E. Atlas, R. J. Weber, R. E. Peltier, J. A. Neuman, J. M. Roberts, A. Swanson, F. Flocke, S. A. McKeen, J. Brioude, R. Sommariva, M. Trainer, F. C. Fehsenfeld, and A. R. Ravishankara (2009), Nocturnal isoprene oxidation over the Northeast United States in summer and its impact on reactive nitrogen partitioning and secondary organic aerosol, *Atmos. Chem. Phys*., *9*, 3027–3042.

Cachier, H., J. Ducret, M. P. Bremond, A. Gaudichet, J. P. Lacaux, V. Yoboue, and J. J. Baudet (1991), Characterisation of biomass burning aerosols in savannah region of the Ivory Coast, in: Global Biomass Burning, edited by: Levine, J., *MIT Press*, Cambridge, 174-180.

Cappa, C. D., and K. R. Wilson (2011), Evolution of organic aerosol mass spectra upon

heating: implications for OA phase and partitioning behavior, *Atmos. Chem. Phys*., *11*, 1895-1911.

CARB (2010), California Air Resources Board, California Emission Inventory Data, Available at: http://www.arb.ca.gov/ei/emsmain/emsmain.htm.

Cahill, T. M., V. Y. Seaman, M. J. Charles, R. Holzinger, and A. H. Goldstein (2006), Secondary organic aerosols formed from oxidation of biogenic volatile organic compounds in the Sierra Nevada Mountains of California, *J. Geophys. Res*., *111*, D16312, doi:10.1029/2006JD007178.

Carrico, C. M., M. H. Bergin, J. Xu, K. Baumann, and H. Maring (2003), Urban aerosol radiative properties: Measurement during the 1999 Atlanta Supersite Experiment, *J. Geophys. Res*., *108*, 8422, doi:10.1029/2001JD001222.

Caseiro, A., I. L. Marr, M. Claeys, A. Kasper-Giebl, H. Puxbaum, and C. A. Pio (2007), Determination of saccharides in atmospheric aerosol using anion-exchange high performance liquid chromatography and pulsed amperometric detection, *J. Chromatogr. A*, *1171*, 37-45.

Chan, A. W. H., M. N. Chan, J. D. Surratt, P. S. Chhabra, C. L. Loza, J. D. Crounse, L. D. Yee, R. C. Flagan, P. O. Wennberg, and J. H. Seinfeld (2010a), Role of aldehyde chemistry and NO_x concentrations in secondary organic aerosol formation, *Atmos. Chem. Phys*., *10*, 7169–7188, doi:10.5194/acp-10-7169-2010.

Chan, M. N., J. D. Surratt, M. Claeys, E. S. Edgerton, R. L. Tanner, S. L. Shaw, M. Zheng, E. M. Knipping, N. C. Eddingsaas, P. O. Wennberg, and J. H. Seinfeld (2010b), Characterization and quantification of isoprene-derived epoxydiols in ambient aerosol in the southeastern United States, *Environ. Sci. Technol*., *44*, 4590-4596.

Chang, W. L., R. J. Griffin, and D. Dabdub (2009), Partitioning phase preference for secondary organic aerosol in an urban atmosphere, *P. Natl. Acad. Sci*., *107*, 6705-6710.

Chebbi, A., and P. Carlier (1996), Carboxylic acids in the troposphere, occurrence, sources, and sink: A review, *Atmos. Environ*., *30*, 4233-4249.

Chen, Y., and T. C. Bond (2010), Light absorption by organic carbon from wood

combustion, *Atmos. Chem. Phys*., *10*, 1773–1787.

Cohan, D. S., J. W. Boylan, A. Marmur, and M. N. Khan (2007), An integrated framework for multipollutant air quality management and its appliation in Georgia, *Environ. Manage*., *40*, 545-554.

Croes, B. E., and E. M. Fujita (2003), Overview of the 1997 Southern California Ozone Study (SCOS97-NARSTO), *Atmos. Environ.*, *37*, S3-S26.

DeCarlo, P. F., J. R. Kimmel, A. Trimborn, M. J. Northway, J. T. Jayne, A. C. Aiken, M. Gonin, K. Fuhrer, T. Horvath, K. S. Docherty, D. R. Worsnop, and J. L. Jimenez (2006), Field-deployable, high-resolution, time-of-flight aerosol mass spectrometer, *Anal. Chem*., *78*, 8281–8289.

de Haan, D. O., A. L. Corrigan, K. W. Smith, D. R. Stroik, J. J. Turley, F. E. Lee, M. A. Tolbert, J. L. Jimenez, K. E. Cordova, and G. R. Ferrell (2009a), Secondary organic aerosol-forming reactions of glyoxal with amino acids, *Environ. Sci. Tech*., *43*, 2818–2824.

de Haan, D. O., M. A. Tolbert, and J. L. Jimenez (2009b), Atmospheric condensed-phase reactions of glyoxal with methylamine, *Geophys. Res. Lett*., *36*, L11819, doi:11810.11029/12009GL037441.

de Gouw, J. A., A. M. Middlebrook, C. Warneke, P. D. Goldan, W. C. Kuster, J. M. Roberts, F. C. Fehsenfeld, D. R. Worsnop, M. R. Canagaratna, A. A. P. Pszenny, W. C. Keene, M. Marchewka, S. B. Bertman, and T.S. Bates (2005), Budget of organic carbon in a polluted atmosphere: Results from the New England Air Quality Study in 2002, *J. Geophys. Res*., *110*, D16305, doi:10.1029/2004jd005623,

de Gouw, J. A., C. A. Brock, E. L. Atlas, T. S. Bates, F. C. Fehsenfeld, P. D. Goldan, J. S. Holloway, W. C. Kuster, B. M. Lerner, B. M. Matthew, A. M. Middlebrook, T. B. Onasch, R. E. Peltier, P. K.Quinn, C. J. Senff, A. Stohl, A. P. Sullivan, M. Trainer, C. Warneke, R. J. Weber, and E. J. Williams (2008), Sources of particulate matter in the northeastern United States in summer: 1. Direct emissions and secondary formation of organic matter in urban plumes, *J. Geophys. Res*., *113*, D08301, doi:10.1029/2007JD009243.

de Gouw, J. A., and J. L. Jimenez (2009), Organic aerosols in the earth's atmosphere, *Environ. Sci. Technol*., *43*, 7614-7618.

de Gouw, J. A., A. M. Middlebrook, C. Warneke, R. Ahmadov, E. L. Atlas, R. Bahreini, D. R. Blake, C. A. Brock, J. Brioude, D. W. Fahey, F. C. Fehsenfeld, J. S. Holloway, M. Le Henaff, R. A. Lueb, S. A. McKeen, J. F. Meagher, D. M. Murphy, C. Paris, D. D. Parrish, A. E. Perring, I. B. Pollack, A. R. Ravishankara, A. L. Robinson, T. B. Ryerson, J. P. Schwarz, J. R. Spackman, A. Srinivasan, and L. A. Watts (2011), Organic aerosol formation downwind from the Deepwater Horizon oil spill, *Science*, *331*, 1295–1299.

Ding, X., M. Zheng, L. P. Yu, X. L. Zhang, R. J. Weber, B. Yan, A. G. Russell, E. S. Edgerton, and X. M. Wang (2008), Spatial and seasonal trends in biogenic secondary organic aerosol tracers and water-soluble organic carbon in the southeastern United States, *Environ. Sci. Technol*., *42*, 5171-5176.

Docherty, K. S., E. A. Stone, I. M. Ulbrich, P. F. DeCarlo, D. C. Snyder, J. J. Schauer, R. E. Peltier, R. J. Weber, S. M. Murphy, J. H. Seinfeld, B. D. Grover, D. J. Eatough, and J. L. Jimenez (2008), Apportionment of primary and secondary organic aerosols in southern California during the 2005 study of organic aerosols in Riverside (SOAR-1), *Environ. Sci. Technol*., *42*, 7655-7662.

Docherty, K. S., A. C. Aiken, J. A. Huffman, I. M. Ulbrich, P. F. DeCarlo, D. Sueper, D. R. Worsnop, D. C. Snyder, R. E. Peltier, R. J. Weber, B. D. Grover, D. J. Eatough, B. J. Williams, A. H. Goldstein, P. J. Ziemann, and J. L. Jimenez (2011), The 2005 Study of Organic Aerosols at Riverside (SOAR-1): instrumental intercomparisons and fine particle composition, *Atmos. Chem. Phys.*, *11*, 12387-12420.

Dockery, D.W., C. A. Pope, X. Xu, J. D. Spengler, J. H. Ware, M.E. Fay, B. G. Ferris, and F. E. Speizer (1993), An association between air pollution and mortality in six U.S. cities, *N. Engl. J. Med*., *329*, 1753-1808.

Dommen, J., A. Metzger, J. Duplissy, M. Kalberer, M. R. Alfarra, A. Gascho, E. Weingartner, A. S. H. Prevot, B. Verheggen, and U. Baltensperger (2006), Laboratory observation of oligomers in the aerosol from isoprene/NO_x photooxidation*, Geophys. Res. Lett*., *33*, L13805, doi:10.1029/2006gl026523.

Duarte, R. M. B. O., C. A. Pio, and A. C. Duarte (2005), Spectroscopic study of the water-soluble organic matter isolated from atmospheric aerosols collected under different atmospheric conditions, *Analytica Chimica Acta*, *530*, 7-14.

Duncan, B. N., R. V. Martin, A. C. Staudt, R. Yevich, and J. A. Logan (2003), Interannual and seasonal variability of biomass burning emissions constrained by

satellite observations, *J. Geophys. Res*., *108*, 4100, doi:10.1029/2002JD002378.

Duvall, R. M., B. J. Majestic, M. M. Shafer, P. Y. Chuang, B. R. T. Simoneit, and J. J. Schauer (2008), The water-soluble fraction of carbon, sulfur, and crustal elements in Asian aerosols and Asian soils, *Atmos. Environ*., *42*, 5872-5884.

Dzepina, K., C. D. Cappa, R. M. Volkamer, S. Madronich, P. F. DeCarlo, R. A. Zaveri, and J. L. Jimenez (2011), Modeling the multiday evolution and aging of secondary organic aerosol during MILAGRO 2006, *Environ. Sci. Technol*., *45*, 3496-3503, doi:10.1021/es103186.

Eatough, D. J., A. Wadsworth, D. A. Eatough, J. W. Crawford, L. D. Hansen, and E. A. Lewis (1993), A multiple-system, multichannel diffusion denuder sampler for the determination of fine particulate organic material in the atmosphere, *Atmos. Environ*., *27*, 1213–1219.

Engling, G., C. M. Carrico, S. M. Kreidenweis, J. L. Collett Jr, D. E. Day, W. C. Malm, E. Lincoln, W. M. Hao, Y. Iinuma, and H. Herrmann (2006), Determination of levoglucosan in biomass combustion aerosol by high-performance anion-exchange chromatography with pulsed amperometric detection, *Atmos. Environ*., *40*, 299-311.

Ervens, B., A. G. Carlton, B. J. Turpin, K. E. Altieri, S. M. Kreidenweis, and G. Feingold (2008), Secondary organic aerosol yields from cloud-processing of isoprene oxidation products, *Geophys. Res. Lett*., *35*, L02816, doi:10.1029/2007GL031828.

Ervens, B., and R. Volkamer (2010), Glyoxal processing by aerosol multiphase chemistry: towards a kinetic modeling framework of secondary organic aerosol formation in aqueous particles, *Atmos. Chem. Phys*., *10*, 8219-8244.

Ervens, B., B. J. Turpin, and R. J. Weber (2011), Secondary organic aerosol formation in cloud droplets and aqueous particles (aqSOA): a review of laboratory, field and model studies, *Atmos. Chem. Phys.*, *11*, 11069–11102.

Eva, H., and E. F. Lambin (1998), Remote sensing of biomass burning in tropical regions: Sampling issues and multisensor approach, *Remote Sens. Environ*., *64*, 292-315.

Fine, P. M., G. R. Cass, and B. R. T. Simoneit (2001), Chemical characterization of fine particle emissions from fireplace combustion of woods grown in the northeastern

United States, *Environ. Sci. Technol*., *35*, 2665-2675.

Fine, P. M., G. R. Cass, and B. R. T. Simoneit (2002), Chemical characterization of fine particle emissions from the fireplace combustion of woods grown in the southern United States, *Environ. Sci. Technol*., *36*, 1442-1451.

Fine, P. M., G. R. Cass, and B. R. T. Simoneit (2004a), Chemical characterization of fine particle emissions from the fireplace combustion of wood types grown in the Midwestern and Western United States, *Environ. Eng. Sci*., *21*, 387-409.

Fine, P. M., G. R. Cass, and B. R. T. Simoneit (2004b), Chemical characterization of fine particle emissions from the wood stove combustion of prevalent United States tree species, *Environ. Eng. Sci*., *21*, 705-721.

Fisseha, R., J. Dommen, K. Gaeggeler, E. Weingartner, V. Samburova, M. Kalberer, and U. Baltensperger (2006), Online gas and aerosol measurement of water soluble carboxylic acids in Zurich, *J. Geophys. Res*., *111*, D12316, doi:10.1029/2005JD006782.

Fountoukis, C., and A. Nenes (2007), ISORROPIA II: a computationally efficient thermodynamic equilibrium model for K^+-Ca^{2+}-Mg^{2+}-NH_4^+-Na^+-SO_4^{2-}-NO_3^--Cl^--H_2O aerosols, *Atmos. Chem. Phys*., *7*, 4639–4659.

Frank, N. H. (2006), Retained nitrate, hydrated sulfates, and carbonaceous mass in Federal Reference Method fine particulate matter for six eastern U.S. cities, *J. Air Waste Manage. Assoc*., *56*, 500-511.

Fuzzi, S., M. O. Andreae, B. J. Huebert, M. Kulmala, T. C. Bond, M. Boy, S. J. Doherty, A. Guenther, M. Kanakidou, K. Kawamura, V.-M. Kerminen, U. Lohmann, L. M. Russell, and U. Pöschl (2006), Critical assessment of the current state of scientific knowledge, terminology, and research needs concerning the role of organic aerosols in the atmosphere, climate, and global change, *Atmos. Chem. Phys*., *6*, 2017-2038.

Gao, S., J. D. Surratt, E. M. Knipping, E. S. Edgerton, M. Shahgholi, and J. H. Seinfeld (2006), Characterization of polar organic components in fine aerosols in the southeastern United States: Identity, origin, and evolution, *J. Geophys. Res*., *111*, D14314, doi:10.1029/2005JD006601.

Giglio, L., J. Descloitres, C. O. Justice, and Y. J. Kaufman (2003), An enhanced

contextual fire detection algorithm for MODIS, *Remote Sens. Environ*., *87*, 273-282.

Goldstein, A. H., C. D. Koven, C. L. Heald, and I. Y. Fung (2009), Biogenic carbon and anthropogenic pollutants combine to form a cooling haze over the southeastern United States, *P. Natl. Acad. Sci*., *106*, 8835–8840, doi:10.1073/PNAS.0904128106.

Grover, B. D., N. L. Eatough, W. R. Woolwine, D. J. Eatough, and R. A. Cary (2009), Modifications to the Sunset Laboratory carbon aerosol monitor for the simultaneous measurements of $PM_{2.5}$ nonvolatile and semi-volatile carbonaceous material, *J. Air Waste Manag. Assoc*., *59*, 1007-1017.

Guenther, A. (1997), Seasonal and spatial variations in natural volatile organic compound emissions, *Ecol. Appl*., *7*, 34–45.

Guenther, A., T. Karl, P. Harley, C. Wiedinmyer, P. I. Palmer, and C. Geron (2006), Estimates of global terrestrial isoprene emissions using MEGAN (model of emissions of gases and aerosols from nature), *Atmos. Chem. Phys*., *6*, 3181–3210.

Gupta, P., W. P. Harger, and J. Arey (1996), The contribution of nitro- and methylnitro-naphthalenes to the vapor-phase mutagenicity of ambient air samples, *Atmos. Environ.*, *30*, 3157-3166.

Hallquist, M., J. C. Wenger, U. Baltensperger, Y. Rudich, D. Simpson, M. Claeys, J. Dommen, N. M. Donahue, C. George, A. H. Goldstein, J. F. Hamilton, H. Herrmann, T. Hoffmann, Y. Iinuma, M. Jang, M. E. Jenkin, J. L. Jimenez, A. Kiendler-Scharr, W. Maenhaut, G. McFiggans, Th. F. Mentel, A. Monod, A. S. H. Prévôt, J. H. Seinfeld, J. D. Surratt, R. Szmigielski, and J. Wildt (2009), The formation, properties and impact of secondary organic aerosol: current and emerging issues, *Atmos. Chem. Phys*., *9*, 5155–5236.

Hand, J. L., B. A. Schichtel, M. Pitchford, W. C. Malm, and N. H. Frank (2012), Seasonal composition of remote and urban fine particulate matter in the United States, *J. Geophys. Res*., *117*, D05209, doi:10.1029/2011JD017122.

Hansen, O. A., E. S. Edgerton, B. E. Hartsell, J. J. Jansen, N. Kandasamy, G. M. Hidy, and C. L. Blanchard (2003), The southeastern aerosol research and characterization study: Part 1-Overview, *J. Air Waste Manage. Assoc*., *53*, 1460–1471.

Hayes, P. L., A. M. Ortega, M. J. Cubison, W. Hu, D. W. Toohey, J. H. Flynn, B. L. Lefer, N. Grossberg, S. Alvarez, B. Rappenglück, J. Taylor, J. D. Allan, J. S.

Holloway, J. B. Gilman, W. C. Kuster, J. A. de Gouw, P. Massoli, X. Zhang, J. Liu, R. J. Weber, A. Corrigan, L. M. Russell, Y. Zhao, S. S. Cliff, A. S. Wexler, G. Isaacman, D. R. Worton, N. M. Kreisberg, S. V. Hering, A. H. Goldstein, R. Thalman, R. Volkamer, Y. H. Lin, J. D. Surratt, J. H. Offenberg, K. D. Froyd, S. Dusanter, S. Griffith, P. S. Stevens, and J. L. Jimenez (2012), Aerosol composition in Los Angeles duing the 2010 CalNex campaign studied by high resolution aerosol mass spectrometry, *J. Geophys. Res.,* under review.

Heald, C. L., D. J. Jacob, R. J. Park, L. M. Russell, B. J. Huebert, J. H. Seinfeld, H. Liao, and R. J. Weber (2005), A large organic aerosol source in the free troposphere missing from current models, *Geophys. Res. Lett*., *32*, L18809, doi:10.1029/2005GL023831.

Hecobian, A., X. Zhang, M. Zheng, N. H. Frank, E. S. Edgerton, and R. J. Weber (2010), Water-soluble organic aerosol material and the light-absorption characteristics of aqueous extracts measured over the Southeastern United States, *Atmos. Chem. Phys.*, *10*, 5965-5977, doi:10.5194/acp-10-5965-2010.

Hennigan, C. J., M. H. Bergin, J. E. Dibb, and R. J. Weber (2008a), Enhanced secondary organic aerosol formation due to water uptake by fine particles, *Geophys. Res. Lett*., *35*, L18801, doi: 10.1029/2008GL035046.

Hennigan, C., A. P. Sullivan, C. I. Fountoukis, A. Nenes, A. Hecobian, O. Vargas, R. E. Peltier, A. T. C. Hanks, L. G. Huey, B. L. Lefer, A. G. Russell, and R. J. Weber (2008b), On the volatility and production mechanism of newly formed nitrate and water soluble organic aerosol in Mexico City, *Atmos. Chem. Phys*., *8*, 3761-3768.

Hennigan, C. J., M. H. Bergin, A. G. Russell, A. Nenes, and R. J. Weber (2009), Gas/particle partitioning of water-soluble organic aerosol in Atlanta, *Atmos. Chem. Phys.*, *9*, 3613-3628.

Hennigan, C. J., A. P. Sullivan, J. L. Collett, Jr., and A. L. Robinson (2010), Levoglucosan stability in biomass burning particles exposed to hydroxyl radicals, *Geophys. Res. Lett*., *37*, L09806, doi:10.1029/2010GL043088.

Henze, D. K., J. H. Seinfeld, N. L. Ng, J. H. Kroll, T.-M. Fu, D. J. Jacob, and C. L. Heald (2008), Global modeling of secondary organic aerosol formation from aromatic hydrocarbons: high- vs. low-yield pathways, *Atmos. Chem. Phys*., *8*, 2405-2421.

Hersey, S. P., J. S. Craven, K. A. Schilling, A. R. Metcalf, A. Sorooshian, M. N. Chan, R. C. Flagan, and J. H. Seinfeld (2011), The Pasadena Aerosol Characterization

Observatory (PACO): chemical and physical analysis of the western Los Angeles Basin aerosol, *Atmos. Chem. Phys.*, *11*, 7417-7443.

Hobbs, P. V., J. S. Reid, R. A. Kotchenruther, R. J. Ferek, and R. Weiss (1997), Direct radiative forcing by smoke from biomass burning, *Science*, *275*, 1776-1778.

Hodzic, A., J. L. Jimenez, S. Madronich, M. R. Canagaratna, P. F. DeCarlo, L. Kleinman, and J. Fast (2010), Modeling organic aerosols in a megacity: potential contribution of semi-volatile and intermediate volatility primary organic compounds to secondary organic aerosol formation, *Atmos. Chem. Phys*., *10*, 5491–5514, doi:10.5194/acp-10-5491-2010.

Hoffer, A., A. Gelencser, P. Guyon, G. Kiss, O. Schmid, G. P. Frank, P. Artaxo, and M. O. Andreae (2006), Optical properties of humic-like substances (HULIS) in biomass-burning aerosols, *Atmos. Chem. Phys*., *6*, 3563-3570.

Hoffmann, T., J. R. Odum, F. Bowman, D. Collins, D. Klockow, R. C. Flagan, and J. H. Seinfeld (1997), Formation of organic aerosols from the oxidation of biogenic hydrocarbons, *J. Atmos. Chem*., *26*, 189–222.

Hoffmann, D., A. Tilgner, Y. Iinuma, and H. Herrmann (2010), Atmospheric stability of levoglucosan: a detailed laboratory and modeling study, *Environ. Sci. Technol*., *44*, 694-699.

Hoyle, C. R., M. Boy, N. M. Donahue, J. L. Fry, M. Glasius, A. Guenther, A. G. Hallar, K. Huff Hartz, M. D. Petters, T. Petäjä, T. Rosenoern, and A. P. Sullivan (2011), A review of the anthropogenic influence of biogenic secondary organic aerosol, *Atmos. Chem. Phys.*, *11*, 321-343.

Huang, X.-F., J. Z. Yu, L.-Y. He, and Z. Yuan (2006), Water-soluble organic carbon and oxalate in aerosols at a coastal urban site in China: Size distribution characteristics, sources, and formation mechanisms, *J. Geophys. Res*., *111*, D22212, doi:10.1029/2006jd007408.

Huang, X.-F., and J. Z. Yu (2007), Is vehicle exhaust a significant primary source of oxalic acid in ambient aerosols? *Geophys. Res. Lett*., *34*, L02808, doi:10.1029/2006GL028457.

IPCC, Fourth Assessment Record: Climate change 2007, Cambridge University Press,

New York, 2007.

Jacob, D. J., J. H. Crawford, H. Maring, A. D. Clarke, J. E. Dibb, L. K. Emmons, R. A. Ferrare, C. A. Hostetler, P. B. Russell, H. B. Singh, A. M. Thompson, G. E. Shaw, E. McCauley, J. R. Pederson, and J. A. Fisher (2010), The Arctic Research of the Composition of the Troposphere from Aircraft and Satellites (ARCTAS) mission: design, execution, and first results, *Atmos. Chem. Phys.*, *10*, 5191-5212.

Jacobson, M. Z. (1998), Studying the effects of aerosols on vertical photolysis rate coefficient and temperature profiles over an urban airshed, *J. Geophys. Res.*, *103*, 10593-10604.

Jacobson, M. Z. (1999), Isolating nitrated and aromatic aerosols and nitrated aromatic gases as sources of ultraviolet light absorption, *J. Geophys. Res.*, *104*, 3527-3542.

Jacobson, M. Z. (2012), Investigating cloud absorption effects: Global absorption properties of black carbon, tar balls, and soil dust in clouds and aerosols, *J. Geophys. Res*., *117*, D06205, doi:10.1029/2011JD017218.

Jaoui, M., E. O. Edney, T. E. Kleindienst, M. Lewandowski, J. H. Offenberg, J. D. Surratt, and J. H. Seinfeld (2008), Formation of secondary organic aerosol from irradiated α-pinene/toluene/NO_x mixtures and the effect of isoprene and sulfur dioxide, *J. Geophys. Res.*, *113*, D09303, doi:09310.01029/02007JD009426.

Jimenez, J. L., M. R. Canagaratna, N. M. Donahue, A. S. H. Prevot, Q. Zhang, J. H. Kroll, P. F. DeCarlo, J. D. Allan, H. Coe, N. L. Ng, A. C. Aiken, K. S. Docherty, I. M. Ulbrich, A. P. Grieshop, A. L. Robinson, J. Duplissy, J. D. Smith, K. R. Wilson, V. A. Lanz, C. Hueglin, Y. L. Sun, J. Tian, A. Laaksonen, T. Raatikainen, J. Rautiainen, P. Vaattovaara, M. Ehn, M. Kulmala, J. M. Tomlinson, D. R. Collins, M. J. Cubison, E. J. Dunlea, J. A. Huffman, T. B. Onasch, M. R. Alfarra, P. I. Williams, K. Bower, Y. Kondo, J. Schneider, F. Drewnick, S. Borrmann, S. Weimer, K. Demerjian, D. Salcedo, L. Cottrell, R. Griffin, A. Takami, T. Miyoshi, S. Hatakeyama, A. Shimono, J. Y. Sun, Y. M. Zhang, K. Dzepina, J. R. Kimmel, D. Sueper, J. T. Jayne, S. C. Herndon, A. M. Trimborn, L. R. Williams, E. C. Wood, A. M. Middlebrook, C. E. Kolb, U. Baltensperger, and D. R. Worsno (2009), Evolution of Organic Aerosols in the Atmosphere, *Science*, *326*, 1525–1529, 10.1126/science.1180353.

Kawamura, K., and K. Ikushima (1993), Seasonal changes in the distribution of

dicarboxylic acids in the urban atmosphere, *Environ. Sci. Technol*., *27*, 2227– 2235.

Kim, E., P. K. Hopke, and E. S. Edgerton (2003a), Source identification of Atlanta aerosol by positive matrix factorization, *J. Air Waste Manage. Assoc*., *53*, 731-739.

Kim, E., P. K. Hopke, P. Paatero, and E. S. Edgerton (2003b), Incorporation of parametric factors into multilinear receptor model studies of Atlanta aerosol, *Atmos. Environ*., *37*, 5009-5021.

Kim, E., and P. K. Hopke (2006), Characterization of fine particle sources in the Great Smoky Mountains area, *Sci. Total Environ*., *368*, 781–794.

Kleinman, L. I., S. R. Springston, P. H. Daum, Y.-N. Lee, L. J. Nunnermacker, G. I. Senum, J. Wang, J. Weinstein-Lloyd, M. L. Alexander, J. Hubbe, J. Ortega, M. R. Canagaratna, and J. Jayne (2008), The time evolution of aerosol composition over the Mexico City plateau, *Atmos. Chem. Phys*., *8*, 1559-1575.

Kondo, Y., Y. Miyazaki, N. Takegawa, T. Miyakawa, R. J. Weber, J. L. Jimenez, Q. Zhang, and D. R. Worsnop (2007), Oxygenated and water-soluble organic aerosols in Tokyo, *J. Geophys. Res*., *112*, D01203, doi:10.1029/2006JD007056.

Kroll, J. H., N. L. Ng, S. M. Murphy, R. C. Flagan, and J. H. Seinfeld (2006), Secondary organic aerosol formation from isoprene photooxidation, *Environ. Sci. Technol*., *40*, 1869-1877.

Kundu, S., K. Kawamura, T. W. Andreae, A. Hoffer, and M. O. Andreae (2010), Molecular distributions of dicarboxylic acids, ketocarboxylic acids and a-dycarbonyls in biomass burning aerosols: implications for photochemical production and degradation in smoke layers, *Atmos. Chem. Phys*., *10*, 2209-2225.

Lack, D. A., and C. D. Cappa (2010), Impact of brown and clear carbon on light absorption enhancement, single scatter albedo and absorption wavelength dependence of black carbon, *Atmos. Chem. Phys*., *10*, 4207-4220.

Lawson, D. R., and J. W. Winchester (1979), Sulfur, potassium, and phosphorus associations in aerosols from South-American tropical rain forests, *J. Geophys. Res*., *84*, 3723-3727.

Lee, E., C. K. Chan, and P. Paatero (1999), Application of positive matrix factorization in

source apportionment of particulate pollutants in Hong Kong, *Atmos. Environ*., *33*, 3201-3212.

Lee, S., K. Baumann, J. J. Schauer, R. J. Sheesley, L. P. Naeher, S. Meinardi, D. R. Blake, E. S. Edgerton, A. G. Russell, and M. Clements (2005), Gaseous and particulate emissions from prescribed burning in Georgia, *Environ. Sci. Technol*., *39*, 9049-9056.

Lee, S., W. Liu, Y. H. Wang, A. G. Russell, and E. S. Edgerton (2008), Source apportionment of $PM_{2.5}$: Comparing PMF and CMB results for four ambient monitoring sites in the southeastern United States, *Atmos. Environ*., *42*, 4126-4137.

Lee, S., Y. Wang, and A. G. Russell (2010), Assessment of secondary organic carbon in the southeastern United States: a review, *J. Air Waste Manage. Assoc*., *60*, 1282-1292.

Lelieveld, J., P. J. Crutzen, V. Ramanathan, M. O. Andreae, C. A. M. Brenninkmeijer, T. Campos, G. R. Cass, R. R. Dickerson, H. Fischer, J. A. de Gouw, A. Hansel, A. Jefferson, D. Kley, A. T. J. de Laat, S. Lal, M. G. Lawrence, J. M. Lobert, O. L. Mayol-Bracero, A. P. Mitra, T. Novakov, S. J. Oltmans, K. A. Prather, T. Reiner, H. Rodhe, H. A. Scheeren, D. Sikka, and J. Williams (2001), The Indian Ocean Experiment: Widespread air pollution from South and Southeast Asia, *Science*, *291*, 1031-1036.

Liggio, J., S.-M. Li, and R. McLaren (2005a), Heterogeneous Reactions of Glyoxal on Particulate Matter: Identificationof Acetals and Sulfate Esters, *Environ. Sci. Technol*., *39*,1532-1541.

Liggio, J., S.-M. Li, and R. McLaren (2005b), Reactive uptake of glyoxal by particulate matter, *J. Geophys. Res*., *110*, D10304, doi:10.1029/2004JD005113.

Lighty, J. S., J. M. Veranth, and A. F. Sarofim (2000), Combustion aerosols: Factors governing their size and composition and implications to human health, *J. Air Waste Manage. Assoc*., *50*, 1565-1618.

Lim, H. J., and B. J. Turpin (2002), Origins of primary and secondary aerosol in Atlanta: Results of time-resolved measurements during the Atlanta Supersite Experiment, *Environ. Sci. Technol*., *36*, 4489-4496.

Lim, Y. B., Y. Tan, M. J. Perri, S. P. Seitzinger, and B. J. Turpin (2010), Aqueous

chemistry and its role in secondary organic aerosol (SOA) formation, *Atmos. Chem. Phys*., *10*, 10521-10539.

Lin, Y.-H., Z. Zhang, K. S. Docherty, H. Zhang, S. H. Budisulistiorini, C. L. Rubitschun, S. L. Shaw, E. M. Knipping, E. S. Edgerton, T. E. Kleindienst, A. Gold, and J. D. Surratt (2012), Isoprene epoxydiols as precursors to secondary organic aerosol formation: Acidcatalyzed reactive uptake studies with authentic compounds, *Environ. Sci. Technol*., *46*, 250-258.

Liu, J., X. Zhang, E. T. Parker, P. R. Veres, J. M. Roberts, J. de Gouw, P. L. Hayes, J. L. Jimenez, L. G. Huey, and R. J. Weber (2012), On the gas-particle partitioning of soluble organic aerosol in two urban atmosphere with contrasting emissions: Part 2. Gas and particle phase formic acid, *J. Geophys. Res.*, under review.

Liu, W., Y. Wang, A. Russell, and E. S. Edgerton (2005), Atmospheric aerosol over two urban-rural pairs in the southeastern United States: Chemical composition and possible sources, *Atmos. Environ*., *39*, 4453-4470.

Lukacs, H., A. Gelencser, S. Hammer, H. Puzbaum, C. Pio, M. Legrand, A. Kasper-Giebl, M. Handler, A. Limbeck, D. Simpson, and S. Preunkert (2007), Seasonal trends and possible sources of brown carbon based on 2-year aerosol measurements at six sites in Europe*, J. Geophys. Res*., *112*, D23S18 10.1029/2006JD008151.

Ma, Y., R. J. Weber, Y.-N. Lee, D. A. Orsini, K. Maxwell-Meier, D. C. Thornton, A. R. Bandy, A. D. Clarke, D. R. Blake, G. W. Sachse, H. E. Fuelberg, C. M. Kiley, J.-H. Woo, D. G. Streets, and G. R. Carmichael (2003), Characteristics and influence of biosmoke on the fine-particle ionic composition measured in Asian outflow during the Transport and Chemical Evolution Over the Pacific (TRACE-P) experiment, *J. Geophys. Res*., *108*, 8816, doi:10.1029/2002JD003128.

Marsik, F. J., K. W. Fischer, T. D. McDonald, and P. J. Samson (1995), Comparison of methods for estimating mixing height used during the 1992 Atlanta Field Intensive, *J. Appl. Meteorol*., *34*, 1802-1814.

Matsunaga, S. N., S. Kato, A. Yoshino, J. P. Greenberg, Y. Kajii, and A. B. Guenther (2005), Gas-aerosol partitioning of semi volatile carbonyls in polluted atmosphere in Hachioji, Tokyo, *Geophys. Res. Lett*., *32*, L11805, 10.1029/2004gl021893.

Miyazaki, Y., Y. Kondo, M. Shiraiwa, N. Takegawa, T. Miyakawa, S. Han, K. Kita, M. Hu, Z. Q. Deng, Y. Zhao, N. Sugimoto, D. R. Blake, and R. J. Weber (2009), Chemical characterization of water- soluble organic carbon aerosols at a rural

site in the Pearl River Delta, China, in the summer of 2006, *J. Geophys. Res*., *114*, D14208, doi:10.1029/2009JD011736.

Morales, J. A., D. Pirela, and J. Durban (1996), Determination of the levels of Na, K, Ca, Mg, Fe, Zn and Cu in aerosols of the western Venezuelan savannah region, *Sci. Total Environ*., *180*, 155-164.

Müller, J.-F., T. Stavrakou, S. Wallens, I. De Smedt, M. Van Roozendael, M. J. Potosnak, J. Rinne, B. Munger, A. Goldstein, and A. B. Guenther (2008), Global isoprene emissions estimated using MEGAN, ECMWF analyses and a detailed canopy environment model, *Atmos. Chem. Phys*., *8*, 1329–1341.

Murphy, D. M., D. J. Cziczo, K. D. Froyd, P. K. Hudson, B. M. Matthew, A. M. Middlebrook, R. E. Peltier, A. Sullivan, D. S. Thomson, and R. J. Weber (2006), Single-particle mass spectrometry of tropospheric aerosol particles, *J. Geophys. Res*., *111*, D23S32, doi:10.1029/2006JD007340.

Myriokefalitakis, S., M. Vrekoussis, K. Tsigaridis, F. Wittrock, A. Richter, C. Brühl, R. Volkamer, J. P. Burrows, and M. Kanakidou (2008), The influence of natural and anthropogenic secondary sources on the glyoxal global distribution, *Atmos. Chem. Phys*., *8*, 4965–4981.

Myriokefalitakis, S., K. Tsigaridis, N. Mihalopoulos, J. Sciare, A. Nenes, K. Kawamura, A. Segers, and M. Kanakidou (2011), In-cloud oxalate formation in the global troposphere: a 3-D modeling study, *Atmos. Chem. Phys*., *11*, 5761-5782.

Nakayama, T., Y. Matsumi, K. Sato, T. Imamura, A. Yamazaki, and A. Uchiyama (2010), Laboratory studies on optical properties of secondary organic aerosols generated during the photooxidation of toluene and the ozonolysis of a-pinene, *J. Geophys. Res.*, *115*, D24204, doi:10.1029/22010JD014387.

Ng, N. L., J. H. Kroll, A. W. H. Chan, P. S. Chhabra, R. C. Flagan, and J. H. Seinfeld (2007), Secondary organic aerosol formation from m-xylene, toluene, and benzene, *Atmos. Chem. Phys*., *7*, 3909–3922.

Ng, N. L., M. R. Canagaratna, Q. Zhang, J. L. Jimenez, J. Tian, I. M. Ulbrich, J. H. Kroll, K. S. Docherty, P. S. Chhabra, R. Bahreini, S. M. Murphy, J. H. Seinfeld, L. Hildebrandt, N. M. Donahue, P. F. DeCarlo, V. A. Lanz, A. S. H. Prevot, E. Dinar, Y. Rudich, and D. R. Worsnop (2010), Organic aerosol components observed in Northern Hemispheric datasets from Aerosol Mass Spectrometry, *Atmos. Chem.*

Phys., *10*, 4625–4641, doi:10.5194/acp-10-4625-2010.

Ng, N. L., S. C. Herndon, A. Trimborn, M. R. Canagaratna, P. L. Croteau, T, B, Onasch, D. Sueper, D. R. Worsnop, Q. Zhang, Y. L. Sun, and J. T. Jayne (2011), An Aerosol Chemical Speciation Monitor (ACSM) for rountine monitoring of the composition and mass concentrations of ambient aerosol, *Aerosol Sci. Technol.*, *45*, 780-794.

Nguyen, T. B., P. B. Lee, K. M. Updyke, D. L. Bones, J. Laskin, A. Laskin, and S. A. Nizkorodov (2012), Formation of nitrogen- and sulphur-containing light-absorbing compounds accelerated by evaporation of water from secondary organic aerosols, *J. Geophys. Res*., *117*, D01207, doi:10.1029/2011JD016944.

NIOSH (1996), Elemental carbon (diesel particulate): method 5040, in *NIOSH Manual of Analytical Methods*, edited by P. M. Eller and M. E. Cassinelli, National Institute for Occupational Safety and Health, Cincinnati.

Noziere, B., and W. Esteve (2005), Organic reactions increasing the absorption index of atmospheric sulfuric acid aerosols, *J. Geophys. Res*., *32*, L03812, doi:10.1029/2004GL021942.

Noziere, B., P. Dziedzic, and A. Cordova (2007), Formation of secondary light-absorbing "fulvic-like" oligomers: A common process in aqueous and ionic atmospheric particles? *Geophys. Res. Lett*., *34*, L21812, doi:10.1029/22007GL031300.

Odum, J. R., T. Hoffmann, F. Bowman, D. Collins, R. C. Flagan, and J. H. Seinfeld (1996), Gas/particle partitioning and secondary organic aerosol yields, *Environ. Sci. Technol*., *30*, 2580-2585.

Odum, J. R., T. P. W. Jungkamp, R. R. Griffin, R. C. Flagan, and J. H. Seinfeld (1997), The atmospheric aerosol-forming potential of whole gasoline vapour, *Science*, *276*, 96-99.

Padró, L. T., R. H. Moore, X. Zhang, N. Rastogi, R. J. Weber, and A. Nenes (2011), Mixing state and compositional effects on CCN activity and droplet growth kinetics of size-resolved CCN in an urban environment, *Atmos. Chem. Phys. Disc.*, *11*, 32723-32768.

Pankow, J. F. (1994), An absorption model of the gas/aerosol partitioning of organic

compounds in the atmosphere, *Atmos. Environ*., *28*, 185-188.

Parikh, H. M., A. G. Carlton, W. Vizuete, and R. M. Kamens (2011), Modeling secondary organic aerosol using a dynamic partitioning approach incorporating particle aqueous-phase chemistry, *Atmos. Environ*., *45*, 1126–1137.

Park, R. J., M. J. Kim, J. I. Jeong, D. Yooun, and S. Kim (2010), A contribution of brown carbon aerosol to the aerosol light absorption and its radiative forcing in East Asia, *Atmos. Environ.*, *44*, 1414-1421.

Patashnick, H., G. Rupprecht, J. L. Ambs, and M. B. Meyer (2001), Development of a reference standard for particulate matter mass in ambient air, *Aerosol Sci. Technol*., *34*, 42-45.

Peltier, R. E., R. J. Weber, and A. P. Sullivan (2007), Investigating a liquid-based method for online organic carbon detection in atmospheric particles, *Aerosol Sci. Technol.*, *41*, 1117-1127.

Penner, J. E., R. E. Dickinson, and C. A. Oneill (1992), Effects of aerosol from biomass burning on the global radiation budget, *Science*, *256*, 1432-1434.

Perraud, V., E. A. Bruns, M. J. Ezell, S. N. Johnson, Y. Yu, M. L. Alexander, A. Zelenyuk, D. Imre, W. L. Chang, D. Dabdub, J. F. Pankow, and B. J. Finlayson-Pitts (2012), Nonequilibrium atmospheric secondary organic aerosol formation and growth, *P. Natl. Acad. Sci*., *109*, 2836-2841.

Pio, C. A., M. Legrand, C. A. Alves, T. Oliveira, J. Afonso, A. Caseiro, H. Puxbaum, A. Sanchez-Ochoa, and A. Gelencser (2008), Chemical composition of atmospheric aerosols during the 2003 summer intense forest fire period, *Atmos. Environ*., *42*, 7530-7543.

Polissar, A. V., P. K. Hopke, and P. Paatero (1998), Atmospheric aerosol over Alaska - 2. Elemental composition and sources, *J. Geophys. Res*., *103*, 19045-19057.

Portmann, R. W., S. Solomon, and G. C. Hegerl (2009), Spatial and seasonal patterns in climate change, temperatures, and precipitation across the United States, *P. Natl. Acad. Sci*., *106*, 7324-7329.

Presto, A. A., K. E. H. Hartz, and N. M. Donahue (2005), Secondary organic aerosol

production from terpene ozonolysis. 2. Effect of NO_x concentration, *Environ. Sci. Technol*., *39*, 7046–7054.

Puxbaum, H., A. Caseiro, A. Sanchez-Ochoa, A. Kasper-Giebl, M. Claeys, A. Gelencser, M. Legrand, S. Preunkert, and C. Pio (2007), Levoglucosan levels at background sites in Europe for assessing the impact of biomass combustion on the European aerosol background, *J. Geophys. Res*., *112*, D23S05, doi:10.1029/2006JD008114.

Pye, H. O. T., and J. H. Seinfeld (2010), A global perspective on aerosol from low-volatility organic compounds, *Atmos. Chem. Phys*., *10*, 4377–4401.

Ramadan, Z., X. H. Song, and P. K. Hopke (2000), Identification of sources of Phoenix aerosol by positive matrix factorization, *J. Air Waste Manage. Assoc*., *50*, 1308-1320.

Roberts, G. C., M. O. Andreae, J. Zhou, and P. Artaxo (2001), Cloud condensation nuclei in the Amazon Basin: "Marine" conditions over a continent? *Geophys. Res. Lett., 28*, 2807-2810.

Robinson, A. L., R. Subramanian, N. M. Donahue, A. Bernardo-Bricker, and W. F. Rogge (2006), Source apportionment of molecular markers and organic aerosol. 2. Biomass smoke, *Environ. Sci. Technol*., *40*, 7811-7819.

Robinson, A. L., N. M. Donahue, M. K. Shrivastava, E. A. Weitkamp, A. M. Sage, A. P. Grieshop, T. E. Lane, J. R. Pierce, and S. N. Pandis (2007), Rethinking organic aerosols: semivolatile emissions and photochemical aging, *Science*, *315*, 1259-1262.

Rogge, W. F., L. M. Hildemann, M. A. Mazurek, G. R. Cass, and B. R. T. Simoneit (1998), Sources of fine organic aerosol. 9. Pine, oak and synthetic log combustion in residential fireplaces, *Environ. Sci. Technol*., *32*, 13-22.

Saarikoski, S., H. Timonen, K. Saarnio, M. Aurela, L. Järvi, P. Keronen, V.-M. Kerminen, and R. Hillamo (2008), Sources of organic carbon in fine particulate matter in northern European urban air, *Atmos. Chem. Phys*., *8*, 6281–6295.

Sandradewi, J., A. S. H. Prevot, E. Weingartner, R. Schmidhauser, M. Gysel, and U. Baltensperger (2008), A study of wood burning and traffic aerosols in an alpine valley using a multi-wavelength aethalometer, *Atmos. Environ.*, *42*, 101-112.

Sareen, N., A. N. Schwier, E. L. Shapiro, D. Mitroo, and V. F. McNeill (2010), Secondary organic material formed by methylglyoxal in aqueous aerosol mimics, *Atmos. Chem. Phys*., *10*, 997–1016.

Saxena, P., and L. M. Hildemann (1996), Water-soluble organics in atmospheric particles: a critical review of the literature and application of thermodynamics to identify candidate compounds, *J. Atmos. Chem., 24*, 57-109.

Schauer, J. J., W. F. Rogge, L. M. Hildemann, M. A. Mazurek, and G. R. Cass (1996), Source apportionment of airborne particulate matter using organic compounds as tracers, *Atmos. Environ*., *30*, 3837-3855.

Schauer, J. J., M. J. Kleeman, G. R. Cass, and B. R. T. Simoneit (1999), Measurement of emissions from air pollution sources. 1. C1 through C29 organic compounds from meat charbroiling, *Environ. Sci. Technol*., *33*, 1566-1577.

Schauer, J. J., and G. R. Cass (2000), Source apportionment of wintertime gas-phase and particle-phase air pollutants using organic compounds as tracers, *Environ. Sci. Technol*., *34*, 1821-1832.

Schichtel, B. A., W. C. Malm, G. Bench, S. Fallon, C. E. McDade, J. C. Chow, and J. G. Watson (2007), Fossil and contemporary fine particulate carbon fractions at 12 rural and urban sites in the United States, *J. Geophys. Res*., *113*, D02311, doi:10.1029/2007JD008605.

Schkolnik, G., and Y. Rudich (2006), Detection and quantification of levoglucosan in atmospheric aerosols: A review, *Anal. Bioanal. Chem*., *385*, 26-33.

Schmidl, C., I. L. Marr, A. Caseiro, P. Kotianova, A. Berner, H. Bauer, A. Kasper-Giebl, and H. Puxbaum (2008), Chemical characterization of fine particle emissions from wood stove combustion of common woods growing in mid-European Alpine regions, *Atmos. Environ*., *42*, 126–141.

Schwartz, J., D. Slater, T. V. Larson, W. E. Pierson, and J. Z. Koenig (1993), Particulate air pollution and hospital emergency room visits for asthma in Seattle, *Am. Rev. Respir. Dis.*, *147*, 826-831.

Seagrave, J. C., J. D. McDonald, E. Bedrick, E. S. Edgerton, A. P. Gigliotti, J. J. Jansen, L. Ke, L. Naeher, S. K. Seilkop, M. Zheng, and J. L. Mauderly (2006), Lung toxicity of ambient particulate matter from southeastern US sites with different contributing

sources: Relationships between composition and effects, *Environ. Health Perspect*., *114*, 1387–1393.

Seinfeld, J. H. and J .F. Pankow (2003), Organic atmospheric particulate material, *Ann. Rev. Phys. Chem*., *54*, 121–140.

Setyan, A., Q. Zhang, M. Merkel, W. B. Knighton, Y. Sun, C. Song, J. E. Shilling, T. B. Onasch, S. C. Herndon, D. R. Worsnop, J. D. Fast, R. A. Zaveri, L. K. Berg, A. Wiedensohler, B. A. Flowers, M. K. Dubey, and R. Subramanian (2012), Submicron particles influenced by mixed biogenic and anthropogenic emissions: high-resolution aerosol mass spectrometry results from the Carbonaceous Aerosols and Radiative Effects Study (CARES), *Atmos. Chem. Phys. Disc.*, *12*, 5601-5658.

Shapiro, E. L., J. Szprengiel, N. Sareen, C. N. Jen, M. R. Giordano, and V. F. McNeill (2009), Light-absorbing secondary organic material formed by glyoxal in aqueous aerosol mimics, *Atmos. Chem. Phys., 9*, 2289-2300.

Simoneit, B. R. T., J. J. Schauer, C. G. Nolte, D. R. Oros, V. O. Elias, M. P. Fraser, W. F. Rogge, and G. R. Cass (1999), Levoglucosan, a tracer for cellulose in biomass burning and atmospheric particles, *Atmos. Environ*., *33*, 173-182.

Simoneit, B. R. T. (2002), Biomass burning - A review of organic tracers for smoke from incomplete combustion, *Appl. Geochem*., *17*, 129-162.

Song, C., K. S. Na, and D. R. Cocker (2005), Impact of the hydrocarbon to NO_x ratio on secondary organic aerosol formation, *Environ. Sci. Technol*., *39*, 3143–3149.

Song, C., R. A. Zaveri, M. L. Alexander, J. A. Thornton, S. Madronich, J. V. Ortega, A. Zelenyuk, X.-Y. Yu, A. Laskin, and D. A. Maughan (2007), Effect of hydrophobic primary organic aerosols on secondary organic aerosol formation from ozonolysis of alpha-pinene, *Geophys. Res. Lett*., *34*, L20803, doi:10.1029/2007GL030720.

Sorooshian, A., F. J. Brechtel, B. Ervens, G. Feingold, V. Varutbangkul, R. Bahreini, S. Murphy, J. S. Holloway, E. L. Atlas, K. Anlauf, G. Buzorius, H. Jonsson, R. C. Flagan, and J. H. Seinfeld (2006), Oxalic acid in clear and cloudy atmospheres: Analysis of data from International Consortium for Atmospheric Research on Transport and Transformation 2004, *J. Geophys. Res*., *111*, D23S45, doi: 10.1029/2005JD006880.

Sorooshian, A., M.-L. Lu, F. J. Brechtel, H. Jonsson, G. Feingold, R. C. Flagan, and J. H.

Seinfeld (2007), On the source of organic acid aerosol layers above clouds, *Environ. Sci. Technol*., *41*, 4647-4654.

Sorooshian, A., S. M. Murphy, S. Hersey, R. Bahreini, H. Jonsson, R. C. Flagan, and J. H. Seinfeld (2010), Constraining the contribution of organic acids and AMS m/z 44 to the organic aerosol budget: On the importance of meteorology, aerosol hygroscopicity, and region, *Geophys. Res. Lett*., *37*, L21807, doi:10.1029/2010gl044951.

Spracklen, D. V., J. L. Jimenez, K. S. Carslaw, D. R. Worsnop, M. J. Evans, G. W. Mann, Q. Zhang, M. R. Canagaratna, J. Allan, H. Coe, G. McFiggans, A. Rap, and P. Forster (2011), Aerosol mass spectrometer constraint on the global secondary organic aerosol budget, *Atmos. Chem. Phys*., *11*, 12109–12136.

Stone, E. A., C. J. Hedman, R. J. Sheesley, M. M. Shafer, and J. J. Schauer (2009), Investigating the chemical nature of humic-like substances (HULIS) in North American atmospheric aerosols by liquid chromatography tandem mass spectrometry, *Atmos. Environ*., *43*, 4205-4213, doi:10.1016/j.atmosenv.2009.05.030.

Stone, E. A., C. J. Hedman, J. B. Zhou, M. Mieritz, and J. J. Schauer (2010), Insights into the nature of secondary organic aerosol in Mexico City during the MILAGRO experiment 2006, *Atmos. Environ*., *44*, 312-319, doi:10.1016/j.atmosenv.2009.10.036.

Sullivan, A. P., R. J. Weber, A. L. Clements, J. R. Turner, M. S. Bae, and J. J. Schauer (2004), A method for on-line measurement of water-soluble organic carbon in ambient aerosol particles: Results from an urban site, *Geophys. Res. Lett*., *31*, L13105, doi:10.1029/2004GL019681.

Sullivan, A. P., R. E. Peltier, C. A. Brock, J. A. de Gouw, J. S. Holloway, C. Warneke, A. G. Wollny, and R. J. Weber (2006), Airborne measurements of carbonaceous aerosol soluble in water over northeastern United States: Method development and an investigation into water-soluble organic carbon sources, *J. Geophys. Res*., *111*, D23S46, doi:10.1029/2006JD007072.

Sullivan, A. P., and R. J. Weber (2006), Chemical characterization of the ambient organic aerosol soluble in water: 2. Isolation of acid, neutral, and basic fractions by modified size-exclusion chromatography, *J. Geophys. Res.*, *111*, D05315, doi:10.1029/2005JD006486.

Sullivan, A. P., A. S. Holden, L. A. Patterson, G. R. McMeeking, S. M. Kreidenweis, W. C. Malm, W. M. Hao, C. E. Wold, and J. L. Collett Jr. (2008), A method for smoke marker measurements and its potential application for determining the contribution of biomass burning from wildfires and prescribed fires to ambient $PM_{2.5}$ organic carbon, *J. Geophys. Res*., *113*, D22302, doi:10.1029/2008JD010216.

Sun, H., L. Biedermann, and T. C. Bond (2007), Color of brown carbon: a model for ultraviolet and visible light absorption by organic carbon aerosol, *Geophys. Res. Lett.*, *34*, L17813, doi:10.1029/2007GL029797.

Surratt, J. D., J. H. Kroll, T. E. Kleindienst, E. O. Edney, M. Claeys, A. Sorooshian, N. L. Ng, J. H. Offenberg, M. Lewandowski, M. Jaoui, R. C. Flagan, and J. H. Seinfeld (2007), Evidence for organosulfates in secondary organic aerosol, *Environ. Sci. Technol*., *41*, 517–527.

Surratt, J. D., Y. Gomez-Gonzalez, A. W. H. Chan, R. Vermeylen, M. Shahgholi, T. E. Kleindienst, E. O. Edney, J. H. Offenberg, M. Lewandowski, M. Jaoui, W. Maenhaut, M. Claeys, R. C. Flagan, and J. H. Seinfeld (2008), Organosulfate formation in biogenic secondary organic aerosol, *J. Phys. Chem. A*, *112*, 8345–8378.

Szidat, S., T. M. Jenk, H. W. Gaggeler, H. A. Synal, R. Fisseha, U. Baltensperger, M. Kalberer, V. Samburova, L. Wacker, M. Saurer, M. Schwikowski, and I. Hajdas (2004), Source apportionment of aerosols by ^{14}C measurements in different carbonaceous particle fractions, *Radiocarbon*, *46*, 475-484.

Tan, Y., A. G. Carlton, S. P. Seitzinger, and B. J. Turpin (2010), SOA from methylglyoxal in clouds and wet aerosols: Measurement and prediction of key products, *Atmos. Environ*., *44*, 5218-5226.

Tanner, R. L., W. J. Parkhurst, M. L. Valente, and W. D. Phillips (2004), Regional composition of $PM_{2.5}$ aerosols measured at urban, rural and "background" sites in the Tennessee valley, *Atmos. Environ*., *38*, 3143-3153.

Terzi, E., and C. Samara (2004), Gas-particle partitioning of polycyclic aromatic hydrocarbons in urban, adjacent coastal, and continental background sites of western Greece, *Environ. Sci. Technol*., *38*, 4973-4978.

Thompson, J. E., P. L. Hayes, J. L. Jimenez, K. Adachi, X. Zhang, J. Liu, R. J. Weber, and P. R; Buseck (2012), Aerosol optical properties at Pasadena, CA during CalNex 2010, *Atmos. Environ*., *55*, 190-200.

Tian, D., Y. T. Hu, Y. H. Wang, J. W. Boylan, M. Zheng, and A. G. Russell (2009), Assessment of biomass burning emissions and their impacts on urban and regional $PM_{2.5}$: A Georgia case study, *Environ. Sci. Technol*., *43*, 299-305.

Tsigaridis, K., and M. Kanakidou (2003), Global modeling of secondary organic aerosol in the troposphere: A sensitivity analysis, *Atmos. Chem. Phys*., *3*, 2879–2929.

Turpin, B. J., and H.-J. Lim (2001), Species contributions to $PM_{2.5}$ mass concentrations: Revisiting common assumptions for estimating organic mass, *Aerosol Sci. Technol.*, *35*, 602-610.

Ulbrich, I. M., M. R. Canagaratna, Q. Zhang, D. R. Worsnop, and J. L. Jimenez (2009), Interpretation of organic components from Positive Matrix Factorization of aerosol mass spectrometric data, *Atmos. Chem. Phys*., *9*, 2891–2918, doi:10.5194/acp-9-2891-2009.

Virtanen, A., J. Joutsensaari, T. Koop, J. Kannosto, P. Yli-Pirila, J. Leskinen, J. M. Makela, J. K. Holopainen, U. Poschl, M. Kulmala, D. R. Worsnop, and A. Laaksonen (2010), An amorphous slid state of biogenic secondary organic aerosol particles, *Nature*, *467*, 824-827.

Veres, P. R., J. M. Roberts, A. K. Cochran, J. B. Gillman, W. C. Kuster, J. S. Holloway, M. Graus, J. Flynn, B. Lefer, C. Warneke, and J. de Gouw (2011), Evidence of rapid production of organic acids in an urban air mass, *Geophys. Res. Lett.*, *38*, L17807, doi:10.1029/2011GL048420.

Volkamer, R., J. L. Jimenez, F. San Martini, K. Dzepina, Q. Zhang, D. Salcedo, L. T. Molina, D. R. Worsnop, and M. J. Molina (2006), Secondary organic aerosol formation from anthropogenic air pollution: Rapid and higher than expected, *Geophys. Res. Lett*., *33*, L17811, doi:10.1029/2006GL026899.

Volkamer, R., F. SanMartini, L. T. Molina, D. Salcedo, J. L. Jimenez, and M. J. Molina (2007), A missing sink for gas-phase glyoxal in Mexiko City: Formation of secondary organic aerosol, *Geophys. Res. Lett*., *34*, L19807, doi:

10.1029/2007GL030752.

Volkamer, R., P. J. Ziemann, and M. J. Molina (2009), Secondary organic aerosol formation from acetylene (C_2H_2): seed effect on SOA yields due to organic photochemistry in the aerosol aqueous phase, *Atmos. Chem. Phys*., *9*, 1907-1928.

Wang, C. F., C. Y. Chang, S. F. Tsai, H. L. Chiang (2005), Characteristics of road dust from different sampling sites in northern Taiwan, *J. Air Waste Manage. Assoc*., *55*, 1236-1244.

Warneck, P. (2003), In-cloud chemistry opens pathway to the formation of oxalic acid in the marine atmosphere, *Atmos. Environ*., *37*, 2423-2427.

Washenfelder, R. A., C. J. Young, S. S. Brown, W. M. Angevine, E. L. Atlas, D. R. Blake, D. M. Bon, M. J. Cubison, J. A. de Gouw, S. Dusanter, J. Flynn, J. B. Gilman, M. Graus, S. Griffith, N. Grossberg, P. L. Hayes, J. L. Jimenez, W. C. Kuster, B. L. Lefer, I. B. Pollack, T. B. Ryerson, H. Stark, P. S. Stevens, and M. K. Trainer (2011), The glyoxal budget and its contribution to organic aerosol for Los Angeles, California, during CalNex 2010, *J. Geophys. Res*., *116*, D00V02, doi:10.1029/2011JD016314.

Watson, J. G., J. C. Chow, L. W. A. Chen, and N. H. Frank (2009), Methods to assess carbonaceous aerosol sampling artifacts for IMPROVE and other long-term networks, *J. Air Waste Manage. Assoc*., *59*, 898-911.

Weber, R. J., D. Orsini, Y. Duan, K. Baumann, C. S. Kiang, W. Chameides, Y.-N. Lee, F. Brechtel, P. Klotz, P. Jongejan, H. ten Brink, J. Slanina, C. B. Boring, Z. Genfa, P. Dasgupta, S. Hering, M. Stolzenburg, D. D. Dutcher, E. Edgerton, B. Hartsell, P. Solomon, and R. Tanner (2003), Intercomparison of near real time monitors of PM2.5 nitrate and sulfate at the U. S. Environmental Protection Agency Atlanta Supersite, *J. Geophys. Res*., *108*, 8421, doi:10.1029/2001JD001220.

Weber, R. J., A. P. Sullivan, R. E. Peltier, A. Russell, B. Yan, M. Zheng, J. de Gouw, C. Warneke, C. Brock, J. S. Holloway, E. L. Atlas, and E. Edgerton (2007), A study of secondary organic aerosol formation in the anthropogenic-influenced southeastern United States, *J. Geophys. Res*., *112*, D13302, doi:10.1029/2007JD008408.

Williams, B. J., A. H. Goldstein, N. M. Kreisberg, and S. V. Hering (2009), In situ measurements of gas/particle-phase transitions for atmospheric semivolatile organic

compounds, *P. Natl. Acad. Sci*., *107*, 6676-6681.

Williams, B. J., A. H. Goldstein, N. M. Kreisberg, S. V. Hering, D. R. Worsnop, I. M. Ulbrich, K. S. Docherty, and J. L. Jimenez (2010), Major components of atmospheric organic aerosol in southern California as determined by hourly measurements of source marker compounds, *Atmos. Chem. Phys.*, *10*, 11577-11603.

Worton, D. R., A. H. Goldstein, D. K. Farmer, K. S. Docherty, J. L. Jimenez, J. B. Gilman, W. C. Kuster, J. de Gouw, B. J. Williams, N. M. Kreisberg, S. V. Hering, G. Bench, M. McKay, K. Kristensen, M. Glasius, J. D. Surratt, and J. H. Seinfeld (2011), Origins and composition of fine atmospheric carbonaceous aerosol in the Sierra Nevada Mountains, California, *Atmos. Chem. Phys*., *11*, 10219–10241.

Yan, B., M. Zheng, Y. T. Hu, X. Ding, A. P. Sullivan, R. J. Weber, J. Baek, E. S. Edgerton, and A. G. Russell (2009), Roadside, urban, and rural comparison of primary and secondary organic molecular markers in ambient $PM_{2.5}$, *Environ. Sci. Technol*., *43*, 4287-4293.

Yan, B., Y. T. Hu, X. Zhang, D. Tian, S. Balachandran, H. K. Kim, R. J. Weber, M. Zheng, and A. G. Russell, Detailed chemical characterization and aging of wildfire aerosols in the southeastern U.S., *in preparation*.

You, Y., L. Renbaum-Wolff, M. Carreras-Sospedra, S. J. Hanna, N. Hiranuma, S. Kamal, M. L. Smith, X. Zhang, R. J. Weber, J. E. Shilling, D. Dabdub, S. T. Martin, and A. K. Bertram (2012), Images reveal that atmospheric particles can undergo liquid-liquid phase separations, *P. Natl. Acad. Sci*., in press.

Zeng, T., Y. H. Wang, Y. Yoshida, D. Tian, A. G. Russell, and W. R. Barnard (2008), Impacts of prescribed fires on air quality over the southeastern United States in spring based on modeling and ground/satellite measurements, *Environ. Sci. Technol*., *42*, 8401-8406.

Zhang, Q., J. L. Jimenez, M. R. Canagaratna, J. D. Allan, H. Coe, I. Ulbrich, M. R. Alfarra, A. Takami, A. M. Middlebrook, Y. L. Sun, K. Dzepina, E. Dunlea, K. Docherty, P. F. DeCarlo, D. Salcedo, T. Onasch, J. T. Jayne, T. Miyoshi, A. Shimono, S. Hatakeyama, N. Takegawa, Y. Kondo, J. Schneider, F. Drewnick, S. Weimer, K. Demerjian, P. Williams, K. Bower, R. Bahreini, L. Cotrell, R. J. Griffin, J. Rautiainen, J. Y. Sun, Y. M. Zhang, and D. R. Worsnop (2007), Ubiquity and dominance of oxygenated species in organic aerosols in anthropogenically-influenced Northern Hemisphere mid-latitudes, *Geophys. Res. Lett*., *34*, L13801,

doi:10.1029/2007GL029979.

Zhang, X., A. Hecobian, M. Zheng, N. H. Frank, and R. J. Weber (2010), Biomass burning impact on $PM_{2.5}$ over the southeastern US during 2007: Integrating chemically speciated FRM filter measurements, MODIS fire counts and PMF analysis, *Atmos. Chem. Phys.*, *10*, 6839-6853, doi:10.5194/acp-10-6839-2010.

Zhang, X., Y.-H. Lin, J. D. Surratt, P. Zotter, A. H. S. Prévôt, and R. J. Weber (2011), Light-absorbing soluble organic aerosol in Los Angeles and Atlanta: A contrast in secondary organic aerosol, *Geophys. Res. Lett*., *38*, L21810, doi:10.1029/2011GL049385.

Zhang, X., Z. Liu, A. Hecobian, M. Zheng, N. H. Frank, E. S. Edgerton, and R. J. Weber (2012a), Spatial and seasonal variations of fine particle water-soluble organic carbon (WSOC) over the southeastern United States: Implications for secondary organic aerosol formation, *Atmos. Chem. Phys. Disc*., *12*, 9621-9664.

Zhang, X., J. Liu, E. T. Parker, P. L. Hayes, J. L. Jimenez, J. A. de Gouw, J. H. Flynn, N. Grossberg, B. L. Lefer, and R. J. Weber (2012b), On the gas-particle partitioning of soluble organic aerosol in two urban atmospheres with contracting emissions: Part 1. Bulk water-soluble organic carbon, *J. Geophys. Res*., under review.

Zheng, M., G. R. Cass, J. J. Schauer, and E. S. Edgerton (2002), Source apportionment of fine particle air pollutants in the southeastern United States using solvent-extractable organic compounds as tracers, *Environ. Sci. Technol*., *36*, 2361-2371.

Zheng, M., G. R. Cass, L. Ke, F. Wang, J. J. Schauer, E. S. Edgerton, and A. G. Russell (2007), Source apportionment of daily fine particulate matter at Jefferson street, Atlanta, GA, during summer and winter, *J. Air Waste Manage. Assoc*., *57*, 228-242.

Zhong, M., and M. Jang (2011), Light absorption coefficient measurement of SOA using a UV-Visible spectrometer connected with an integrating sphere, *Atmos. Environ.*, *45*, 4263-4271.

Zuend, A., and J. H. Seinfeld (2012), Modeling the gas-particle partitioning of secondary organic aerosol: the importance of liquid-liquid phase separation, *Atmos. Chem. Phys.*, *12*, 3857-3882.

VITA

Xiaolu Zhang

Xiaolu Zhang was born in Beijing, China in 1984. She grew up in Beijing and attended Peking University, where she received a bachelor degree in Environmental Sciences in 2006. Shortly after her graduation, Ms. Zhang came to the United States to pursue a doctorate degree in Atmospheric Chemistry at Georgia Tech. When she is not working on her research, Ms. Zhang enjoys food and travel. Ms. Zhang's favorite activities include going shopping and playing with her cat, Xiaoming.